Design and Analysis of a Nested Halbach Permanent Magnet Magnetic Refrigerator

by

Armando Tura

BEng, University of Victoria, 2002
MASc, University of Victoria, 2005

A Dissertation Submitted in Partial Fulfillment
of the Requirements for the Degree of

"DOCTOR OF PHILOSOPHY"

in the Department of Mechanical Engineering

Supervisory Committee

Design and Analysis of a Nested Halbach Permanent Magnet Magnetic Refrigerator

by

Armando Tura
BEng, University of Victoria, 2002
MASc, University of Victoria, 2005

Supervisory Committee

Dr. Andrew Rowe, Department of Mechanical Engineering
Supervisor

Dr. Peter Wild, Department of Mechanical Engineering
Departmental Member

Dr. Sadik Dost, Department of Mechanical Engineering
Departmental Member

Dr. Aaron Gulliver, Department of Electrical Engineering
Outside Member

Abstract

Supervisory Committee
Dr. Andrew Rowe, Department of Mechanical Engineering
Supervisor
Dr. Peter Wild, Department of Mechanical Engineering
Departmental Member
Dr. Sadik Dost, Department of Mechanical Engineering
Departmental Member
Dr. Aaron Gulliver, Department of Electrical Engineering
Outside Member

A technology with the potential to create efficient and compact refrigeration devices is an active magnetic regenerative refrigerator (AMRR). AMRRs exploit the magnetocaloric effect displayed by magnetic materials whereby a reversible temperature change is induced when the material is exposed to a change in applied magnetic field. By using the magnetic materials in a regenerator as the heat storage medium and as the means of work input, one creates an active magnetic regenerator (AMR). Although several laboratory devices have been developed, no design has yet demonstrated the performance, reliability, and cost needed to compete with traditional vapor compression refrigerators. There are many reasons for this and questions remain as to the actual potential of the technology.

The objective of the work described in this thesis is to quantify the actual and potential performance of a permanent magnet AMR system. A specific device configuration known as a dual-nested-Halbach system is studied in detail. A laboratory scale device is created and characterized over a wide range of operating parameters. A numerical model of the device is created and validated against experimental data. The resulting model is used to create a cost-minimization tool to analyze the conditions needed to achieve specified cost and efficiency targets.

Experimental results include cooling power, temperature span, pumping power and work input. Although the magnetocaloric effect of gadolinium is small, temperature spans up to 30 K are obtained. Analysis of power input shows that the inherent magnetic work is a small fraction of the total work input confirming the assumption that potential

cycle efficiencies can be large. Optimization of the device generates a number of areas for improvement and specific results depend upon targeted temperature spans and cooling powers. A competitive cost of cooling from a dual-nested-Halbach configuration is challenging and will depend on the ability to create regenerator matrices with near-ideal adiabatic temperature change scaling as a function of temperature.

Table of Contents

List of Tables

List of Figures

Nomenclature

Acronyms

AMR(R)	Active Magnetic Regenerator (Refrigerator)
MCE	Magnetocaloric Effect (adiabatic temperature change)
COP	Coefficient of Performance
AMRTA	Active Magnetic Regenerator Test Apparatus
PMMR	Permanent Magnet Magnetic Refrigerator

Symbols

a, b, c, d	Discrete points in a cycle	-
A	Surface area	m^2
B	Magnetic Field	T
Bi	Biot number	-
c	Specific heat	$JkgK^{-1}$
d	Diameter	m
Fo	Fourier number	-
h	Convection coefficient, enthalpy	$Wm^{-2}K^{-1}$, $kJkg^{-1}$
H	Enthalpy rate	W
k	Thermal conductivity	$Wm^{-1}K^{-1}$
L	Length	m
m	Mass	kg
n	MCE scaling exponent	-
Pr	Prandtl number	-
p	Pressure	Nm^{-2}
Q	Heat transfer rate	W
R	Thermal mass ratio	-
Re	Reynold's number	-
s	Entropy	$kJkg^{-1}K^{-1}$
t	Non-dimensional time coordinate	-
T	Temperature	K

U	Utilization	-
W	Power	W
x	Non-dimensional spatial coordinate	-

Greek

α	Thermal diffusivity	m^2s^{-1}
β	Balance	-
Λ	Coefficient of merit	
ε	Porosity	-
Γ	Geometric form factor	-
κ	Non-dimensional conductance	-
ρ	Density	kgm^{-3}
σ	Symmetry	-
τ	Period	s
Φ	Utilization	-

Subscripts

C	Cold or cooling capacity	-
c	Cycle	-
eff	Effective	-
f	Fluid	-
H	Hot or high-field	-
h	Hydraulic	-
m	Magnetic	-
p	Constant pressure, parasitic	-
s	Solid	-
$'$	Per unit length	-

Acknowledgments

Just about 11 years ago I was nervously sitting in an office chair for the most improvised job interview I can ever remember. I was made aware of this work term opportunity just minutes before, and for that I have to thank my dear friend Rodney Katz, the machine shop technician. To be honest, I think even Rodney did not realize at the time how much trouble I would have given him for the decade to come: complex little mechanical parts, late days in the shop…But if we were friends then, and we are far closer now, probably because of that. I cannot think of myself being successful without his incredible support. I like to take pride, when I visit other universities, of how quickly, in our experimental research, we move from an idea to a working device. For this I really owe a big thank you to him.

Back to that office in the Mechanical Engineering Office Wing. I am nervous and I am trying to understand this young professor, fresh from his PhD defence, telling me stories about the magnetocaloric effect. No idea of what he is talking about, I did not even understand his pronunciation… is it something about chlorine and magnetism? Well, let him talk more about it, eventually I should be able to make something out of this nonsense.

He gets deeper in the topic, talks like I am already an expert in the field, is it because I am trying to show confidence, or is it just the way he talks about his research? Lost, intimidated… But wait! He is finally writing some definitions on the white board, that's it! MAGNETOCALORIC effect: The fog is rarifying, I am starting to see what this is all about.

Then the proposal. A work term is what I walked in his office for, but as he is going along I realize that this is just the beginning. Young and brave professor: he does not even know me and yet he is already offering me a Masters Student position, to start right after my work term. Being the leader of the first Formula SAE built at UVic must have helped my reputation, but still, brave. Surprised and confused, yet drawn by the

enthusiasm and the impressively clear description of the objectives and expected outcome of my potential graduate program, I am ready to accept the offer.

It is uncommon to enroll in a Master program and then in a PhD with the same supervisor, same research area, and same laboratory. It is also strongly discouraged for an academic carrier. Yes, magnetic refrigeration is an engaging field, but I could have applied to other universities, I even had start-up companies offering attractive research positions. Continuing to work supervised by Prof. Andrew Rowe was the most natural path as the human factor has always meant the most for me.

I really need to acknowledge Prof. Rowe for his outstanding ability to perform as supervisor, educator, professor and researcher. I admire him for is ability to motivate and support a graduate student. I am always baffled by how easily he embraces student solutions and design ideas, even if they differ from his original plan. His theoretical expertise is exceptional and paired with excellent experimental skills. In simple words it is a joy working for him. He is a role model.

With eleven years in the research area and six in the PhD program I have a long list of acknowledgments, but I am here already toward the end of my second page, so I should keep it brief.

Life in the lab has been an incredible experience, and for that I need to thank my coworkers, dear friends. Danny Arnold, working with you is fun and rewarding. I cannot believe we never had conflicts trying to impose each other ideas, design, and solutions. Thank you for being caring, tactful, respectful, and so much fun. Sandro Schopfer, the lab misses you so badly, and not just because you are the Matlab God. Tom Burdyny and Oliver Campbell, my eyes will definitely be wet when you leave the Lab.

None of this would have happened if I did not have a loving family, role models, support, and joy for my life. Thank you dad, mom, Alfredo and Emanuela.

Chapter 1

Introduction

1.1 Motivation

Refrigeration is a pervasive technology that has been instrumental in transforming industrial societies throughout the world. Modern refrigeration equipment is reliable, inexpensive, and mature. It is not unrealistic to say there are few design variables that have not been thoroughly studied and optimized in conventional near-room temperature devices. However, one of the difficulties with vapour-compression refrigeration cycles is that most of the better refrigerants are ozone depleting substances consisting of chlorinated fluorocarbons (H/CFCs) which can also be powerful greenhouse gases. In contrast, magnetic refrigeration (MR) makes use of a magnetic solid as the refrigerant. In addition magnetic refrigeration has the potential to offer significantly higher efficiencies than conventional gas cycles in more compact devices. Since refrigeration based devices draw approximately 15% of the worldwide energy consumption, improved efficiency could have a significant positive impact on the global energetic demand, and carbon emissions [1].

1.2 Background

Magnetic refrigeration exploits a property of magnetic materials called the magnetocaloric effect (MCE): the temperature of ferromagnetic materials is observed to rise upon application of a magnetic field. When a material is magnetized, its magnetic moments are aligned, leading to a reduction in its magnetic entropy. If this process is done adiabatically and reversibly the total entropy is constant. Thus, a reduction in magnetic entropy is compensated by an increase in lattice entropy resulting in a temperature increase. MCE can be defined as adiabatic temperature change due to magnetization, or, alternatively, isothermal magnetic entropy change. This property is a strong function of magnetic field intensity and temperature, and is maximized at the

magnetic material ordering temperature, known as the Curie temperature (where magnetization is a strong function of temperature and magnetic field). Thus thermal cycles can be envisioned by magnetizing and demagnetizing solid state refrigerants just like it can be done by compressing and expanding compressible substances.

Figure 1-1 shows gadolinium MCE for a 2 T field [2]. Gadolinium is often used as prototype refrigerant for near room temperature applications.

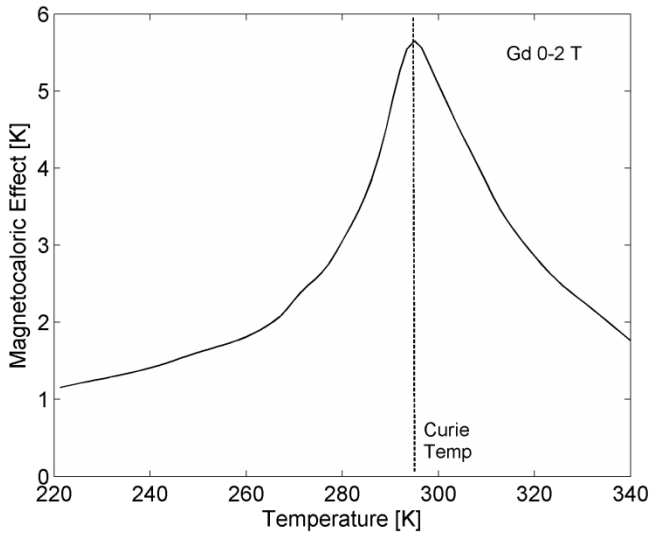

Figure 1-1. Magnetocaloric effect of Gd for a 0-2 T applied field change [4].

The MCE is a strong function of temperature and is related to the rate of change of magnetization with respect to temperature; hence it is most significant in the proximity of the Curie temperature where spontaneous magnetic ordering occurs. This concept will be made clearer in Chapter 2 where further details of this physical property are given. MCE is a function of the applied field and, for gadolinium near the Curie temperature, follows the law [3]

$$\Delta T_{MCE} = 3.675 H^{0.7}, \tag{1.1}$$

where H is the applied magnetic field in Tesla. This highlights that a magnetic cycle is most effective if the low field is as close as possible to zero; in other words operating between 0-1 T is preferred to 1-2 T, because of the diminishing returns.

Until the 1970s, magnetic refrigeration remained a means of cooling for low temperatures only. For a material to have a significant magnetocaloric effect, the magnetic entropy change must be large relative to the total entropy of the material. At low temperatures, the lattice and electronic contributions to the entropy are relatively small. Thus, with moderate field changes, it was presumed that magnetic cooling was only effective at low temperatures where the small magnetic entropy changes are relatively large compared to the total entropy [1]. Additionally early applications of magnetic refrigeration had very specific applications such as experiments below 1 K.

In 1974, significant progress occurred in magnetic refrigeration with a breakthrough with the work of Brown [1][5]. He developed a magnetic refrigerator near room temperature using a reciprocating device based on the magnetic-sterling cycle. Gd was used as the refrigerant, a water-alcohol mixture as heat transfer fluid, and a water-cooled 7 T electromagnet. The device consisted in a vertical column filled with the heat transfer fluid (regenerator) placed inside an annular coil (Figure 1-2). Gadolinium was used as magnetic refrigerant consisting of 1 mm thick parallel plates. Two heat exchangers, one at the top and another at the bottom of the cylinder, ensure the isothermal magnetization and demagnetization, while constant field regeneration is obtained by moving alternatively up and down the fluid-filled column. Brown reported temperature spans up to 47 °C, although cooling power was extremely low due to the low cycle frequency imposed by both isothermal processes and energizing/de-energizing of the electromagnet. Brown's work was innovative because he proved not only that magnetic refrigeration is feasible near room temperature, but also that a regenerative cycle is instrumental in effectively producing a temperature lift much larger than the ΔT_{MCE}.

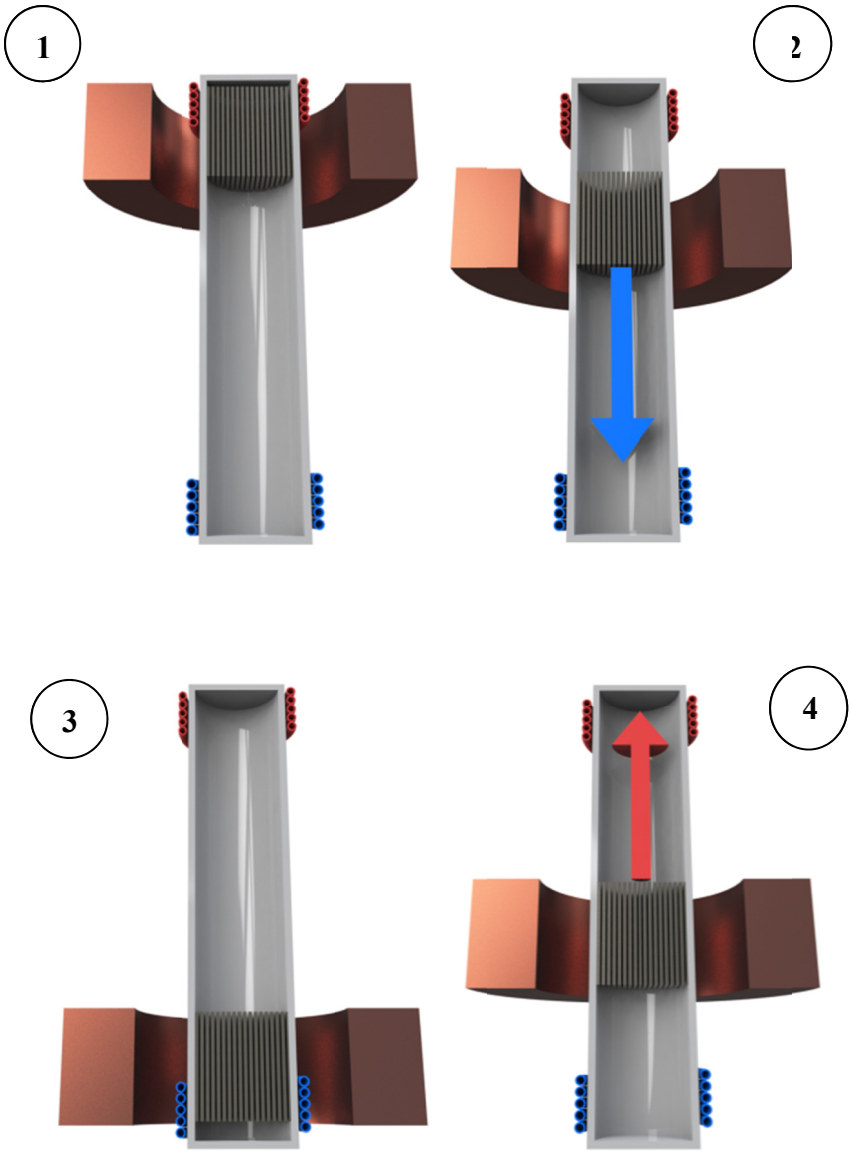

Figure 1-2. Schematic of cycle steps of Brown's device. 1) isothermal magnetization 2) isomagnetic cooling 3) isothermal demagnetization 4) isomagnetic heating.

In 1982 a new concept was introduced by Barclay that became known as an Active Magnetic Regenerator (AMR). Unlike previous gas cycles, or magnetic cycles, the AMR concept coupled what had been two separate processes into a single component [1]. Instead of using a separate material as a regenerator to recuperate the heat from the magnetic material, the AMR concept made use of the refrigerant itself as the regenerator. In essence, a temperature gradient is established throughout the AMR and a fluid is used

to transfer heat from the cold end to the hot. This subtle but important idea produced a new magnetic cycle distinct from Carnot, Ericsson, Brayton, or Stirling. In the AMR, each section of the regenerator bed undergoes its own cycle; the entire mass of working material no longer experiences a similar cycle at uniform temperature. This concept was given further complexity when the use of multiple magnetic refrigerants in a single AMR was introduced. Early AMR development was focused on the 20 to 77 K range to liquefy hydrogen [1]. Barclay's research group intensely worked for over a decade on natural gas liquefier which is illustrated in Figure 1-3. A superconducting magnet is the core of a C shaped field generator and a magnetic wheel consisting in radially arranged regenerators spins, alternatively exposing the individual AMRs to the intense magnetic field in the air gap. During the magnetization phase (inside the air gap) the refrigerant generates heat that the fluid (i.e. helium or nitrogen) extracts and then rejects to the environment, while during the demagnetization phase the refrigerant cools down and the heat transfer fluid is pumped across the regenerators to extract cooling power.

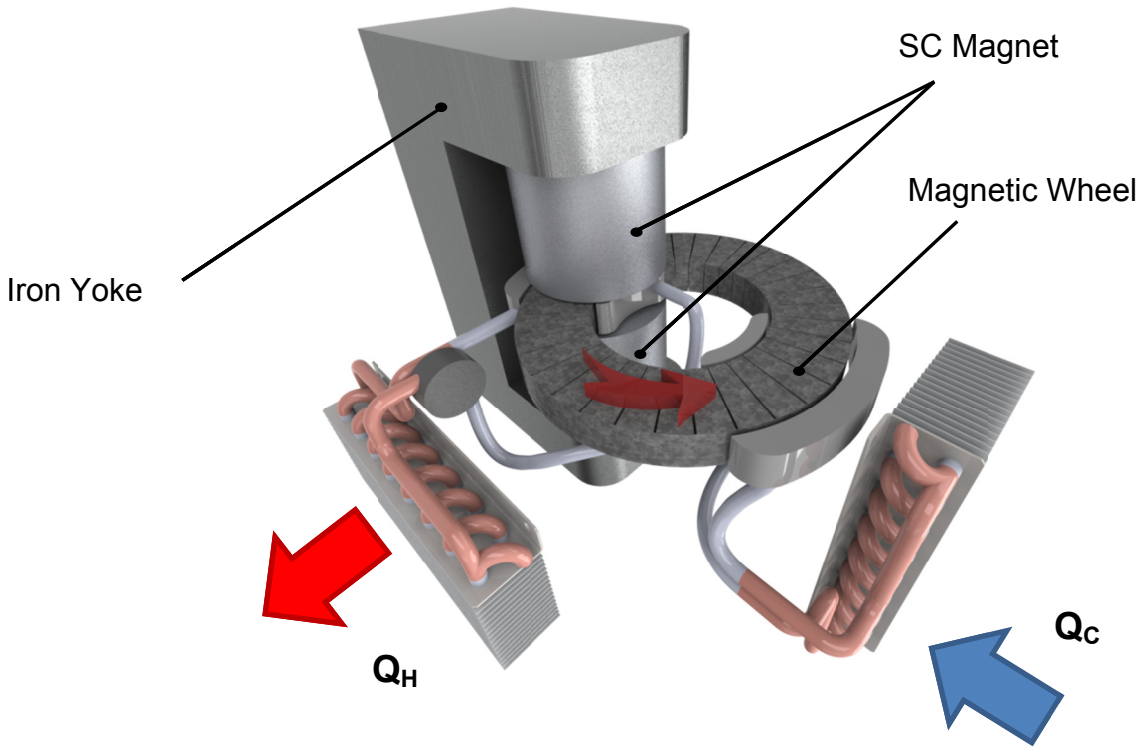

Figure 1-3. Simplified schematic of the concept patented by J. Barclay of a SC system for LNG production [6].

This design principle has been also exploited for near room application by a number of research institutions [7], replacing the superconducting magnet with permanent magnets.

During the past two decades materials research has been prolific and there have been some interesting new alloys discovered that have the potential to be good magnetic refrigerants for room temperature applications. In particular, a series of ternary alloys such as $Gd_5(Si_{1-x}Ge_x)_4$, $Mn(As_{1-x}Sb_x)$, $MnFe(P_{1-x}As_x)$, $La(Fe_{13-x}Si_x)$ are found to display high entropy changes due to a first-order phase transition [8]. Second-order transition alloys, such as Gd, Gd_xEr_{1-x}, Gd_xTb_{1-x} have also been extensively tested [9]. As a result experimental devices have progressed to room temperature applications as time has passed. In 1990 the US Navy David Taylor Research Center in Maryland, conducted a test for room temperature refrigeration using a layered regenerator with a mixed composition of gadolinium and terbium [10]. The magnetic field intensity was varied between 0 and 7 T by ramping the current in the superconducting magnet up and down, in 70 second cycles. Temperature spans up to 50 K were obtained, however the layering concept failed (larger temperature spans were achieved using a single material). While the Cryofuels group at the University of Victoria began working on their rotary AMR to liquefy natural gas, the Astronautics Corporation in cooperation with the Oak Ridge National Laboratory built and tested a medium scale magnetic refrigerator near the liquefaction temperature of nitrogen [11]. The design made use of two 2 kg regenerators reciprocating in a 7 T superconducting magnet. The device produced up to 25 W of cooling, and under no load and a heat rejection temperature of 82 K the cold end of the regenerator reached 44 K. Later, at the Ames Laboratory in Iowa, the Astronautics Corporation built and successfully tested a proof of concept reciprocating room temperature device capable of producing 500 W of cooling power and a coefficient of performance (COP) of 6 or more [12]. A helium-immersed superconducting magnet with a field up to 7 T was used. In 1998, researchers at Astronautics Corporation reported a room-temperature device using Gd refrigerant and a water-glycol heat transfer fluid. The cooling power of this device was high, but more significantly, they were able to show refrigeration with an applied field as low as 1.7 Tesla with use of permanent magnets. A rotating “magnetic wheel” machine developed at Astronautics was operated for over 1500 hr between 2001 and 2007 [7]. In 2002 an Active Magnetic Test Apparatus

(AMRTA) was completed and tested by the Cryofuel Systems group at the University of Victoria (Figure 1-4). The reciprocating device made use of a 2 T superconducting magnet and two AMRs with a mass of up to 135 g each. The refrigerator was designed for flexibility, with the main objective of characterizing a broad range of regenerators, for room temperature and cryogenic applications [13]. In 2003, the device received a superconducting field generator upgrade, allowing a maximum field of 5 T. Designed to operate from near room temperature to the cryogenic regime, the system encloses the regenerators in a vacuum chamber, with the objective of thermally disconnecting them from the environment. This allows operating near room temperature with very well controlled thermal leaks, in the order of 1 W or less [14]. Thus small regenerators with cooling powers in the order of 5 to 20 W can be tested with confidence. The device obtained no load temperature spans up to 86 °C (tests performed in 2004), which is still the largest recorded no-load span from an AMR system to date.

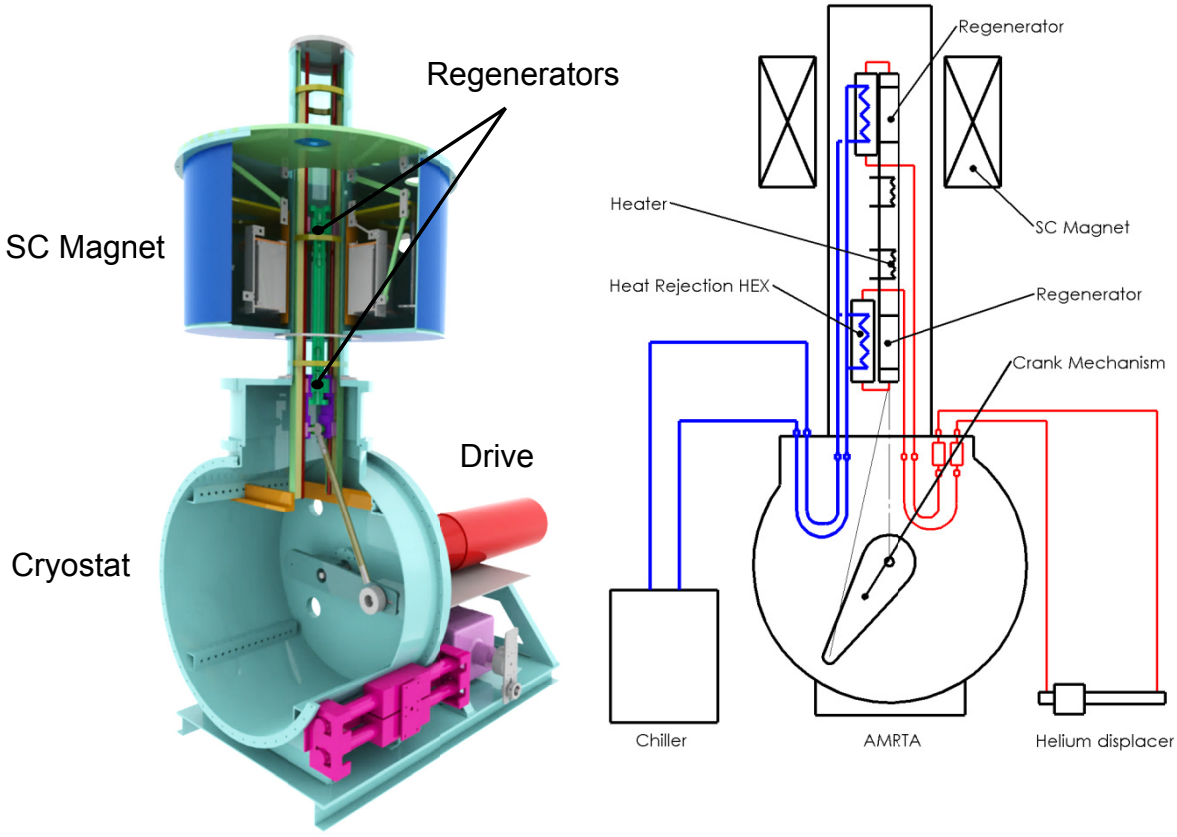

Figure 1-4. Active regenerator test apparatus developed by Rowe in 2002.

Given the progress in the material development for both permanent magnets and solid magnetic refrigerants, prototype design, and the interest in more environmentally friendly and efficient refrigeration systems, the International Institute of Refrigeration (IIR) took a step into promoting the development of commercial devices [15]. In 2005 the IIR sponsored the first *International Conference on Magnetic Refrigeration at Room Temperature*, named *Thermag*. This biennial event has so far given substantial momentum to research and development across the world. Material discovery and system development has flourished and the number of related annually published papers has exponentially increased (Figure 1-5).

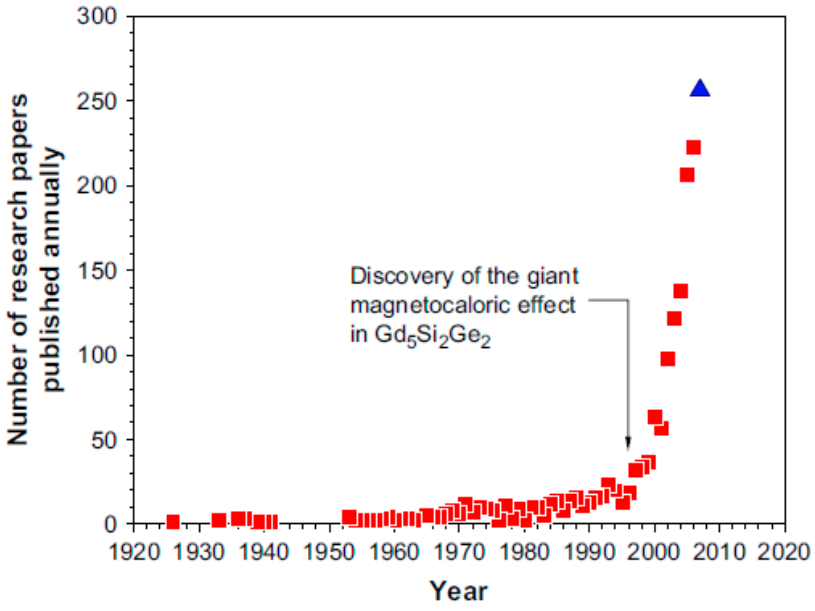

Figure 1-5. Number of publications per year [15].

Among all, the most interesting cooling machines developed during the past decade are the Astronautics Corporation's second and third generation magnetic refrigerator, the Tokyo Institute of Technology's rotating magnet refrigerator (Chubu Electric Power Co.), and the developments at Risø National Laboratory. These represent the state of the art in MR prototyping in terms of design and performance.

Astronautics Corporation second generation magnetic refrigerator (Figure 1-6) is the first development for near room temperature applications using permanent magnets. This device was a proof of concept that such refrigerator is conceivable and has potential

applications. It consists of a stationary C shaped magnet/yoke assembly creating a 1.5 T field in the gap. A "magnetic wheel" pertaining of three active magnetic regenerators spins up to 4 Hz alternatively magnetizing each of them as they cut through the field in the magnet air gap. Using approximately 200 g of gadolinium in small spheres (0.25 – 0.5 mm) it recorded a cooling power of 50 W and 25 °C temperature span under no thermal load [7].

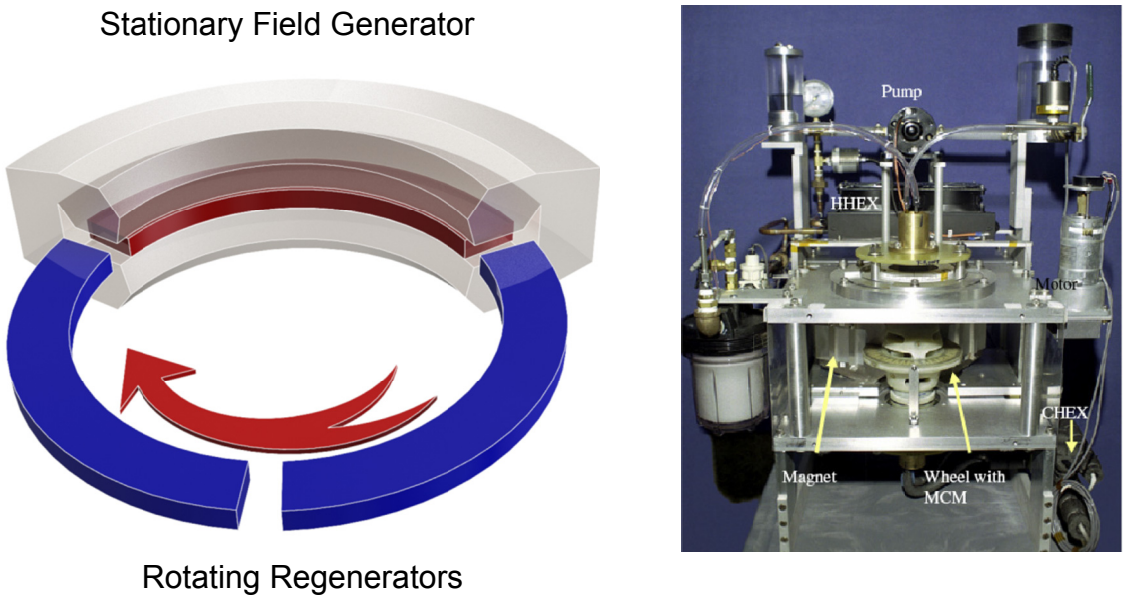

Figure 1-6. Second generation Astronautics magnetic refrigerator. First one using a permanent magnet [7].

Astronautics Corporation developed their third generation refrigerator in 2007. The new design uses a rotating permanent magnet of 1.5 T field and twelve *stationary* active regenerators, simplifying the heat transfer liquid sealing (similar choice as Chubu's group). Using 0.9 kg of gadolinium as refrigerant, the machine produced a cooling power up to 840 W with no temperature span, and approximately 400 W with 10°C temperature span. A maximum span of 19°C was obtained with no thermal load [16]. More recently the device operated with a six layer LaFeSiH refrigerant composition with a much improved performance. A cooling power with no temperature span of 2049 W was measured and peak performance of 1704 W over a span of 11.1 °C, with COP = 2.24

[17]. The device was designed as a supplemental electronics cooler with a cooling span of approximately 12 °C, between 44 °C and 32 °C.

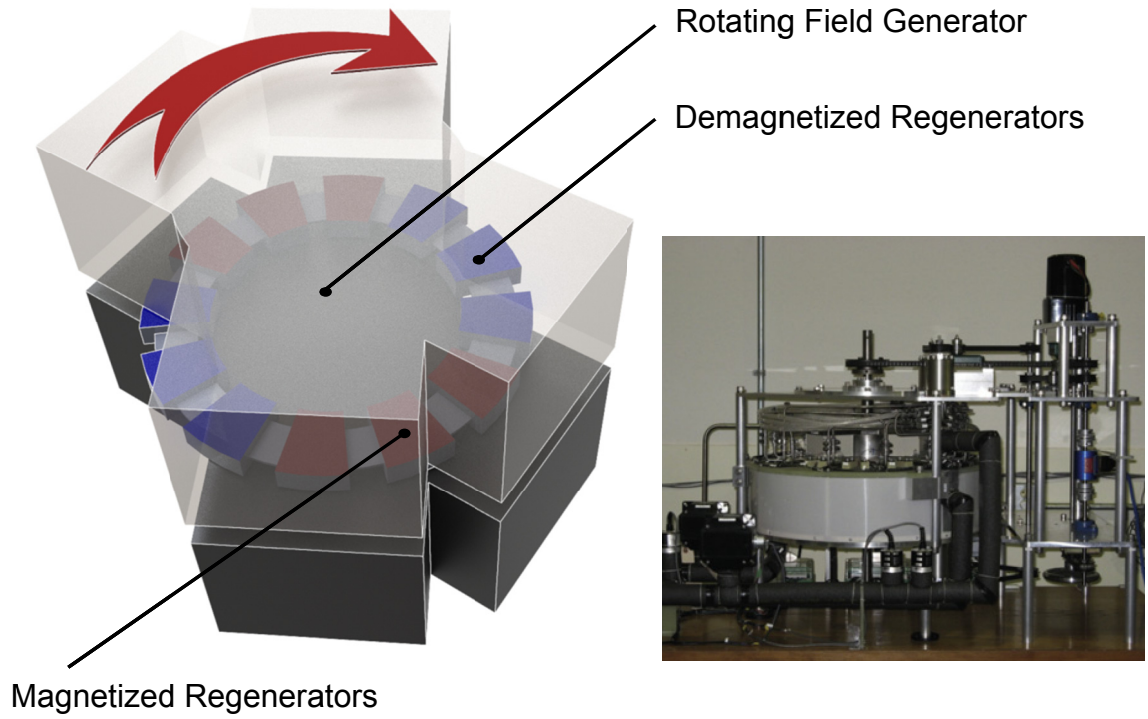

Figure 1-7. Third generation Astronautics' magnetic refrigerator [7].

Chubu's group targeted a refrigeration machine with a cooling capacity of 500 W and a COP of 3 or greater [18] mainly for air conditioning applications. This was their second generation machine after a proof of concept reciprocating device was previously built and tested [19]. In 2005 the results of the rotary magnetic refrigeration system based on moving permanent magnets and stationary regenerators were published. The machine originally produced a cooling power of 60 W. Through redesigning the magnets, magnetic yoke, and regenerator flow path, the group finally obtained a cooling capacity of 540 W and a COP of 1.8 over a 0.2 K temperature span. Figure 1-8 illustrates its working principles. A permanent magnet field generator rotates inside a cylindrical iron yoke generating two rotating high fields (0.77 T) in the air gaps. The mechanism allows four AMRs with a total mass of 1 kg to be alternatively magnetized and demagnetized.

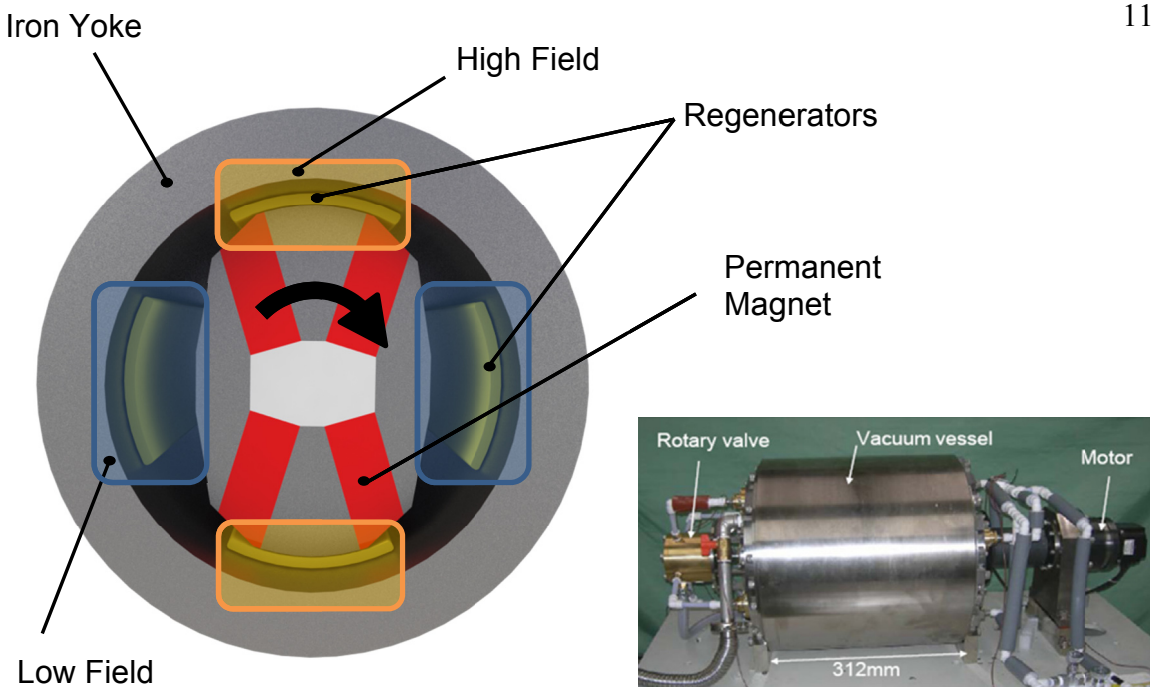

Figure 1-8. Chubu field generator and regenerators arrangement. Four regenerators and an external iron yoke are stationary, while the inner magnet is rotated alternating the high fields on the refrigerant [7].

Risø National Laboratory recently developed a novel rotary magnetic refrigerator using a quadripole stationary magnet array (Figure 1-9) with 24 rotating regenerators [20]. Such a design allows for high power densities with a relatively low permanent magnet volume. Given the rather low inertia of the refrigerant compared to the magnets and potential magnetic torque cancellation, the device is designed to operate up to a relatively high frequency (2.5 Hz results have been published). Each regenerator performs a complete thermal cycle four times in a full rotation, thus if the device operating speed is 1 Hz, cycle speed is effectively 4 Hz and a total of 96 regenerator cycles per revolution: a very elegant, simple, and effective design. The challenge of this approach is managing friction and wear of the dynamic seals located at the flow distribution valve, which exacerbate exponentially with angular velocity. The seal could induce substantial thermal losses and frequent costly maintenance. Performance results have been published using 2.8 kg of gadolinium as refrigerant. A maximum of 1010 W of cooling with no span, 200 W with a span of 18.9 °C, and a maximum span of 25.4 °C under no load were observed.

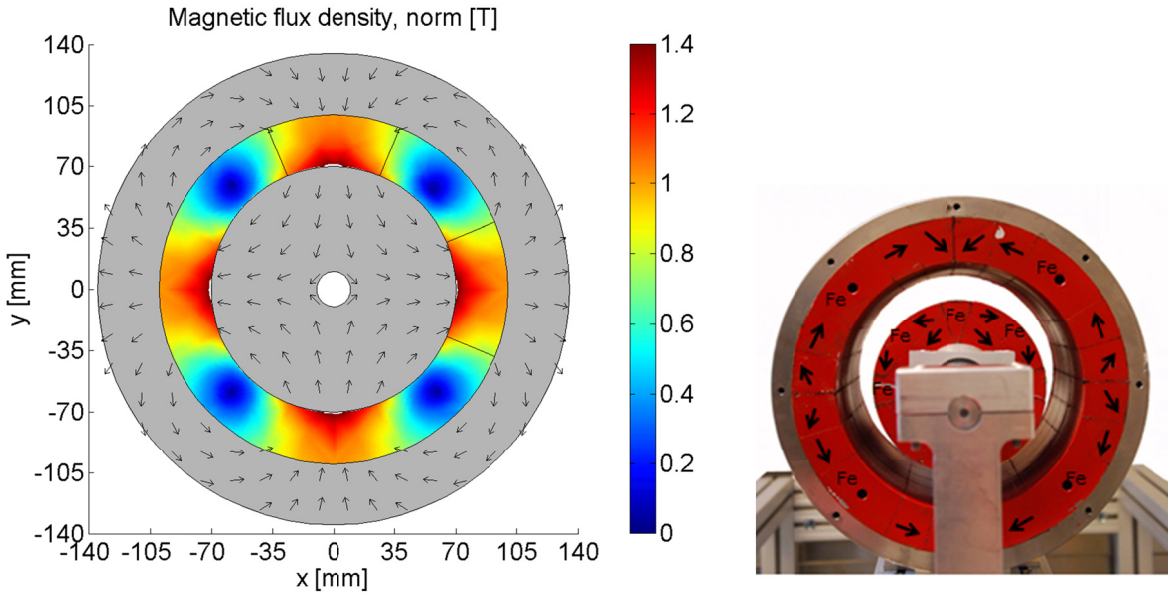

Figure 1-9. Risø quadripole field generator showing the high and low field regions [21].

1.3 Magnetic Refrigeration Classification

Since the work of Brown in the 1970s the number of lab apparatuses and prototypes has been growing. In 2008 more than 25 devices were reported [5] and over 40 by 2010 [7]. While almost the entirety of the devices is based on the AMR cycle, each system has been developed uniquely. Indeed although the magnetic refrigeration cycle can be described simply as an alternation of magnetization and demagnetization applied to a solid state refrigerant coupled with a fluid with reversing flux, the principle can be applied in a multitude of different physical solutions. Therefore the designs can be classified based on the design choices of the 1) field generator, 2) regenerator, 3) heat transfer system, and 4) device configuration. The following sections describe more in the details this categorization.

1.3.1 Field Generator

The magnetic system solution is critical for both the performance and cost of the refrigeration unit. The magnetic field can be generated in a number of ways, typically using permanent magnets or coil magnets. The design of choice depends on the type of application (Figure 1-10).

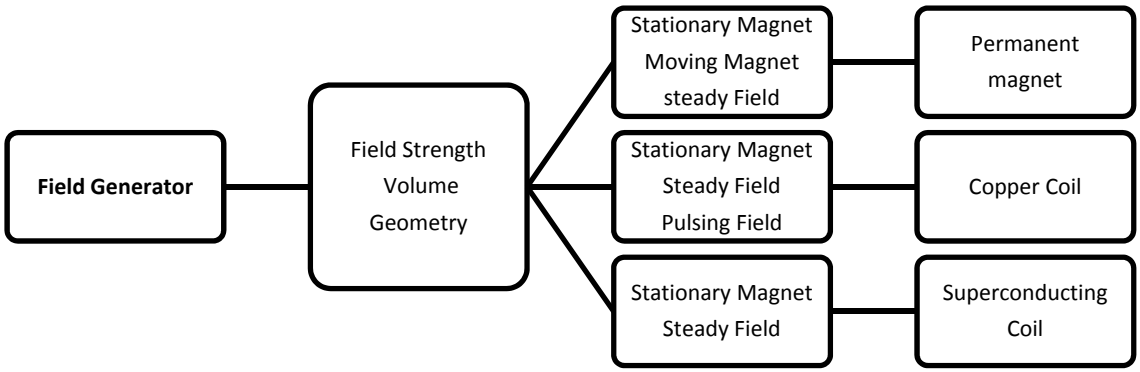

Figure 1-10. Design criteria for magnet characteristics

Permanent magnets are a convenient solution because the field is energized all the time at no cost, however they are limiting in terms of magnetized volume and field intensity. In addition, since the field cannot be modulated, magnet-magnet or magnet-regenerator relative motion is required. Magnet-magnet motion exploits the additive property of magnetic fields, i.e. superimposing same or opposite sign fields can amplify or annihilate them. This methodology is further explained in Chapter 3 and generally exploited with the use of Halbach arrays [22]. The most common solution adopted by MR apparatuses is Magnet-regenerator motion, which relies on the spatial magnetic field distribution to modulate the field surrounding the regenerator.

Conversely, coils are compact and light, their field is only limited by the amount of circulating current, and high magnetic fields can be much more easily obtained for greater volumes. However, differently from permanent magnets, they require a certain amount of power to operate. For field intensities above 1 T a copper coil may draw a large amount of electric power (inefficient and the heat generated needs to be dissipated), while a superconducting magnet can relatively easily generate fields up to 7 T with minimal electrical power. Nevertheless a substantial amount of power (~ 7.5 kW) is required to maintain a superconducting coil at subcritical temperatures. This is done either by conduction cooling, i.e. by means of a compact cryocooler, or liquid helium immersion. Clearly this can be justified only if a combination of large magnetized volumes and high field strengths (above 2 T) are required, where the implementation of permanent magnets is virtually impossible. Recent theoretical research suggests that

superconducting magnetic refrigerators could potentially outweigh the SC cooling requirement for capacities in excess of 100 kW [23]. Theoretically the field intensity can be modulated by varying the electric current, which is extremely desirable as the device design can be considerably simplified because of the lack of moving parts. However modulating the field in the coil for practical refrigeration cycle speeds (in the order of 1 Hz or faster) is unfeasible with superconducting systems because of the heating of the coil induced by the rate of change the current, and very difficult with conventional copper coils unless the field and volume requirements are relatively small. Thus for practical applications, even when using coils, relative motion is still the preferred method of creating a magnetic cycle. Given the bulk and complexity of the magnet systems, regenerators are moved and coils are stationary.

1.3.2 Regenerator

The regenerator is the heart of the Active Magnetic Regenerator cycle. It is responsible for performing the required magnetothermal and regenerative cycle and consists in a porous matrix of a magnetocaloric refrigerant coupled with a modulated magnetic field opportunely synchronized with an alternating heat transfer fluid. A well-known challenge [24] in the development of an AMR is finding an optimal matrix geometry that offers adequate heat transfer with acceptable thermal losses, viscous dissipation, eddy currents, and structural integrity to withstand magnetic forces. The pursuit of an optimal regenerator is an iterative process and device specific. For instance (Figure 1-11) application constraints can be cooling demand, temperature span, efficiency, cost, durability, while device constraints are the field characteristics (ie intensity, distribution), magnet geometry (physical size constraints), heat transfer fluid (chemical stability, viscous losses), or field modulation (forces and eddy currents). The performance can be tuned to fit the above constraints by choosing the overall shape (aspect ratio), matrix structure, and composition.

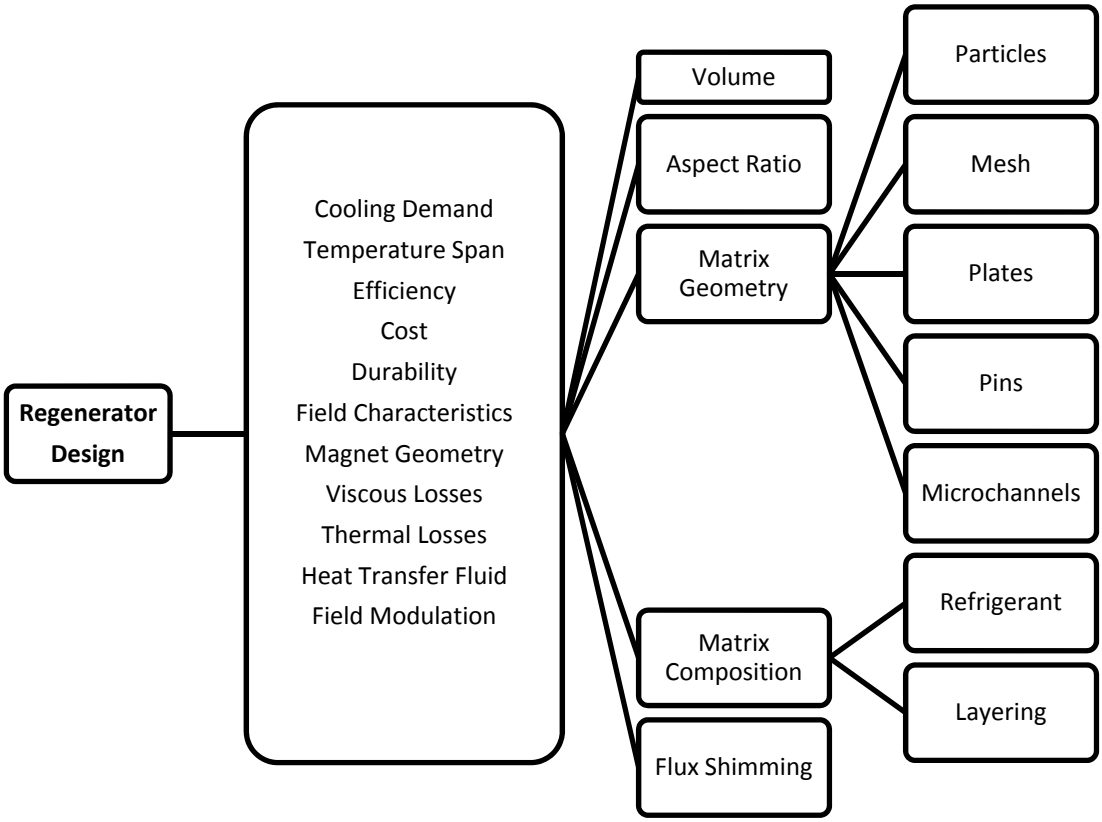

Figure 1-11. Design criteria for regenerators.

When designing a regenerator the most emphasis is on composition (including number and types of refrigerant) and matrix geometry. The porous internal structure has a pivotal role in the heat transfer effectiveness and low viscous losses, two competing factors. Figure 1-12 illustrates examples of common regenerator structures: spheres (generally with diameter of a fraction of mm), mesh, microchannel, pins, and parallel plates. Spheres and parallel plates represent the extreme opposite of the spectrum in terms of heat transfer and viscous losses. Another important factor is the matrix porosity, which is defined as the void space fraction of the regenerator volume. Increasing porosity reduces pressure drop, at the cost of increasing entrained fluid thermal mass, reducing refrigerant mass, and potentially increasing thermal leaks due to axial conduction/diffusion in the fluid phase.

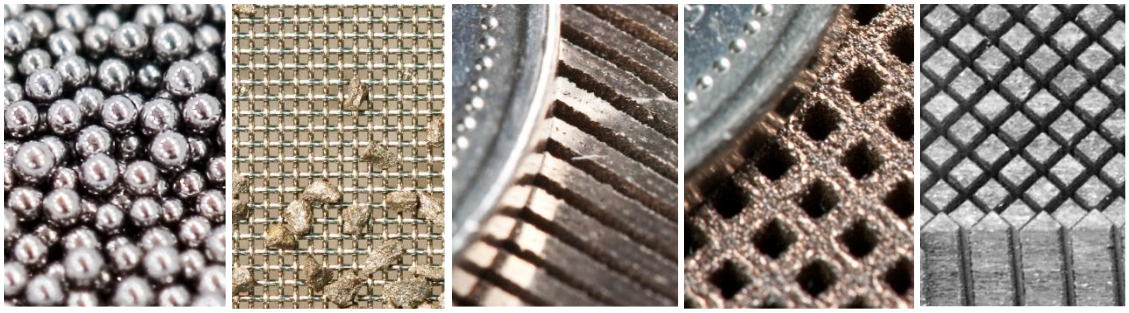

Figure 1-12. Common matrix geometries, from left to right: spheres, crushed particles on mesh, parallel plates, microchannels, and pins. Features in the pictures scale between 100 μm to 500 μm.

Another aspect that can greatly affect the regenerator performance is geometrical demagnetization [25]. Fields below 2 T and low aspect ratio regenerator macro and micro structure can negatively impact the effective magnetization. This can clearly be a performance issue when utilizing permanent magnets (small air gaps and relatively low fields). The use of high permeability passive materials, strategically placed adjacent to the AMR can help in locally enhancing the field, counteracting the demagnetization effect. This technique is known as “flux shimming” [26].

1.3.3 Heat Transfer System

The heat transfer system consists of the fluid vessels, heat exchangers, pumping and valving. The heat transfer system needs to ensure oscillating fluid flow in the matrix while it can be either alternating or unidirectional for the remaining circuit.

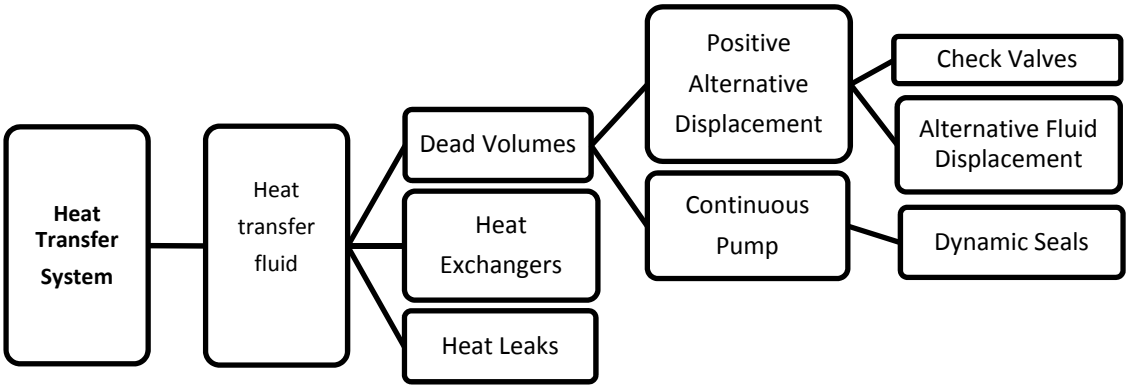

Figure 1-13. Design criteria for heat transfer fluid system.

Figure 1-13 illustrates common design choices for the heat transfer fluid system. Key parameters in the determination of design solutions are the heat transfer fluid of choice, complexity of the system, heat leaks, and dead volumes. The two main approaches are (more simplistic) an alternating displacer driving the fluid throughout the entire system, or (more complex) a pump associated with a distribution valve. The first choice is convenient because of its simplicity as no dynamic sealing is required (made exception of the piston seal). It also allows evaluating the flow rates directly from the displacer motion, and mechanically coupling the cycle operating frequency with the flow rate. Thus no flow meters and complex control system are required. On the downside the displacer seals might have larger friction losses. Also vibrations and noise may be induced by the inertial forces of the reciprocating mechanism. Additionally, oscillating flow is not ideal for heat transfer in the heat exchangers and dead volumes can severely limit the performance of the device. The reciprocating device built by Rowe produced good results in this configuration [13], however the choice of a low density heat transfer fluid like He has likely helped in minimizing losses due to dead volumes. If higher density fluid is a requirement, then the system can be improved introducing two sets of check valves at each end of the regenerators. This solution allows minimizing dead volumes by imposing unidirectional flow in the circuit, with the exception of the regenerators and displacer.

Alternatively, a conventional pump can be used for a continuous flow circulation while a distribution valve is responsible for alternating the flow in the regenerators. Such configuration is commonly used in the implementation of GM or pulse tube cryocoolers, where compressed helium is used both as heat transfer and working fluid. However if incompressible heat transfer fluid is chosen, accumulators might be required to accommodate for pressure spikes. Risø's magnetic refrigerator elegantly circumvented the problem by allowing several of the 24 regenerators to be simultaneously in the active blow phase in either directions all the time, so that pressure spikes are never observed.

1.3.4 Device Configuration

Design configuration describes the field generator system and regenerators arrangement. Rowe [27] suggested using four parameters with a discrete regenerator structure (that is when multiple regenerators can be identified rather that a single structure achievable with regenerator matrices with no transversal flow, like parallel plates, microchannels etc). These are the number of regenerators *r*, the number of high field regions *b*, the number of regenerators filling each one high field region *d*, the number of regenerators that are magnetized by each of the high field regions divided by the total number of regenerators *a*. Figure 1-14 illustrates how the parameters are used to describe four examples of different design configurations. The dashed lines represent the high field regions, the grey rectangles the regenerators, the crossed white boxes the magnets, and the arrows the relative regenerator-magnet motion.

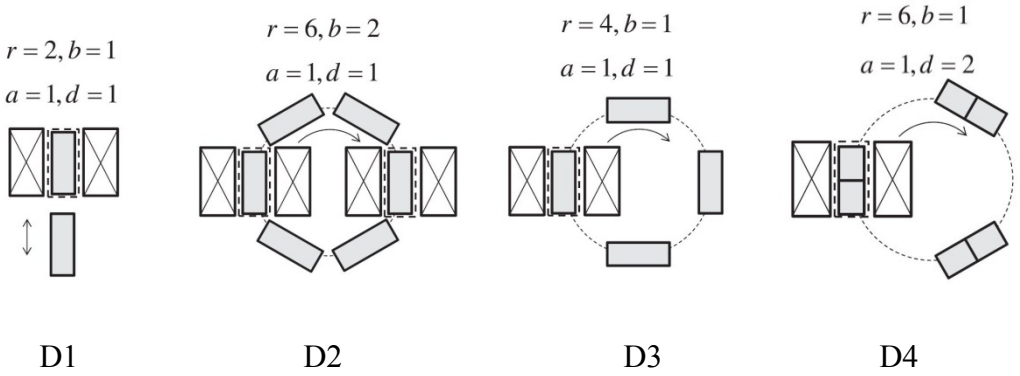

Figure 1-14. Four device schematics and their configurations [27].

The first device (D1) is a classic reciprocating arragement with two regenerators alternatively entering the single high field region. This is one of the simplest lab test apparatuses concepts frequently adopted. All the other devices represented are of rotating type. The second device illustrates a system based on six regenerator and two high field regions, the third uses one high field with four regenerators, and the last one one high field also but with six regenerators and two simultaneousy in each high field region. We will see that the devices descriptors *r, b, d* a have a role in the performance metrics as defined in the following section.

1.4 Performance Metrics

The ultimate objective of the research on MR is device commercialization. While proof of concept devices have been built and characterized, performance targets need to be set to meet the market demand. As much as this might boil down to capital and operating cost of the devices, performance metrics needs to be in place to compare different device configurations and what influences each configuration to meet the performance targets. Rowe proposed a number of performance metrics, which included the previously defined device descriptors, with the objective of correlating the device design parameters to performance and cost of cooling [27].

Following is listed a set of equations defining performance metrics currently used by the scientific community. The *exergetic cooling power*,

$$Ex_Q = Q_C\left(\frac{T_H}{T_C} - 1\right) \tag{1.2}$$

where Q_C is the cooling rate obtained between the environment temperature T_H and the cold reservoir temperature T_C. While the *exergetic efficiency* is defined as:

$$\eta = \frac{Ex_Q}{W} = COP\left(\frac{T_H}{T_C} - 1\right) \tag{1.3}$$

with W as work input and COP coefficient of performance. Since the performance of a magnetic refrigerator depends on the field intensity and amount of refrigerant used, a useful parameter normalizing these factors is the *specific exergetic cooling power*,

$$\mu = \frac{Ex_Q}{B_0 V_{MCM}} \tag{1.4}$$

where B_0 is the applied field and V_{MCM} is the total refrigerant volume.

Field generator performance is associated with intensity B_0 in the high field region, volume V_B of the high field region, and volume V_{mag} of the field generator itself. It is desirable to maximize B_0 and V_B, while minimizing V_{mag}, thus:

$$\Lambda = \frac{B_0 V_B}{V_{mag}}. \tag{1.5}$$

Cost for unit of useful cooling can be expressed in terms of the operational and design performance characteristics described by the defined metrics. For instance, the cost rate can be expressed as:

$$c_Q = CRF\left(c_{mag} \frac{V_{mag}}{Ex_Q} + c_{MCM} \frac{V_{MCM}}{Ex_Q} \right) + \frac{c_e}{\eta} \tag{1.6}$$

where CRF is the capital recovery factor, c_{mag} is cost of magnet for unit volume, c_{MCM} is the cost of the refrigerant per unit volume and c_e is the electricity cost ($/kWh). This expression represents the sum of the capital and operating cost rate, where the capital cost has been reduced to the cost by volume of the magnet and refrigerant while the operating cost is merely the electric power consumed. If capital cost is expressed by Z and $z = Z/Ex_Q$, by using Equation 1.4 and Equation 1.5 we have

$$z = \left(\frac{c_{mag}}{\Lambda} \frac{V_B}{V_{MCM}} + \frac{c_{MCM}}{B_0} \right) \frac{1}{\mu}. \tag{1.7}$$

By defining a *device configuration descriptor D* as

$$D = \frac{r}{bd} \tag{1.8}$$

we can express Equation 1.7 in its final form:

$$z = \left(\frac{c_{mag}}{\omega \Lambda D} + \frac{c_{MCM}}{B_0} \right) \frac{1}{\mu}, \tag{1.9}$$

where ω accounts for space inside the high field region not filled by refrigerant. This expression illustrates clearly the impact on cost of design parameters. The preferred configuration is difficult to determine because Λ, D, B_0, μ are inter-related.

Another performance metric has been introduced by Bjørk [28], the magnet figure of merit Λ_{cool}. It can be treated, to some extent, as a refined definition of Λ as presented in Equation 1.5, being a measure of how efficiently the field generator is used:

$$\Lambda_{cool} = \left(H_{\max}^{2/3} - H_{\min}^{2/3} \right) \frac{V_{field}}{V_{mag}} P_{field} \tag{1.10}$$

where V_{field} is the volume with the high field and V_{mag} is the volume of the magnet itself and P_{field} is the portion of the total cycle period that the magnet is actively used. Compared to the definition Λ in Equation 1.5, Λ_{cool} adds emphasis to the non-linear relation *MCE-H*. With the introduction of the P_{field} factor, the figure of merit now accounts for the efficient use of the magnet not only spatially, but also temporally. The point made here is that, if the magnet is the largest investment in the device, it should be exploited constantly to maximize its potential. Typically configurations designed around magnet-magnet motion for field modulation, rather than magnet-regenerator motion, are the most penalized by Λ_{cool} as defined, because their field is needed for generating *both* high and low field regions. The type of application and cost/performance constraints might dictate which is the preferred solution.

1.5 Problem Description

Since the late ‘80s a number of devices have been developed and tested in various laboratories around the world. These machines explored a broad range of operating

conditions and design configurations. Figure 1-15 summarizes published temperature spans and cooling powers. Additional details of each of the devices are tabulated in Appendix I. Nevertheless, it is still unclear if magnetic refrigeration technology can become commercially viable.

Although proof of concept has been demonstrated, devices have struggled in developing useful temperature spans unless very intense fields are applied (> 2 T). Indeed when using permanent magnets with fields confined below 2 T for practical refrigeration applications, maximum reported temperature spans are under 40 °C.

Large cooling powers have been only obtained for relatively low temperature spans (in the range of 10-15 °C), suggesting that possibly air conditioning and heat pumps could be suitable applications for these machines [29][30]. Generally, devices reported a nearly linear and strong dependency of temperature span to thermal load [13] when single material AMRs are used. If multi-material layering (which consists of varying the regenerator composition along its length) is implemented, cooling load sensitivity within the design operating range can be reduced significantly; however the performance degrades faster if the device is forced to operate beyond such a regime [17].

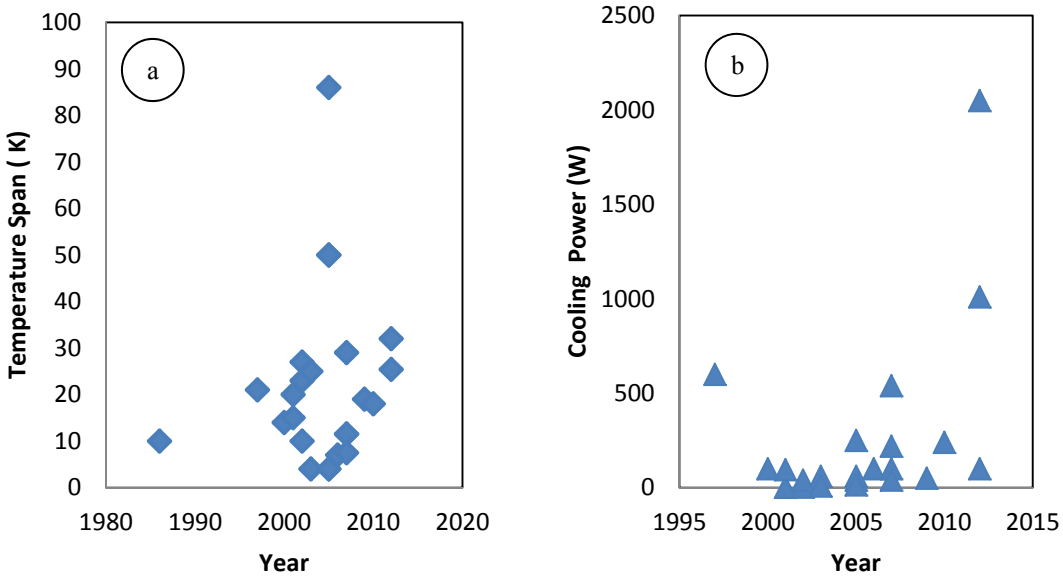

Figure 1-15. a) Temperature span and **b)** cooling power for published MRs to date.

AMR cycles can be very efficient. Magnetocaloric materials can be magnetized and demagnetized with virtually no entropy generation. It has been shown that, theoretically, an AMR cycle could approach the efficiency of the Carnot cycle [41] [42]. Nevertheless current lab devices have shown poor efficiency, largely due to viscous losses, thermal leaks, ineffective hydraulic design, eddy currents, and large magnetic forces to overcome during regenerator magnetization/demagnetization (Appendix I and II). The better devices reported COPs between 0.5 and 3 for relatively low temperature spans (10 – 15 °C).

Possibly the biggest challenge in MR, and the true objective for all researchers in this area is to determine the conditions required to create competitive AMR devices. This includes design characteristics, operating parameters, regenerator structure and, most importantly, the magnetocaloric properties. This is a multidisciplinary challenge, where magnetism, thermodynamics, structural mechanics, fluid dynamics, and heat transfer meet. Researchers are developing models using a variety of approaches [7] in an attempt to understand the fundamentals of AMR cycles. Such models require validation and this is where experimentation is valuable. To generate useful data, experimental devices need to allow for easy manipulation of functional parameters and facilitate the use of different regenerator structures and compositions.

Modeling has given the scientists tools to understand the physics of AMR cycles and experimental apparatuses have helped in validating models. However, many questions remain as to what implications AMR physics have on device design. High level questions such as:

1. What is required for a commercially viable device?
2. How good do refrigerant properties need to be?
3. How sensitive is cost to device configuration? and,
4. What efficiency can be realized?

Only a few investigations have directly addressed these questions, attempting to quantify the effective potential of MR. The most relevant published work is the minimizing of the cost of a magnetic refrigerator by Bjørk and al. [29]. Using an

advanced numerical model to predict AMR performance, and using Λ_{cool} as fundamental parameter for magnet cost minimization, Bjørk estimated theoretical cost of magnet and refrigerant for a system operating with a temperature span of 20 °C and a load of 100 W.

1.6 Objectives

Magnetic refrigeration is an attractive technology because of its intrinsic efficiency and the use of solid state refrigerants that can be benign to the environment. While the technology has been proven feasible, the question of market potential is unanswered. This is a complex problem. Nevertheless, even a simplified assessment would help to identify the main challenges to development, upon which further details and complexity can be built.

The objective of this thesis is to determine potential costs and efficiencies of a permanent magnet based AMR refrigerator. This objective will be addressed by the following activities:

1. create a test apparatus to experimentally quantify AMR performance,
2. develop a validated performance model of an AMR refrigerator; and,
3. create a cost-minimization design tool to determine optimal structures, designs, and operating parameters.

Together, these goals combine to create a framework for device development. Results will indicate what characteristics and material properties may be needed to achieve performance targets. In doing so, areas where further research is needed can be identified.

Given the large parameter space to be explored both in terms of device operability and AMR composition and matrix structure, experimentation can be extremely time consuming and expensive, yet necessary. The first goal is then developing a novel device specifically designed to be able to replace and characterize AMRs over a useful range of operating conditions effectively in terms of time and cost. No published prototype seemed to be designed for explicitly addressing such objectives.

Characterization of the refrigerator is done with a given regenerator composition and matrix geometry. The results can be used as benchmark for comparing the performance to

other AMRs to be tested. The regenerator of choice is a packed bed of small gadolinium spheres. The scientific community is moving toward using such regenerators as the standard test because of the well characterized MCE of Gd and its good mechanical and chemical stability. Additionally, a bed of packed spheres is a convenient matrix solution because of good heat transfer and ease of manufacture (in the specified composition) and implementation.

An efficient mathematical model capable of capturing performance of the device is to be developed and validated against the experimental data. The objective is an analytical method that can evaluate the cooling capacity for a given temperature span orders of magnitude faster than a numerical method. The aim is to be able to estimate hundreds or thousands of optimized solutions sweeping a number of design variables, such as cooling demand or MCE. This way is possible to observe the performance sensitivity in respect to key parameters, helping in understanding the critical performance factors to be tackled. The model does not need to use AMR real properties, but rather idealized properties so that it can help in quantifying goals in material research. The method differentiates from any of the work so far published because it is designed to minimize the contributions of both capital and operating cost of the refrigerator, based on the amount of refrigerant and permanent magnet, and power consumption.

1.7 Dissertation Organization

This document is structured in manuscript format, meaning that the articles included in the appendices detail the research work, while the thesis serves as a framework, providing background and motivation, research strategy, and a summary of the results.

Background and motivation, leading to the research objective are presented in Chapter 1, while Chapter 2 presents the basic principles of magnetic refrigeration and active magnetic regenerators. Chapter 3 and 4 describe the research strategy, from the objectives of the MR prototype and how these lead to the design choice, to the optimization objectives and how the theory and the experimentation can be leveraged to develop an effective model. Chapter 5 is a summary of the findings and Chapter 6 outlines conclusions, recommendations, and areas for future work.

1.8 Summary

This Chapter presented background on magnetic refrigeration and motivation for the thesis. While an attractive technology, current AMR prototypes are far from matching cost and performance of conventional refrigeration devices. The Chapter closes by raising the question of what is the potential for commercialization. The next Chapter introduces the basic theory of magnetic refrigeration and the active magnetic regenerator cycle.

Chapter 2

Magnetic Refrigeration Theory

2.1 The Magnetocaloric Effect

Magnetic refrigeration exploits a property displayed by certain magnetic materials: the magnetocaloric effect (MCE). In these materials, a significant change in entropy can be effected by the application or removal of a magnetic field, H. For materials with a simple magnetic work mode, the MCE depends only on the absolute temperature of the material, T and the magnetic field change, ΔH (which expresses the difference H_f-H_i) [32]. The MCE can be interpreted as the isothermal entropy change or adiabatic temperature change as it is defined in the following expressions:

$$\Delta s_M(T,H_f,H_i) = s(T,H_f) - s(T,H_i) \quad \textbf{(2.1)}$$

$$\Delta T_{ad}(s,H_f,H_i) = T(s,H_f) - T(s,H_i)\ . \quad \textbf{(2.2)}$$

Equations and 2.1 and 2.2 are graphically illustrated in Figure 2-1, where the vertical

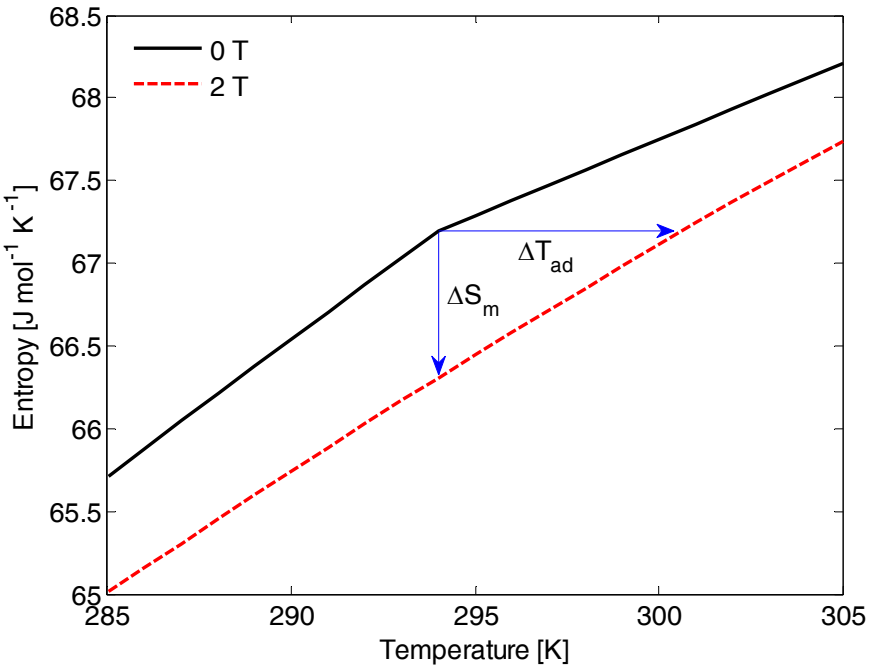

Figure 2-1. Graphical representation of the MCE [33].

axis is the isothermal entropy change and the horizontal line is the isentropic (adiabatic) temperature change. Both transformations occur between the same *S(T,H)* curves. Figure 2-1 illustrates ΔS_M and ΔT_{ad} for a range of temperatures in the proximity of the Curie temperature, T_{Curie} for $\Delta H = H_f - H_i$. Also a correlation between the MCE and magnetization can be derived. By varying the magnetic field, work is performed and the internal energy of the system changes. Thus, a differential variation in internal energy can be accomplished by a magnetic work interaction given by the product of the applied magnetic field, *H*, and the variation in magnetization, *M* [1]:

$$\delta w_m = \mu_0 H dM \tag{2.3}$$

Since for a material that has a simple magnetic work mode, $s = s(T,H)$, a differential change in entropy can be written as:

$$ds = \left(\frac{\partial s}{\partial T}\right)_H dT + \left(\frac{\partial s}{\partial H}\right)_T dH \tag{2.4}$$

where *s* is the entropy per unit mass. Using the definition of heat capacity, the above can be rewritten as,

$$ds(T,H) = \frac{c_B(T,H)}{T} dT + \left(\frac{\partial s}{\partial H}\right)_T dH. \tag{2.5}$$

If an isentropic field change is produced, the temperature change is:

$$dT = -\frac{T}{c_B(T,H)}\left(\frac{\partial s}{\partial H}\right)_T dH \tag{2.6}$$

and using Maxwell's relations for the equivalence of the second derivatives

$$dT = -\frac{T}{c_B(T,H)}\left(\frac{\partial M(T,H)}{\partial T}\right)_H dH \tag{2.7}$$

where *M* is the mass specific magnetization of the material. From this simple explanation, one can deduce that a material with no significant work modes other than magnetic

should have a high ratio of magnetic entropy change to total entropy to produce a large adiabatic temperature change. The MCE for a change in magnetic field from 0 to H is related to Equation 2.7 by

$$MCE = -\int_0^H \frac{T}{c_H(T,H)}\left(\frac{\partial m(T,H)}{\partial T}\right)_H dH \ . \qquad \textbf{(2.8)}$$

Different research groups have placed more emphasis on adiabatic temperature change (mostly system developers) or isothermal entropy change (material developers). The two properties are competing in the sense that if we try to maximize one, this is often done at the expenses of the other. This is because of the inverse relationship with the heat capacity. Both properties are relevant as the temperature change is necessary to produce a useful temperature lift, while the entropy change delivers the cooling power. The optimal balance between these properties may be system and application dependent [34].

Although a broad range of materials with a significant MCE for a wide spectrum of temperatures are available, research on the development of new materials is still more active than research on AMR cycles. In general, a good refrigerant needs to feature a number of properties to perform satisfactorily in an AMR [4]:

a. An MCE as large as possible over a broad temperature range allows large cooling power and temperature span, with low sensitivity to heat rejection temperature.

b. Minimal magnetic and thermal hysteresis are needed for high efficiencies.

c. High specific heat improves power density.

d. High thermal conductivity improves regenerator effectiveness.

e. Large electrical resistance minimizes eddy currents.

f. Good mechanical properties simplify manufacturing process.

g. Low cost materials increase commercial viability.

h. Chemically stable.

Second order transition alloys (based on rare earth elements) are good candidates for magnetic refrigerant; however current material research is mostly focused on first order material composition because of the larger magnetic entropy change and lower costs.

2.2 AMR Theory

Given the small temperature change induced in most materials, a regenerative cycle is required for any practical application. An active magnetic regenerator is a simple and elegant concept that performs the regeneration and thermal cycle simultaneously. During operation a temperature gradient is established in the refrigerant matrix and each cross section performs its own local thermal cycle (Figure 2-2).

Like any refrigerator, an AMR operating at periodic steady-state produces a net flow of heat from a cold source to a hot sink. Although, the net heat transfer cycle occurs between reservoirs at T_C and T_H, the bulk of the working material does not have to interact with these reservoirs directly. This is conceptually similar to a cascade system of a large number of magnetic refrigerators.

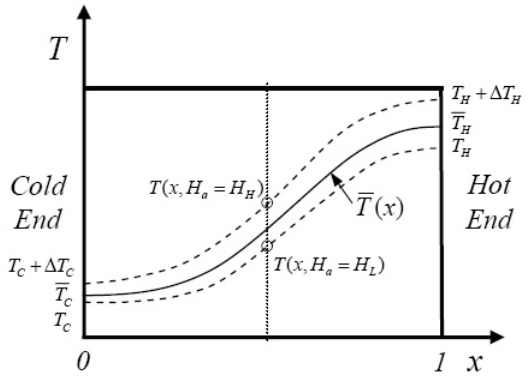

Figure 2-2. AMR temperature profile at periodic steady state [4].

Let's consider the systems shown schematically in Figure 2-3. The envelope of an AMR bed is shown with a dashed line while a section of infinitesimal thickness is drawn with a solid line. The bed is made up of a porous solid material that is the magnetic refrigerant and a fluid within the pores acts as the heat transfer medium. The fluid transfers heat between a cold heat exchanger, the refrigerant, and a hot heat exchanger.

The capacity rates of the fluid are shown as $\dot{\varphi}$ ($\dot{\varphi} = \dot{m}c_p$). Over a complete cycle, heat is absorbed at the cold end and rejected at the hot end.

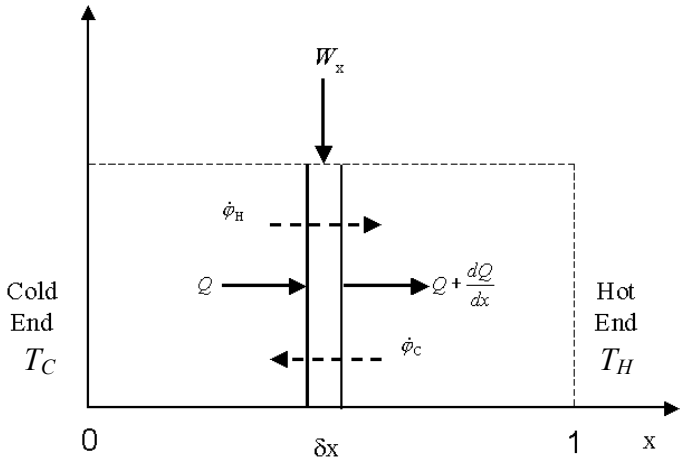

Figure 2-3. A schematic representation of an AMR showing the net work and heat flux at a differential section [4].

Most AMR devices built and tested to date have mimicked a reverse magnetic Brayton cycle in each section of the regenerator bed by using four distinct steps represented in Figure 2-4:

a. The regenerator is in a demagnetized state. Fluid flows through the regenerator entering the bed at a temperature T_H. As the fluid flows through the bed it exchanges heat with the solid refrigerant and exits the bed at T_C
b. The bed is exposed to a high magnetic field and the temperature of the refrigerant increases due to the magnetocaloric effect by $\Delta T(T)$
c. After absorbing a heat load and increasing its temperature by ΔT_C, the fluid enters the cold end of the regenerator, absorbs heat from the solid and exits the AMR at a temperature $T+\Delta T_H$
d. The AMR is demagnetized, the temperature decreases due to the magnetocaloric effect, and the cycle repeats

Figure 2-4 shows the assumed refrigerant cycle occurring in the differential section at some location in the AMR. The cycle as described above is equivalent to the process starting at point '*a*' and proceeding alphabetically to return to the starting point.

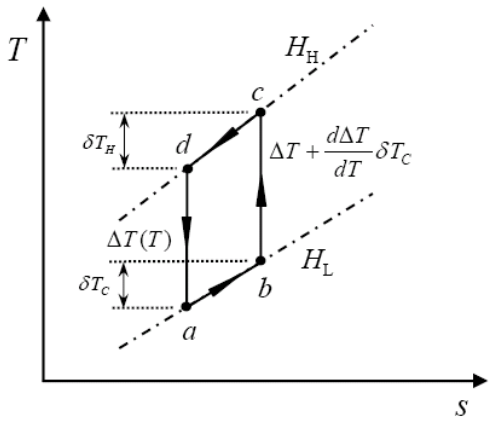

Figure 2-4. Hypothetical cycle for the magnetic refrigerant at some cross-section of the AMR [4].

It is assumed that the magnitude of the MCE for the process b-c is described by a first order Taylor series approximation in reference to point *a*. In the reversible case, the resulting area within the T-s diagram is equivalent to the magnetic work input per unit mass for a complete cycle.

Ideally, to create a reverse Brayton cycle the regenerator requires a stepwise waveform in the magnetic field application and heat transfer fluid blow across the solid matrix. Real devices only approximate such a cycle. In the most optimistic scenarios ramp up and down phases are required for both magnetic field and fluid velocities. Most devices based on relative motion, relying on a crank mechanism and constant drive rotational speed, are limited to a pseudo-sinusoidal waveform.

If the details of the AMR are ignored and one focuses on the absorption of heat by the fluid flowing through the cold reservoir, the cooling power can be determined from,

$$Q_C = \frac{1}{\tau_C}\oint \dot{m}_f c_p T_f(t)dt \qquad \textbf{(2.9)}$$

where $\dot{m}_f$ is the fluid mass flow rate as a function of time, c_p is the fluid heat capacity, and T_f is the fluid temperature at the exit of the AMR. For a complete cycle the integral can be written as,

$$Q_C = \frac{1}{\tau_C} m_d c_p \Delta T_f \tag{2.10}$$

where ΔT_f is the effective temperature change of the fluid as it flows through the cold heat exchanger, and m_d is the mass of fluid that flows through the AMR when it is demagnetized (or *displaced* fluid). If the regenerator has a very high number of thermal transfer units (*NTU*), the temperature of the fluid exiting the AMR will closely match the temperature of the solid refrigerant at the cold end. In addition, if the thermal mass of the refrigerant is much greater than the thermal capacity of the total fluid flux through the regenerator, the temperature of the solid will not change much. The ratio of the fluid thermal capacity to the regenerator thermal mass is called the utilization and is defined as,

$$\Phi = \frac{m_d c_p}{m_s c_H} \tag{2.11}$$

where m_s is the mass of refrigerant in the regenerator and c_H is the average heat capacity of the refrigerant. In the limit of very small utilization and large NTU, and assuming parasitic heat leaks are insignificant, the temperature change of the fluid as it absorbs heat through the cold heat exchanger is equal to the magnetocaloric effect of the refrigerant at the cold end of the regenerator, $\Delta T_f = \Delta T_C$. In terms of passive regenerators, Φ is sometimes referred to as the matrix capacity rate ratio and varies little throughout the regenerator for constant fluid heat capacity. For an AMR, the local utilization is a function of field and temperature and, in general, is position dependent.

If the AMR cycle is a reversible process no entropy is generated in the regenerator and therefore the same amount of entropy flows in and out. In addition, if the regenerator is assumed to behave as a cascade system of an infinite number of magnetic refrigerators, the following relation is true throughout the regenerator length [35]:

$$\dot{S}(x) = \frac{Q(x)}{T(x)} = const \tag{2.12}$$

where $\dot{S}$ and Q are the entropy and heat flow rate and T is the absolute temperature, all at the same axial location *x*. Furthermore, the boundary conditions at the hot and cold end are:

$$Q_c = \dot{m}_f c_p \Delta T_{ad_c} \tag{2.13}$$

$$Q_h = \dot{m}_f C_p \, \Delta T_{ad_h}. \tag{2.14}$$

Thus, using Equations 2.13 and 2.14 with 2.12 we obtain

$$\frac{\Delta T_{ad_c}}{T_c} = \frac{\Delta T_{ad_h}}{T_h}. \tag{2.15}$$

The above expression suggests that the magnetocaloric effect must scale with temperature according to the following relation:

$$\Delta T_{ad}^{ideal}(T) = \Delta T_{ref} \frac{T}{T_{ref}} \tag{2.16}$$

where ΔT_{ad}^{ideal} is the ideal MCE at temperature T, ΔT_{ref} is the MCE at a reference temperature, $T_{ref.}$ Equation 2.16 states the ideal magnetocaloric effect should be a linearly increasing function of temperature. Additionally, since the temperature is expressed in Kelvin, for near room temperature application the MCE at the cold end should be at the most 15% less than at the hot end, implying that the slope is small and in first approximation the ideal MCE could be assumed constant (assuming $T_H \approx 300$ K and $T_C \approx 260$ K).

By layering the AMR with magnetic refrigerants that have increasing Curie temperatures, it may be possible to more closely match the ideal MCE at different locations in the AMR. An example of this concept is shown in Figure 2-5. Although it has been proven that layering is possible, its implementation needs to be closely tailored to the specific application [13].

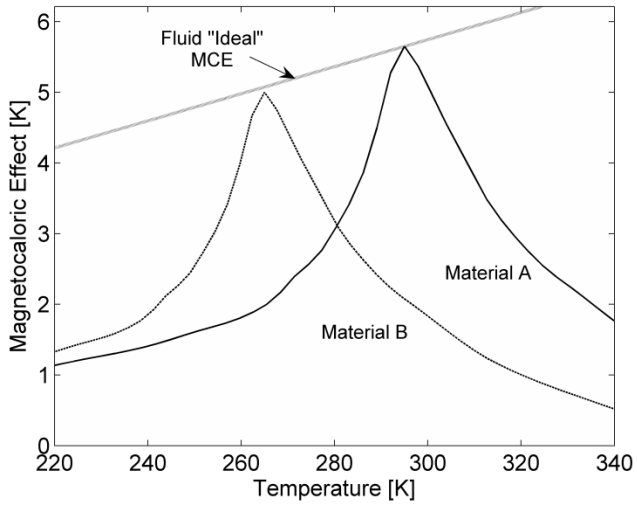

Figure 2-5. The ideal MCE as compared to gadolinium with a 0-2 T field change (Material A), and another material with a Curie temperature near 265 K (Material B)[13].

Governing equations for an AMR system have been developed throughout the years with the objective of analytically or numerically describe its thermo-magnetic state at a specific time and for a given set of boundary conditions. They consist of a system of two equations, one for the fluid and the other for the solid matrix. These equations are derived from the energy balance expressions for each phase. Since they are coupled, they must be solved simultaneously.

The energy balance for a heat transfer fluid flowing through a regenerator can be summarized by the following [36]:

$$\rho_f C_p A_f \frac{\partial T_f}{\partial t} = -\dot{m}_f C_p \frac{\partial T_f}{\partial x} + \frac{\partial}{\partial x}\left(k_f A_f \frac{\partial T_f}{\partial x} \right) + hP_w \left(T_s - T_f \right) + \left| \frac{\partial p}{\partial x} \frac{\dot{m}}{\rho_f} \right| \qquad \textbf{(2.17)}$$

where ρ_f is the density, A_f is the area of fluid flow, k_f is the thermal conductivity, h is the convection heat transfer coefficient, P_w is the wetted perimeter, or cross-sectional contact area between the fluid and the regenerator matrix, and p is the fluid pressure. All parameters with the subscript f refer to the fluid. The viscous losses are a function of the pressure drop $\frac{\partial p}{\partial x}$, which strongly depends on the operating frequency. Pressure drop

decreases AMR efficiency, thus, much work is focused on its minimization through the choice of heat transfer fluid, regenerator matrix, and AMR aspect ratio.

Similarly the energy balance for the solid matrix can be expressed as follows:

$$\rho_S A_S \left(\frac{\partial u_S}{\partial t} - B \frac{\partial m}{\partial t} \right) = \frac{\partial}{\partial x} \left(k_S A_S \frac{\partial T_S}{\partial x} \right) + h P_W \left(T_f - T_S \right) \tag{2.18}$$

where the magnetic work term has been grouped on the left side with the internal energy term. Both the fluid and matrix expressions assume uniform properties in the radial direction and adiabatic walls. In Equation 2.18 the viscous dissipation term is not present, however there is an additional magnetic work term. Equations 2.17 and 2.18 can be expressed as:

$$\kappa \frac{\partial T_f}{\partial t^*} = -\Phi \frac{\partial T_f}{\partial x^*} + \frac{\partial}{\partial x^*} \left(\frac{\varphi}{Pe_f} \frac{\partial T_s}{\partial x^*} \right) + NTU \Phi \left(T_s - T_f \right) \tag{2.19}$$

and

$$\kappa \frac{\partial T_s}{\partial t^*} = \psi \frac{\partial}{\partial x^*} \left(\frac{1}{\mathrm{K}s} \frac{\partial T_s}{\partial x^*} \right) + NTU \Phi \left(T_s - T_f \right) + \frac{\dot{Q}_{in} \tau}{m_s c_s} \tag{2.20}$$

where the following non-dimensional parameters have been introduced:

$$\Phi = \frac{\dot{m}_f c_p \tau}{m_s c_B} \tag{2.21}$$

$$NTU = \frac{h A_w}{\dot{m}_f c_p} \tag{2.22}$$

$$\kappa = \frac{m_f c_p}{m_s c_B} \tag{2.23}$$

$$Pe_f = \frac{\dot{m} c_f L}{k_{eff} A_f} \tag{2.24}$$

$$\psi = \frac{c_{s,ref}}{c_s} \tag{2.25}$$

$$\mathrm{K}s = \frac{m_s c_{s,ref} L}{k_s A_s \tau} \tag{2.26}$$

$$t^* = \frac{t}{\tau}; \quad x^* = \frac{x}{L} \tag{2.27}$$

where A_w is the wetted area, m_f the mass of the gas within the regenerator pores, L the length of the regenerator, and k_{eff} is the effective thermal conductivity of the regenerator and fluid, taking into account dispersion effects, $c_{s,ref}$ are solid reference heat capacity.

The non-dimensional governing equations define key parameters determining the temperature distribution for fluid and solid throughout an AMR. Two important parameters are utilization (Equation 2.21) and NTU (Equation 2.22). In practice, adjusting utilization will change the cooling power, temperature span, and efficiency of an AMR cycle. A value that is too high or too low can lead to poor performance. In a well-designed apparatus, the ability to vary and quantify utilization over a range of 0.2 to 1.5 is desirable. NTU is an indication of the thermal effectiveness of a regenerator, and large values of NTU are desired; unfortunately, NTU decreases as utilization increases. This can be compensated by the regenerator matrix structure, but often results in increased pressure drop. These issues are discussed further in later Chapters.

2.3 Summary

In this Chapter a brief introduction to magnetic refrigeration theory is given. It was explained how the MCE can be used to produce thermal cycles, and how this can be incorporated into a regenerative cycle to create an AMR. The definition of an ideal MCE was given and shown how this differs from real refrigerant properties. The idea of layering refrigerants as a way to approximate ideal behavior was shown. Finally, the fluid and solid energy balance equations were given and governing non-dimensional parameters were defined. The next Chapter describes the development of the magnetic refrigerator starting from the design requirements and specifications.

Chapter 3

Permanent Magnet Magnetic Refrigerator (PMMR) Development

Chapter 1 summarized some of the most relevant refrigerators built in the past, giving an overview of the progression in the development of the technology and the current state of the art work. Appendix I reports, in tabulated form, most of the published work to date, while a detailed description of most devices can be found in published review articles [1][5][7]. This chapter describes a novel MR prototype, the technical specifications of the apparatus, and explains the experimental strategy implemented to generate performance data.

3.1 Background

The development of a reliable predictive model requires validation against experimental data. In theory, this can be done by utilizing existing published results; however, there is limited data available in the literature for AMR devices and most of it is for a limited range of operating conditions. Thus, an experimental device was designed and constructed.

A theoretical model is always an idealization of a real system, where simplifications are generally employed. In this regard, without an experimental system it is often challenging to judge which phenomena can be omitted, simplified or linearized. Additionally, experimental apparatuses can help in determining physical effects of importance that may have been overlooked by the theorist. Reconciliation of theoretical and experimental results using published data might be impossible or misleading. For instance if a model over-predicts the cooling power of the refrigerator, this deviation may be attributed either to model inaccuracy or measurement error and in any case it can depend on a number factors. Having access to a dedicated device simplifies the task of segregating the possible causes.

Another motivation for building a magnetic refrigerator is that the experiments can be tailored to match simulation objectives, rather than adapting the simulation to existing data. Also, experimental results can map out the refrigerator characteristics as needed (i.e.

data point resolution per parameter sweep), not to mention that the physical quantities can also be probed to best suit the model boundary conditions and output.

The most relevant reason for developing an in-house magnetic refrigerator is that it is desirable to have access to a system with specifications unmatched by any of the devices published to date. Devices currently fall under two main categories. One is what would be best defined as "strictly lab testing apparatuses", with no presumption of operating as magnetic refrigerators, but designed with the specific purpose of testing the performance of materials and magnetocaloric cycles. These are generally flexible devices, capable of easily replacing the regenerators and components, with easy access to measurable quantities. While very useful for characterizing the refrigerant performance, they are of little help in suggesting what a real device performance and cost can realistically be. The other category of devices is "MR prototypes". This is a relatively new category, with the exception of the second generation MR by Astronautics Corporation. These machines can lack the flexibility and modularity needed for examining a vast parameter space, while monitoring critical data can become cumbersome and, at times, impossible. Modifying these machines for different testing configurations can be expensive and time consuming.

3.2 Magnetic Refrigerator Apparatus Objectives

A number of desirable characteristics for a test apparatus have been described in previous sections. These will be discussed here in more detail in addition to other features of importance. These requirements are largely based on information gathered from the literature as well as experience with another experimental apparatus, the Superconducting Magnet Test Apparatus [4][13], often referred as "AMR Test Apparatus" or "AMRTA".

An important design feature is the use of a configuration that can be easily characterized by an analytical expression; for example, the magnetic field strength as a function of magnet size. The use of analytic expressions can assist the optimization algorithm in terms efficiency, reliability, and simplicity.

Accessibility and modularity of the AMRs is another important criterion. It was learned from previous experience that a significant amount of experimental downtime can occur

due to AMR inspection and replacement. With the AMRTA this can take days, while it is desirable to perform such routine operations within minutes.

A practical goal is for a device to be capable of high power densities. This is necessary in order to operate as a “prototype” and not only as a “lab testing apparatus”. The idea is to develop a relatively compact device operating at high frequency (5-10 Hz). Maximizing the operating frequency might not be the optimal operating regime but it is one way to reduce costs and is therefore of interest to be able to experimentally determine sensitivities to high frequency.

High power density leads to reduced device size and amount of refrigerant. Many refrigerant alloys or composites are costly and difficult to manufacture when not mass produced. If an objective is to test a range of compositions and configurations, the cost can become prohibitive if large volumes are needed. Additionally the device itself can be both financially and technologically more manageable if downscaled. Yet the system needs to generate sufficient cooling power at non-zero temperature spans to overcome the effect of parasitic losses, reduced efficiency, and measurement error.

An attractive feature in an experimental system is one designed for versatility and modularity. If it is desirable to explore a different range, or even test a functionally different component (i.e. replacing an alternating positive displacement device with a centrifugal pump), it is convenient to have a modular device which is easily modified. In addition, modularity can help a system evolve with time, starting with a simple and reliable solution, and gradually moving toward more complex and refined concepts. This is not just useful in terms of added flexibility by expanding operability, it can truly be a life saver if some design choices were inadequate to start with, which is not uncommon when prototyping.

3.3 MR Design Specifications

The design process starts with establishing specifications so as to meet a target performance. Cooling power comparable to a small appliance is desirable for a number of reasons: (1) it can provide a direct comparison to current technology, (2) performance can be easily measured with readily available laboratory instruments, and (3) minimize the

cost of prototype refrigerant supply. It was decided that 200 W could be a good target to start with, as this is comparable to a medium sized household refrigerator. Because single magnetic refrigerants tend to produce useful cooling powers over small temperature spans, it was decided that the target cooling power should be at a temperature span in the range of 0 - 10 °C.

Once the cooling power, Q_c, has been decided, the next step is to choose the approximate maximum field intensity, and the mass of the refrigerant. For a compact and low power magnetic refrigerator, rare earth permanent magnets are currently the only viable solution for a field generator. This choice limits the maximum magnetic field intensity to approximately 1.5 T. As a first approximation, reducing the maximum field scales up the amount of refrigerant needed and device size. Once the maximum field intensity has been established, utilization and frequency are the other two fundamental operating parameters to be fixed.

Utilization is the thermal mass ratio between the fluid blown through the regenerator matrix in a period, and the thermal mass of the solid. Once the refrigerant mass is fixed, this parameter can only be varied by changing the amount of fluid mass per pulse. Intuitively this has an impact on cooling power. Also, as utilization is increased, the thermal perturbation of the solid, induced by the fluid advection, increases. In general cooling power grows with utilization up to a point; if it is increased any further the induced temperature fluctuation becomes progressively more destructive reducing cooling power. Literature suggests that, depending on the conditions, utilization factor should be between 0.4 and 1.2 [37], however values larger than 1 might be difficult to attain because of the large viscous losses.

The main limitation we face with operating frequency is the pressure drop due to viscous effects. If water or a water glycol mixture is used as heat transfer fluid and crushed or spherical particles with characteristic length in the order of 300-500 μm constitute the regenerator matrix geometry, maximum operating frequency is likely limited to 3 to 4 Hz. Operating pressure should be kept below 1 MPa as most common hydraulic components are rated within this limit.

As maximum field (1 T), utilization range (0.4 -1.0) and maximum frequency (4 Hz) have finally been specified, it is now possible to estimate, by order of magnitude, the amount of refrigerant required for the desired cooling power. Model results reported by Li, P. et al. [37] show predicted cooling power for an AMR using spherical particles operating at 0.5 Hz. A variety of heat transfer fluids are examined including water and a water-glycol mixture.

Q_c evaluation, estimates by Li et al. are scaled as required to estimate the expected performance of the prototype device. Li predicts that at 0.5 Hz with a water-glycol heat transfer fluid and 1.8 kg of Gd, utilizations of 0.4 – 1 result in a cooling powers ranging from ~200 – 400 W with a 10 °C temperature span. Normalizing by the volume of refrigerant gives a cooling power of 0.87 – 1.7 W/cm^3.

If the prototype uses 25 cm^3 (approximately 200 g) of Gd alloy and operate at 3-5 Hz, applying the results of Li gives an estimated cooling power between 22 and 43 W at 0.5 Hz. Assuming linear scaling in frequency the cooling power at 4 Hz would range between 175 – 340 W with utilizations between 0.4 and 1. The model of Li does not account for parasitic heat leaks, eddy diffusivity effects in the regenerator, or the effects of entrained fluid mass in the pores of the regenerator matrix. These effects will all lead to lower performance. Such estimate can be cross-referenced with some of the results obtained with the AMRTA. Using thermal load tests applied to two 90 g of Gd regenerators for a total of 180 g, using a linear scaling and assuming 1.5 T, Φ ranging 0.4–1, and 4 Hz, the expected Q_c is 141-354 W (Figure 3-1). This result is remarkably close to the estimate based on the Li et al.

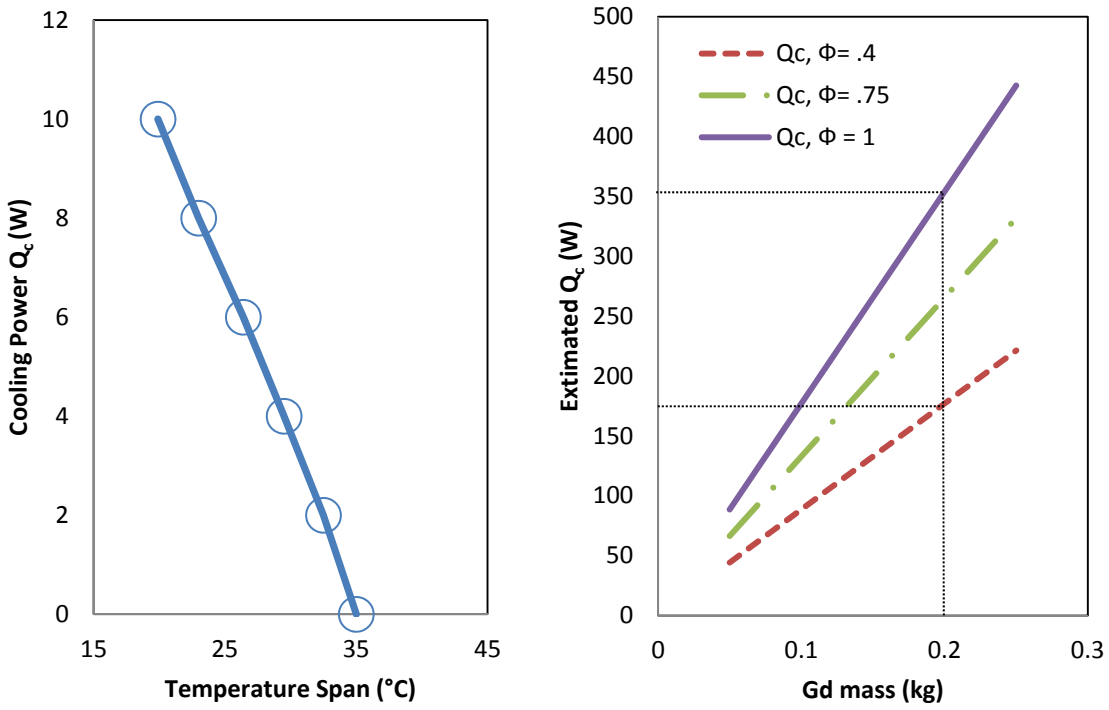

Figure 3-1. AMARTA cooling power sensitivity results (left) and cooling power predictions for PMMR (right).

3.4 MR Design Solution

This section describes the PMMR design choice and justifies it in merit of the objectives stated in 3.2.

The key components making up the test apparatus (PMMR) and the assembly are shown in Figure 3-2 and Figure 3-3. Two active magnetic regenerators (1) are connected by a fluid transfer loop (water) with oscillating flow driven by a fluid displacer (2). A cold heat exchanger (3) separates the two AMRs and two hot heat exchangers (4) reject heat from the system. The AMR beds are alternatively magnetized and demagnetized by nested Halbach cylinders (5), where an inside magnet rotates with respect to the outside one. The AMR cycles are synchronized such that they operate in opposite phases. An electric motor (6) drives both the inner magnets and the fluid displacer by means of a timing belt (7) and a crank mechanism (8). Additional components are present to instrument the apparatus and to facilitate filling, pressurizing, and draining the hydraulic

lines. AMR temperature spans are measured by the thermocouples T_{H1}, T_{C1}, T_{H2}, and T_{C2}. The hot heat exchangers are thermally sunk to a chiller external loop for heat rejection temperature control.

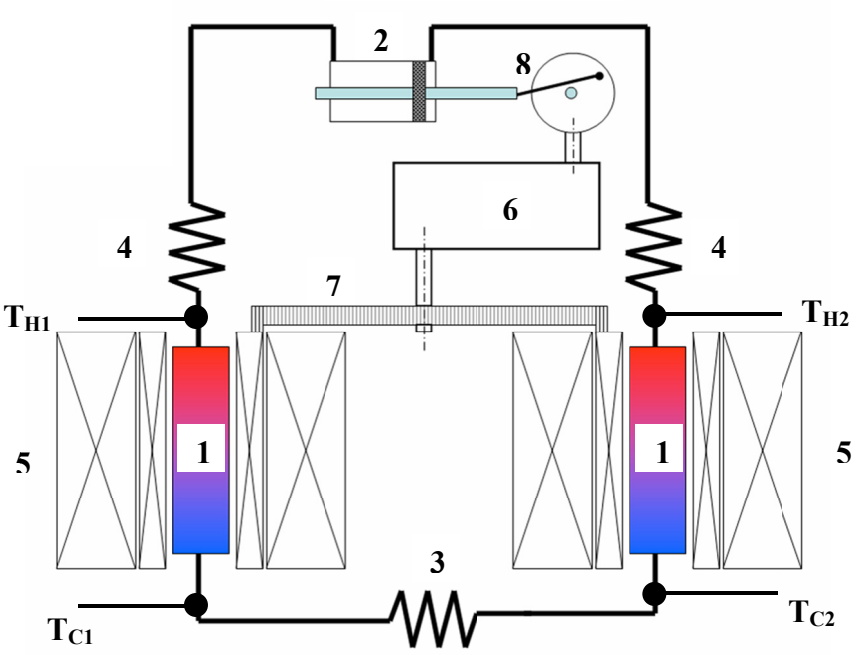

Figure 3-2. PMMR schematic.

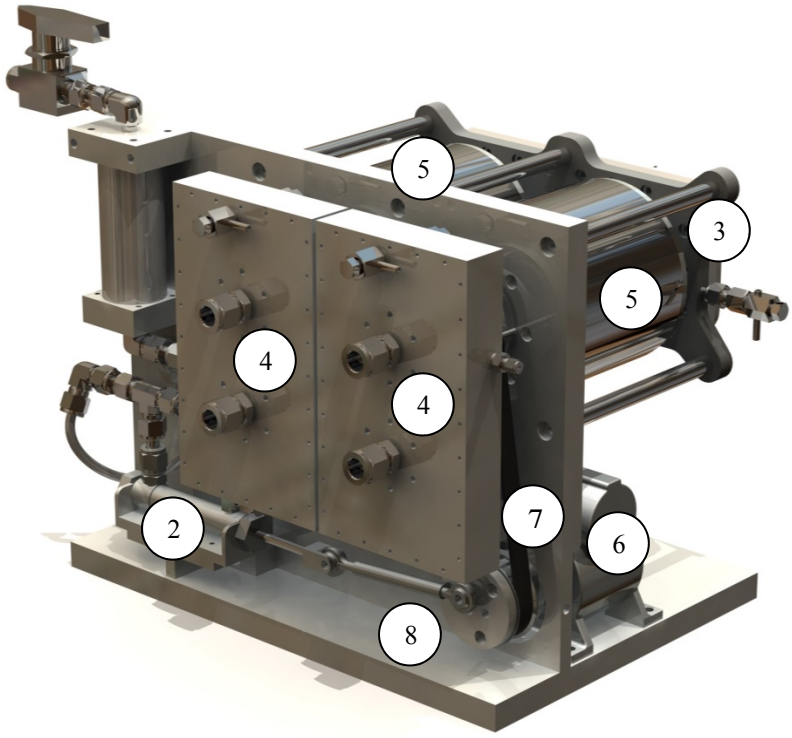

Figure 3-3. PMMR assembly.

3.4.1 Field generator

Halbach cylinders are cylindrical structures comprised of permanent magnets. The direction of polarization in the structure determinates the external magnetic field distribution. In ideal Halbach cylinders the magnetization direction is a continuous function of angular position, as described in polar coordinates by [38]:

$$M = M_r\left[\cos(k\phi)\hat{\rho} + \sin(p\phi)\hat{\phi}\right] \quad \textbf{(3.1)}$$

where $\hat{\phi}$ is the tangential direction, ϕ is angular position, $\hat{\rho}$ is the radial direction, p is a parameter determining the specific type of Halbach cylinder, and M_r is the magnetic remanence. Figure 3-4 illustrates cylinder magnetization for values of p between -3 and 2.

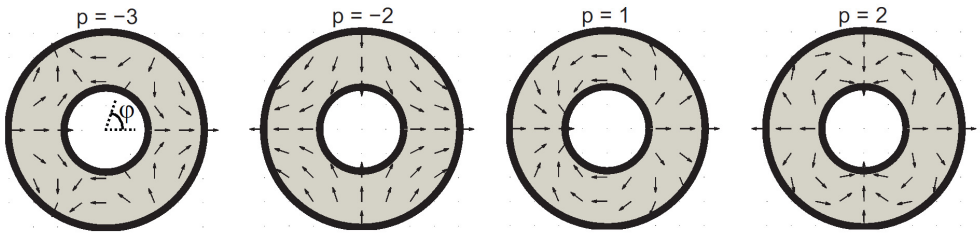

Figure 3-4. Halbach cylinder configuration for a number of *p* values [38]. Arrows represent the direction of the magnetic field.

Real Halbach cylinders require a discrete number of segments to be magnetized in a constant direction, therefore they only approximate the ideal case. The finer the segmentation the closer to ideal it becomes. If the configuration with $p = 1$ is chosen, the field is entirely confined within the outer diameter, and it has relatively uniform distribution in the bore, with a transversal orientation. The field intensity in the inner bore can be analytically predicted using the following correlation [39]:

$$H = M_r \ln \frac{D_o}{D_i}, \tag{3.2}$$

where H is the magnetic field D_o the outer diameter, and D_i the inner diameter. Although this relation is for ideal cylinders of infinite length, it predicts the field in real ones satisfactorily with the appropriate correction factors accounting for length and number of segments.

If two of such cylinders are nested within each other and they are designed so that they produce the same field intensity in the bore, they can be used for modulating the field in the inner-most bore by relative rotation (Figure 3-5) between zero (cancellation) and twice the intensity of each (addition). As the magnets are rotated to the respect to each other the field intensity in the bore varies and the magnetic waveform over a full rotation is close to a squared sine wave (Figure 3-6). For this specific case the field generated by the two cylinders does not match exactly, thus there is some residual field in the cancellation phase.

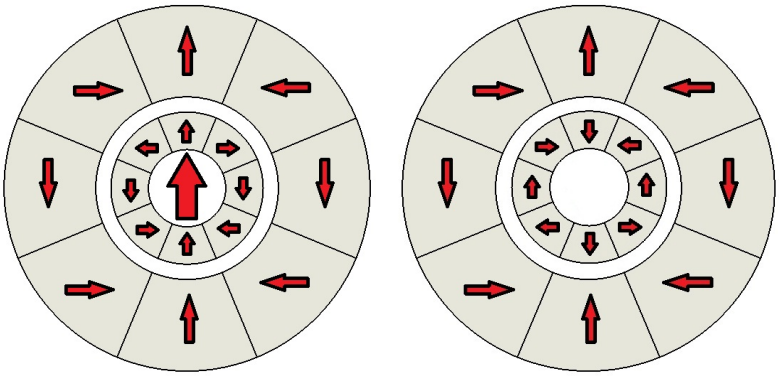

Figure 3-5. Nested Halbach cylinders in the high field (aligned) and zero field (counter-aligned) relative position. Arrows represent the direction of the magnetic field.

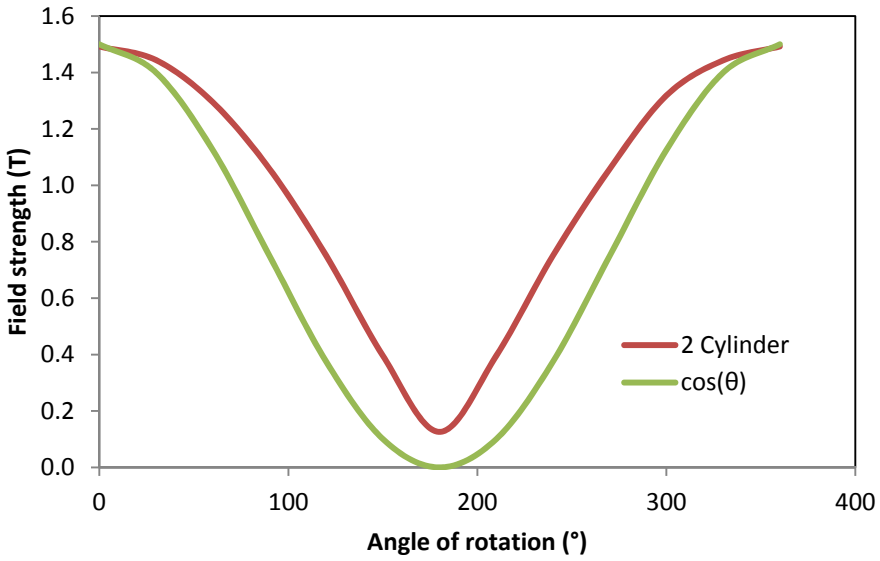

Figure 3-6. Field strength versus angle of rotation compared to a cosine wave.

Nested Halbach cylinders have been used in a number of applications, mostly as part of measurement instruments. For instance they are commonly used in the characterization of magnetocaloric materials for direct measurement of specific heat or adiabatic temperature change [40].

The magnetic waveform in Figure 3-6 is not ideal for magnetic refrigeration applications because it deviates considerably from a square or trapezoidal waveform. However nested Halbach cylinders are a very convenient configuration for the objectives summarized in 3.2. Indeed it is possible to modulate the field with simple mechanical

solutions up to relatively high frequencies. The inner bore is easily accessible, and the AMR replacement can be done simply and with minimal force as its insertion and extraction is orthogonal to the field. Also, the regenerators are stationary requiring only static seals. Other important features are the simple mathematical description of the field generator properties (length, inner and outer diameter), and the fact that field is almost entirely confined inside the magnets, with very moderate stray field at the top and bottom end of the cylinders. Additionally, nested Halbach cylinders might offer good magnetic forces cancellation contributing to cycle efficiency. Ideal nested cylinders of infinite length should require no magnetic torque when rotated, however real ones have end effects due to the stray field in these region. It has been shown that in first approximation the torque necessary for a full rotation is close to sinusoidal and its magnitude is proportional to D_o^3 [39]. If, as shown in Figure 3-6, two nested assemblies are used and operated in opposite phase, a good torque cancellation may be possible. It is worth noting that this is a novel field generator approach for magnetic refrigeration apparatuses, as no similar systems have been published to date.

A segmented Halbach cylinder has a bore field reduced with respect to an ideal cylinder. Halbach suggested that the H evaluated in Equation 3.2 should be reduced by the factor [38]

$$H_n = H(\infty)\frac{\sin(2\pi/n)}{2\pi/n}, \tag{3.3}$$

where H_n is the field intensity if an n-segment cylinder and H(∞) is given by Equation 3.2. The impact on the effective field is illustrated in Figure 3-7. Halbach cylinders of 8 segments were chosen for the MR because a satisfactory compromise between field (about 90% of ideal) and fabrication cost.

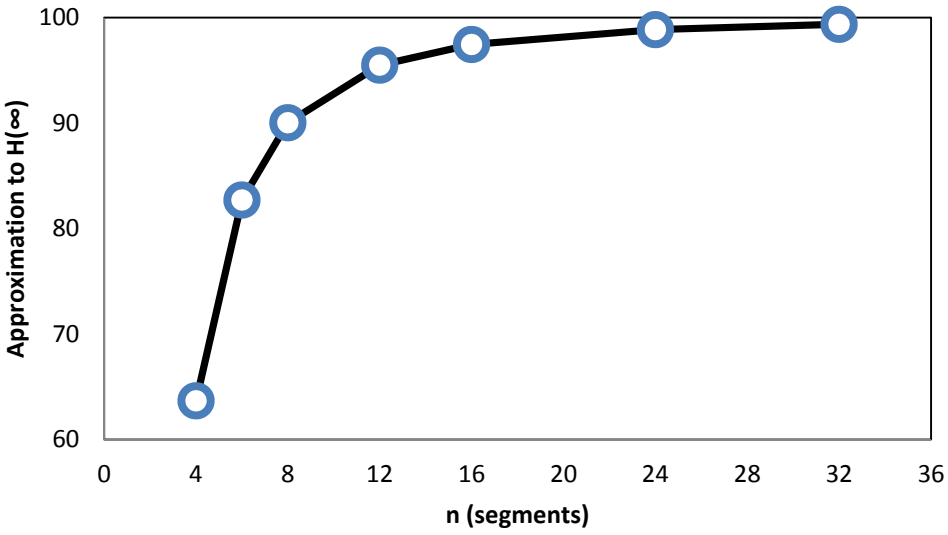

Figure 3-7. Approximation to ideal field intensity due to segmentation.

3.4.2 Regenerators and hydraulic system

A linear alternating fluid displacer mechanically coupled to the magnet drive was chosen to create fluid flow through the system (Figure 3-9). This solution, as explained in 1.3.3, is simple and effective, however it requires care in minimizing dead volumes between the regenerator and the heat exchangers. The initial design used alternating flow in the entire system, exactly the same as the AMRTA. However the small fluid displacement required due to the use of liquid rather than gaseous heat transfer fluid (~ 5 – 20 cm^3) suggested that unidirectional flow in the heat exchangers would noticeably improve their effectiveness. Integrated check valves were designed and added at the cold heat exchanger ends, while the hot-end heat exchangers were left as in the original design because they were already performing well with a good thermal connection to the temperature controlling chiller.

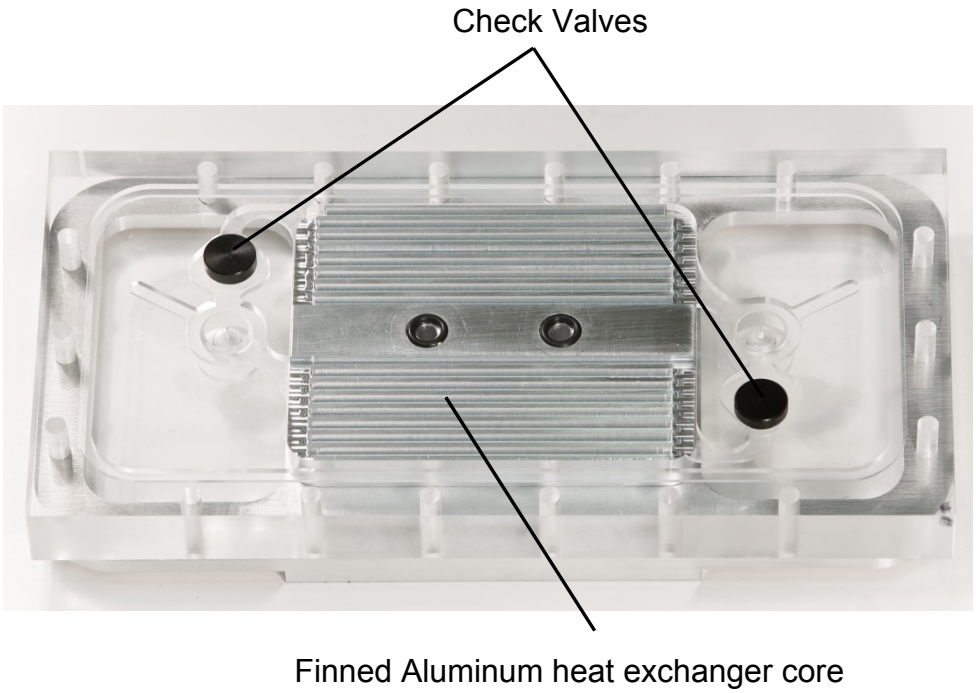

Figure 3-8. Cold heat exchanger assembly including the finned aluminum cold plate, check valves, and acrylic clear housing.

The fluid displacement assembly (Figure 3-9) is mechanically coupled to the drive motor. As operating the frequency is increased, flow rate increases while the volume of fluid pumped per cycle stays constant. Characterization of an active magnetic regenerator requires measuring performance with frequency and utilization mapped independently. If utilization needs to be varied, the crank arm length can be adjusted to provide for a different stroke. The choice of a pump and distribution valve might offer higher efficiency and less maintenance. It also permits varying utilization during operation, by simply adjusting the flow rate; however, it can lead to a more complex hydraulic and control system.

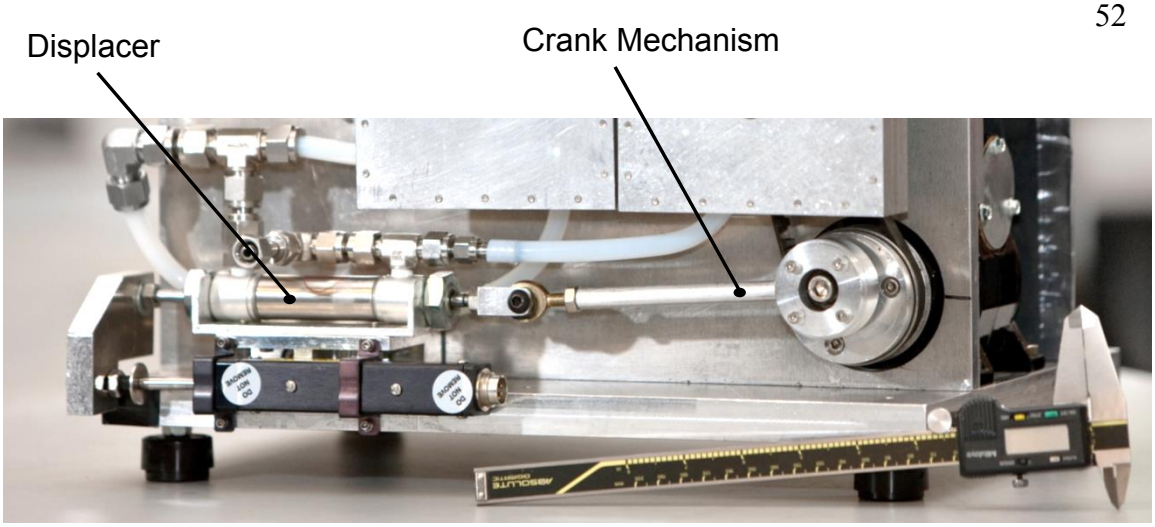

Figure 3-9. Hydraulic displacer and crank arm subassembly.

3.4.3 PMMR Design Summary

The exploded view of the prototype in Figure 3-10 shows the drive system details and the arrangement of the main components. The nested cylinders (1) are installed horizontally with the outer magnet (2) stationary and the inner one (3) rotating. Two G10 composite tube (4) housings the refrigerant run from end to end of the field generator assemblies bridging between the hot (5) and cold heat exchangers (6). The refrigerant (7) can be accessed by removing six screws securing the cold heat exchanger which can then be slid out with the two regenerator housings. The G10 tube is bonded onto a flange bolted and sealed against the cold heat exchanger back plate, while it is simply pushed inside the hot heat exchanger bore and sealed by a radial O-ring. Therefore, a small amount of force (to overcome seal friction) is required for both installation and extraction. The timing belt (8) drives the two inner magnets and the crank arm plate (9) by engaging the relative pulleys. Also the temperature measurements (10) are performed inside the heat exchangers in the proximity of the regenerator hot and cold outlet. This compact design is also convenient for limiting thermal leaks to the environment because of the material choice, small surfaces, and because the distance the fluid needs to travel between the heat exchangers and the AMRs is minimal. Simulations show thermal losses as low as 0.3 W/K. This means that if the device operates with a temperature span of 20 K a 5 W thermal leak is expected.

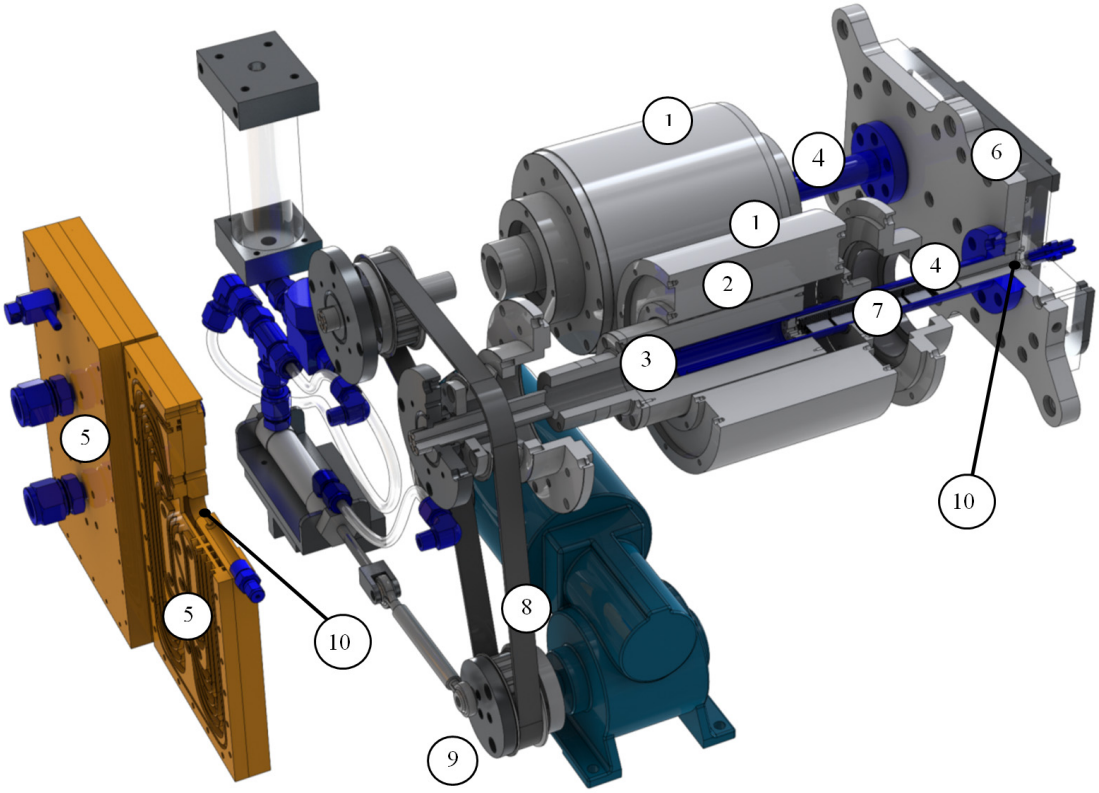

Figure 3-10. PMMR exploded view of the main components.

A summary of design specifications is given in Table 3-1. Further details on the design and testing of the device can be found in Appendix II.

Table 3-1: PMMR Specifications

Property	Range	Units
Magnetic field (average over regenerator volume)	0.1-1.4	T
Operating frequency	0-5	Hz
Heat transfer fluid	Water-glycol	
Available regenerator volume (each)	20	cm^3
Regenerator diameter	16	mm
Available regenerator length	110	mm
Motor output power	180	W

3.5 Experimentation Plan

Characterizing the refrigerator performance means measuring dependent variables such as temperature span, cooling power, and power input over a range of operating conditions. Given the large parameter space to explore, it is necessary to be selective as to which factors should be focused on.

Parameters that are fixed are the regenerator mass and composition. Based on the theory described in Chapter 2, two operating parameters of importance are utilization and frequency. Both variables affect performance and efficiency. Also, given the nature of the refrigerant and the variation in properties as a function of temperature, performance is mapped over a range of heat rejection temperatures.

As described in Chapter 2, AMR performance is strongly dependent on heat transfer properties because of the regenerative nature of the cycle [24]. The smaller the MCE the more effective the regenerator needs to be as the temperature gradient driving the heat transfer is reduced. While high effectiveness regenerators are not difficult to develop, devising geometry with low viscous losses is. Good heat transfer at high flow rates requires large contact area between the liquid and solid phases. The result is that effectiveness and pressure drop are competing characteristics. Most passive regenerators are conventionally used in conjunction with gases (i.e. Stirling, GM, thermoacoustic coolers), which cause modest viscous losses. In contrast a compact refrigerator for near room temperature application typically operates with liquids, such as a water-glycol mix. Spheres in the 300-600 μm range have a satisfactory heat transfer rate, however the pressure drop can be limiting the device flow rate and cooling power. On the opposite side of the spectrum is a parallel plate matrix configuration, which typically delivers a much reduced heat transfer, with the benefit of considerably lower viscous losses. It is conceivable that a matrix structure can be devised to deliver heat transfer performance close to small spheres with a pressure drop closer to a parallel plate configuration. Optimizing the regenerator matrix in terms of heat transfer and viscous losses is vital. Consequently, testing regenerators with different matrix geometries but constant composition and mass can provide valuable information.

Figure 3-11 shows the testing plan with the design parameters in the order of progression. The order is dictated by experimental logistics. For instance, once matrix geometry, utilization, frequency and heat rejection temperature are fixed, temperature span is evaluated for a range of heat loads. This operation is then repeated for each of heat rejection temperatures, and so for frequency, utilization and matrix geometry. If, for example, 5 scenarios per parameter are to be measured, 5^5= 3125 cases need to be tested. Assuming one hour per test, it is immediately seen that the sensitivity analysis needs to be narrowed down to a tighter parameter range.

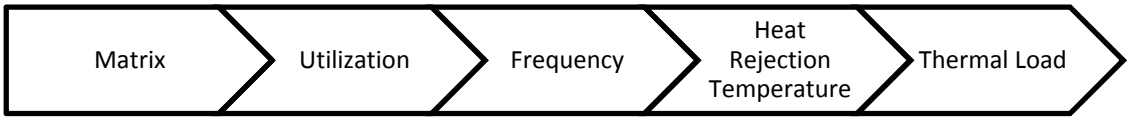

Figure 3-11. Design parameters progression order

Given the objectives in Section 1.6, it was decided to limit the matrix geometry to two cases (spheres and parallel plates). It was also decided to limit frequency of operation to two cases (2 and 4 Hz) while the other parameters are limited to four operating conditions each, reducing the number of tests to 254 (Table 3-2).

Table 3-2. Parameter range for the experimentation

Matrix Geometry	Utilization	Frequency	T_H	Q_c
300 μm spheres	0.62	2 Hz	17 °C	0 W
0.5 mm parallel plates	0.94	4 Hz	22 °C	20 W
	1.03		27 °C	30 W
	1.28		32 °C	40 W

Astronautics Corporation kindly offered gadolinium spheres of a narrow size distribution, between 250 - 300 μm. The minimum utilization set in Table 3-2 is about 20% higher (0.62 vs 0.5) than the original target because of pressure drop limitations. The high pressure drop due to regenerator aspect ratio and the small sphere diameter limits the total maximum Gd mass to 110 g. Thus, the minimum mechanically allowable stroke, with the smallest diameter displacer piston, limits the utilization at the low end to

0.62. For the parallel plate configuration, the gadolinium plate thickness chosen is also limited by the available supply. The heat rejection temperature (T_H) range is chosen to ensure the refrigerant operates in a temperature range close to its Curie Temperature (~ 22 °C). The 0 W to 40 W range of cooling load is based on the expected cooling capacity in the specified operating conditions. Further specifics on the regenerator design, experimental procedures, and instrumentation are given in the relative manuscripts in Appendix II and III.

3.6 Summary

Chapter 3 described the design requirements and the technical specifications of the PMMR. The chosen design reflects the need for a device that can operate effectively as a flexible laboratory-testing tool while still performing as a prototype magnetic refrigerator. A list of desirable specifications was given, such as modularity, compactness, ease of use, and short downtime when replacing refrigerant. Also, given a target cooling capacity of approximately 200 W, the amount of refrigerant was estimated once frequency and utilization range was established. A nested Halbach cylinder design solution was chosen because of the accessibility of the regenerators, and ease of magnet rotation up to moderate speeds for field modulation. The hydraulic system was also designed for compactness and simplicity. Finally a detailed plan for testing and device characterization was developed. Chapter 4 describes the model development, while the Chapter 5 will summarize experimental and model results.

Chapter 4

The Cost Analysis Optimization Model

This chapter describes the development of an AMR performance model and a cost-minimization algorithm. The purpose of the performance model is to quantify AMR cooling power as a function of regenerator properties, matrix structure, operating and design parameter. The performance model is used in a cost-minimization model to determine design values that minimize the total cost of the system (capital and operating cost). This section details the objectives and describes the development of such mathematical tool.

4.1 Model Objectives

In Section 1.6 it was stated that it is desirable to understand what conditions need to be met for magnetic refrigeration to be commercially viable. It is challenging to answer such a question because of both its breadth in terms of potential applications and design solutions, and its complex interdisciplinary nature. Therefore, it is beneficial to have a limited scope for analysis. For instance, targeting a single MR configuration is more manageable than attempting to find an answer to a more general scenario. When a particular design has been assessed, the model can then be adapted to other device configurations. The model should satisfy the following requirements:

- It should be validated against experimental data.
- It should solve rapidly even at the cost of reduced accuracy of the prediction (within a tolerable margin - the model should be able to capture trends and cost order of magnitude).
- The model should minimize the total cost for a specified performance requirement (temperature span and cooling power).

- The model should show sensitivity to design parameters such as MCE, pressure drop, temperature span, and required cooling power that are consistent with experimental findings.

The overall objective of the optimization model is to determine the conditions for a specific device configuration that provide the least cost of cooling. This information can be used to direct changes in system design, or to understand what factors need to be improved so that performance targets are achieved.

4.2 Model Development

The model is developed using a representation of the AMR that can be evaluated efficiently, with little computational demand. Once coded, the numerical model is validated against experimental data and then embedded in an optimization routine with the objective of cost minimization.

Rowe [40][42] proposed a simplified method for evaluating the cooling capacity of an AMR and the temperature distribution in the regenerator when the temperature span is set by the boundary conditions. The framework was used by Burdyny to create a numerical model which was validated against a range of experimental data [43]. This formulation can be simplified to create an analytic expression for cooling power (instead of a system of partial differential equations) and is potentially orders of magnitude faster than a numerical solution. Following is a summary of the equations and assumptions used for the analysis, while a detailed derivation can be found in the original publications. The model replaces the coupled partial differential equations 2.17 and 2.18 with a single one:

$$(m'_f c_p + m'_s c_b)\frac{\partial T}{\partial \tilde{t}} + \dot{m} c_p \frac{\partial T}{\partial \tilde{x}} - \frac{\partial T}{\partial \tilde{x}}\left(\kappa_{eff} A \frac{\partial T}{\partial \tilde{x}}\right) = -m'_s T \left(\frac{\partial M}{\partial T}\right)_H \frac{\partial \mu_0 H}{\partial \tilde{t}} \qquad \textbf{(4.1)}$$

under the assumption that $T_f \approx T_s = T(x,t)$, valid for a high heat transfer coefficient, where m'_f is the mass of fluid per unit length of the regenerator entrained in the pores and m'_s is the mass of magnetocaloric material per unit length, M is the magnetization per unit

mass, c is mass specific heat, κ_{eff} is effective conductivity, including the solid and fluid terms, and A is the cross-sectional area of the regenerator.

The left side of Equation 4.1 includes the rate of change in temperature due to conduction and advection, while the right side expresses the heat generation due to the magnetocaloric effect. A *real* magnetocaloric refrigerant is a non-linear function of T (Figure 1-1) and a number of other physical parameters and it is quite well described by the *Mean Field Theory* [38]. To arrive at an analytic solution for cooling power an *ideal* refrigerant is assumed [44] where the MCE is a linear function of temperature:

$$\Delta T_{MCE}(x) = \left(\frac{\Delta T}{T}\right) T(x). \tag{4.2}$$

This was shown in Section 2.3, as Equation 4.2 is derived from Equation 2.16. This assumption is convenient as it simplifies the evaluation of Q_c and W_{input}. Cooling power and magnetic work can be derived from the governing Equation 4.1 combined with the expressions for magnetic work and losses. If entrained fluid is taken into account (R > 1), solid specific heat is assumed constant, and a step-wise cycle is adopted, we have:

$$Q_c = \frac{m_s c_s}{\tau_c} U \left(\frac{\Delta T}{T}\right) T_{a0} \left(1 - \frac{p}{\sin p}\left(\frac{U}{\kappa}\frac{\Delta T}{T}\right)^{-1}\left(\frac{T_{a1}}{T_{a0}} - \cos(p)\right)\right) \tag{4.3}$$

and

$$W_M = \frac{m_s c_s}{\tau_c}\left(\frac{\Delta T}{T}\right)\left[\frac{R-1}{R}\left(\frac{\Delta T}{T}\right)\int_0^1 T dx + U\left(T_{a1} - T_{a0}\right)\right] \tag{4.4}$$

where

$$\int_0^1 T dx = \frac{1-\cos(p)}{p\sin(p)}(-T_{a1} + T_{a0}), \text{ with } p \equiv \left(\frac{\Delta T}{T}\right)\left(\frac{1}{\kappa}\frac{R-1}{R}\right)^{\frac{1}{2}}. \tag{4.5}$$

T_{a0} and T_{a1} are the temperatures at the ends of the regenerator at the final phase of the demagnetization process before the cold blow (T_{ax} is the temperature at a generic position x), and κ is the non-dimensional conductance. The non-dimensional parameter U can be

considered an alternative definition of utilization where it is determined by Φ and the thermal mass ratio R:

$$U \equiv \frac{\Phi}{R} \quad \text{with } \Phi \equiv \frac{\dot{m} c_p \tau_B}{m'_s L c_b}, \quad R \equiv 1 + \frac{m'_f c_p}{m'_s c_b} \tag{4.6}$$

The boundary conditions T_{a0} and T_{a1} can be determined from:

$$T_C = \left(1 - \frac{U}{2}\frac{p\cos(p)}{\sin(p)}\right) T_{a0} + \frac{U}{2}\frac{p}{\sin(p)} T_{a1} \tag{4.7}$$

$$T_H = -\frac{U}{2}\frac{p}{\sin(p)} T_{a0} + \left(1 + \frac{U}{2}\frac{p\cos(p)}{\sin(p)}\right) T_{a1} \tag{4.8}$$

where T_C, and T_H are the average fluid temperatures at the cold and warm ends of the regenerator. The non-dimensional conductance κ is defined as:

$$\kappa = \frac{\tau_c}{m'_s L c_s}\frac{k_{eff} A}{L} \tag{4.9}$$

where effective conductivity, k_{eff}, is divided into a static component, which takes into account the amount of solid and fluid in the regenerator, and a dispersive component, which accounts for the effects of fluid mixing [45]. As shown by Burdyny, this loss mechanism can also include imperfect convective heat transfer between the solid and the fluid.

While it is possible to estimate the temperature distribution through an AMR, it is not required. Only Equations 4.2 and 4.3 are needed to estimate the cooling power and cycle input power.

For the model described here, the impact of finite convective heat transfer in the regenerator is included by modeling it as a parasitic heat leak through the regenerator. This accounts for the regenerator ineffectiveness, while maintaining a simple analytical approach. The parasitic heat loss Q_L is modeled as a function of the regenerator *NTU*. Using the Hausen model with infinite thermal mass for regenerator effectiveness [46]:

$$Q_L = (1-\in)\frac{2m_d c_p}{\tau_c}(T_H - T_C) \tag{4.10}$$

with

$$\in = \frac{NTU}{NTU+2} \text{ and } NTU \equiv \frac{hA_w}{\dot{m}c_p} = \left(\frac{k_f}{D_h}Nu\right)\frac{A_w}{\dot{m}c_p} \tag{4.11}$$

where m_d is the fluid mass displaced per cycle and τ_c the cycle period, and $\in$ the regenerator effectiveness. The Nu is evaluated by the Whitaker correlation [45]:

$$Nu = 2 + \left(0.Re^{\frac{1}{2}} + 0.2Re^{\frac{2}{3}}\right)Pr^{0.4}, \text{ with } Re = \frac{\rho u_p}{\mu} \tag{4.12}$$

where ρ is fluid density, u_p pore velocity, and μ dynamic viscosity. Additionally, the field dependence of the MCE is assumed to obey Equation 1.1 which is consistent with a material like Gd near the Curie temperature and most refrigerant.

In order to model a complete system additional terms are needed such as thermal losses to the environment, torque required to rotate the magnets, viscous losses, and scaling laws for magnetic field with magnet geometry. These are detailed in the related manuscript in Appendix IV.

4.2.1 The Optimization Routine

An optimization model was constructed in Matlab with the objective of minimizing the total cost rate of a MR. Given the non-linearity of the problem the function *fmincon* was used. The variables in the optimization are utilization Φ, frequency f, outer magnet diameter D_o, inner magnet diameter D_i, and length of the magnet L. The objective function (*OF*) is the sum of capital cost rate and operating cost rate

$$C_Q = C_{cap} + C_{op} \tag{4.13}$$

Capital cost is obtained by simply evaluating the volumes of the magnet and refrigerant, and multiplying them by their cost per weight and the capital recovery factor *CRF*. Operating cost is evaluated by multiplying the cost of electricity C_e, by the hourly power consumption W_{tot} and the duty cycle. The total power consumption is given by the

sum of cycle work W_M, fluid pumping power W_P, and the power required to overcome the drive torque W_{drive}. The total input power includes the motor efficiency, η_{motor}.

W_M is derived from Equation 4.4 and it is function of ΔT_{MCE}, utilization, frequency, mass of the refrigerant and other fixed parameters. ΔT_{MCE} is obtained from the magnetic field intensity, which is function of the magnet geometry. The mass of the refrigerant also depends on the magnet geometry. W_P represents the hydraulic losses, which are function of the regenerator geometry, utilization, and frequency. Finally W_{drive} is function of the magnet geometry. The cooling capacity is not present in the objective function, but, instead, is a constraint to be met, and evaluated using Equation 4.3. Because of this the *Active Set* algorithm was chosen (an optimal solution will be searched starting from a solution set with active constraints). The optimization problem is formalized as,

$$OF: \quad \textbf{Minimize } C_{tot} = C_{cap} + C_{op} = f(\Phi, f, D_o, D_i, L)$$

$$ST: \quad H_a < 1.5\ T$$
$$Q_c > \text{set value (between 70 W and 400 W)}$$
$$P < 0.7\ MPa.$$

The constraints include the field intensity upper limit, minimum cooling power, and maximum pressure drop. The maximum field constraint is based on limits imposed by the permanent magnet remanence. As shown in Equation 3.2, the field intensity of a Halbach cylinders is proportional to the logarithm of the external diameter. As will be shown in the results, this constraint is never active at 1.5 T (cost-limiting factor).

The Q_c boundary constraint is necessary to avoid trivial solutions and its range is chosen to match the cooling power requirements for household refrigerators. Larger cooling capacities can be obtained by aggregating a number of pairs of cylinders and regenerators. Under such scenario linear scaling of the results can be applied.

The pressure drop is limited to a maximum of 0.7 MPa, because of design limitations on conventional hydraulic components. Displacers and pumps can be specified to operate at higher pressure drops, however they become more costly and the system less efficient and more prone to wear.

The temperature span chosen is based on CECOMAF high back pressure standards, with T_C set at a temperature equivalent to an evaporator at 5º C and T_H to a condenser temperature of 55 ºC [47]. Model parameters are listed in Table 4-1. Upper and lower bounds are in place for the objective function variables as listed in Table 4-2. The optimization search is performed using a number of different start points and all results converge to the same optimized solution, suggesting that the *OF* is convex in the selected region.

Table 4-1. Model Parameters

Parameter	Value/Range
T_H [ºC]	55
T_C [ºC]	5
Porosity (α) [-]	0.36
Spheres diameter [mm]	0.3
B_r [T]	1.35
R thermal mass ratio [-]	1.7
Q_c [W]	70-400
MCE_{ideal}/MCE_{Gd} @ 22 ºC [-]	0.6-1.1
Q_{amb} heat leak coeff. [W/K]	0.2
Capital Recovery [years]	10

Table 4-2. OF variable upper and lower bounds

Parameter	Lower Bounds	Upper Bounds
Utilization [-]	0.2	2
Device frequency [Hz]	.5	5
Magnet length [m]	0.02	0.3
Cylinder outside diameter [m]	0.03	0.3
Cylinder inside diameter [m]	0.01	0.1

4.3 Summary

This Chapter discusses the objectives of the performance model, how energy balance equations are implemented, and how the optimization was formalized. The objective is a model capable of evaluating capital and operating cost of a dual nested Halbach cylinder MR. In addition, the optimization model minimizes the total cost rate so that optimal operating and design parameters are found. The model simplifies the governing equation by merging the coupled differential equations presented in Chapter 2 into a single one, and post evaluating the loss in performance due to finite heat transfer. This approach allows for evaluation of the cooling power for a given temperature span using an analytical expression. An optimization routine is then presented. The objective function is the sum of the capital and operating cost rate assuming a lifecycle of 10 years. The optimization variables are the magnet inner and outer diameter, length, utilization, and frequency. The constraints are the cooling capacity, maximum field, and maximum pressure drop.

Chapter 5 presents a summary of experimental results obtained using the PMMR, and optimized results from the model.

Chapter 5

Summary of Key Results

5.1 Experimental results

Experimental Results are divided in two subsets, and their investigations are published in their respective publications. Experiments using 300 μm gadolinium spheres are described in Tura et al, 2011 [48] (Appendix II) and results for gadolinium parallel plates are described in Tura et al, 2012 [49] (Appendix III).

5.1.1 AMR of Packed Spheres

In order to characterize the refrigerator, temperature span between hot and cold heat exchangers, pressure drop (viscous losses), power input, and cooling power are measured. Each measurement is recorded once the refrigerator reaches a periodic steady state condition for a specific operating regime. Periodic steady state is assumed if the recorded peak temperature span does not change over a period of 120 seconds. Each operating parameters is mapped over the ranges reported in Table 3-2. Appendix II presents the complete set of results. This section describes the main results relevant to the validation of the performance model. The dataset of interest includes all tests performed operating at 2 Hz and 4 Hz with a heat rejection temperature of 22 °C. That is varying frequency, Q_c and Φ in conformity with Table 3-2. The results are summarized in Figure 5-1.

The plots show that in the operating range the relationship between cooling capacity and temperature span is approximately linear. This has been observed in other devices [12][15]. This linearity is generally lost if instead of a single material regenerator, a multiple composition layered regenerator is adopted. Also, in the range of the tested conditions, cooling load sensitivity is reduced if either utilization or frequency are increased. As mentioned earlier increasing Φ induces larger perturbations in the regenerator temperature distribution during a cycle. This effect is required to actually perform a thermal cycle (to reject heat and provide cooling), if it is too small the cooling

capacity is reduced (smaller cycle area), however if it is too large it reduces the regenerator effectiveness. This can be observed by the reduction in temperature span at lower cooling loads when utilization increases. Note that the case of 4 Hz and Φ = 1.28 could not be experimentally performed due to pressure drop exceeding the device maximum pressure rating, thus the data presented is a linear extrapolation from the other two cases. The effective cooling capacity is only 42% of what was predicted, in first approximation, from the simple linear scaling obtained from the AMRTA experimental data in Section 3.3. This is to be expected as the performance of a device does not depend only on the ΔH, refrigerant mass, frequency, and utilization; neither these quantities scale linearly with performance in real devices. Although not presented here, results are similar if the heat rejection temperature is decreased, in which case the performance scales simply down, due to the reduced MCE in the operating temperature range. If the T_H is raised above T_{Curie}, the results are similar as long as $T_C < T_{Curie}$, otherwise the operating conditions become unstable. This behavior was previously observed and documented [13].

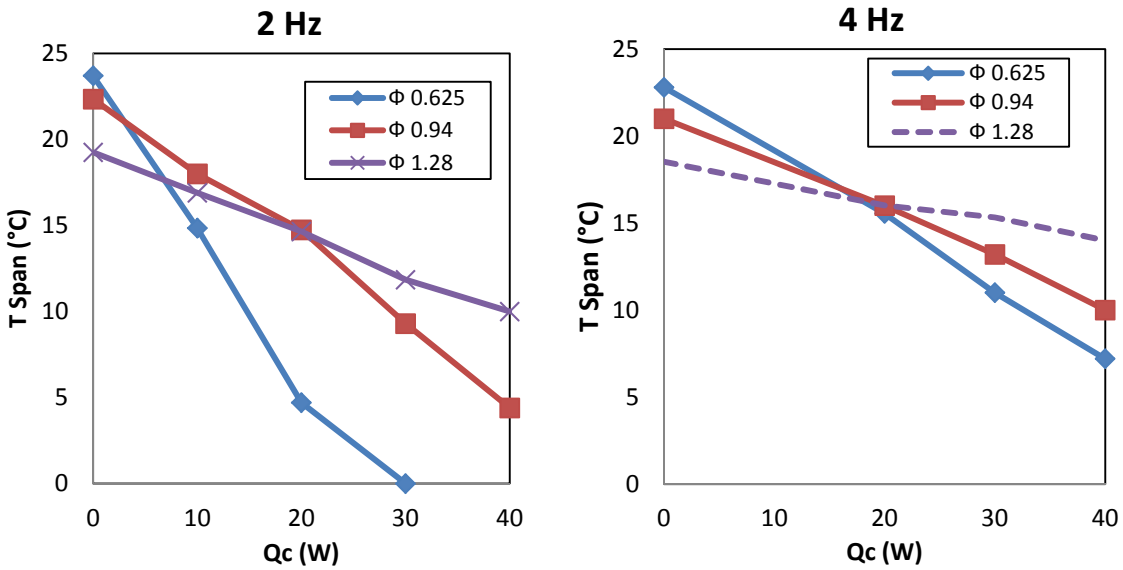

Figure 5-1. PMMR experimental results with T_H set at 22 °C. The figure on the left shows temperature span as a function of applied load for three different utilizations at 2 Hz. The plot on the right is for 4 Hz.

Figure 5-2 illustrates the apparatus power consumption with an approximate breakdown of loads. *Base* power is the power to run the gearmotor with nothing attached to the shaft; the *mechanical* drive power is the power required to rotate the magnets with no fluid flow (i.e. mechanical losses only); the *cycle* power is the power required to drive the displacer mechanism and the magnetic work. Data refers to a utilization of 0.62. The input power is evaluated by measuring voltage and current drawn by the electric motor. Between 2–4 Hz the motor requirement is ~ 50–110 W, thus COP is typically less than 1. The device efficiency is low because of 1) the cooling capacity is low, and 2) the power required to drive the refrigerator is comparably high.

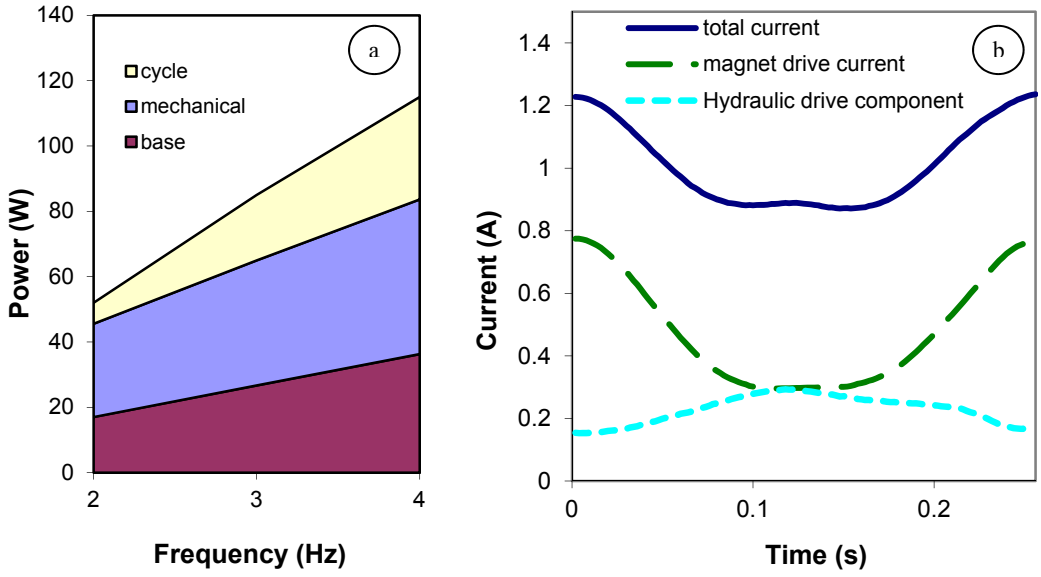

Figure 5-2. a) Power input breakdown as function of frequency, and b) instantaneous current draw over a cycle.

The plots in Figure 5-2 show that although the efficiency is low, increases are possible if losses can be reduced. Indeed most of the power requirement is to overcome mechanical losses, whereas the viscous losses are relatively low. The instantaneous current draw during the magnet rotation is nonuniform because the torque cancellation is not as effective as planned. This is due to imperfections to Halbach cylinder fabrication and to field stray magnetic interaction between the nested cylinders. These effects can be reduced with better manufacture and design. Viscous losses may be reduced using more

efficient regenerator matrix geometry or by changing the aspect ratio. Small spheres are well known for good heat transfer but high pressure drop.

Figure 5-3 compares the performance of the PMMR to published results of other prototypes using the specific exergetic cooling power metric (Equation 1.4). It can be seen that the device performs comparatively well mostly because of its relatively high power density, thanks to relatively high operating frequencies (Figure 5-3).

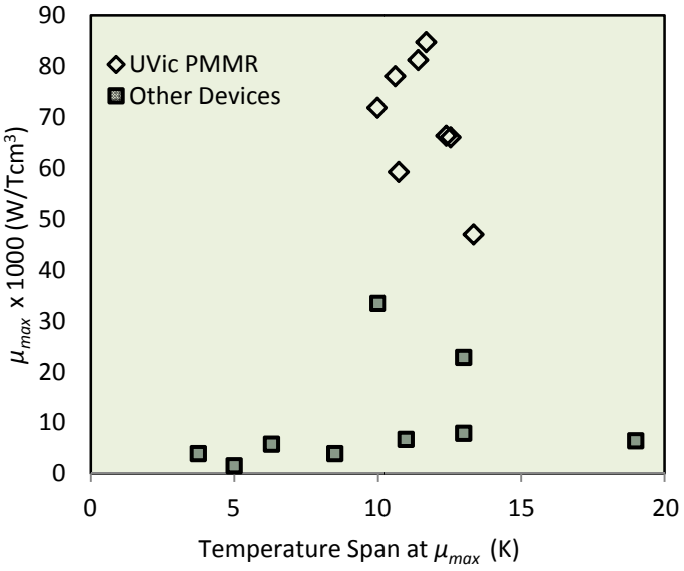

Figure 5-3. Maximum specific exergetic cooling power or PMMR compared to other devices as function of temperature span [50].

5.1.2 Parallel Plates Matrix AMR

An effective AMR must balance the demand for good heat transfer between the solid and fluid against hydraulic losses. For instance, when using 0.3 mm diameter gadolinium spheres (55 g, 36 % porosity) in a cylindrical volume of 16 mm diameter and 55 mm length, a pressure drop of ten atmospheres or larger can be observed when operating at 4 Hz. Such viscous losses are unacceptable because they significantly reduce device efficiency.

A geometry that can be operated at much higher frequencies and fluid flow rates is a parallel plate type of regenerator. Flat plates can be stacked together with equally spaced gaps necessary for the fluid to flow and exchange heat with the solid medium. Parallel

plates can be one order of magnitude better in terms of viscous losses than spheres; however, surface area and heat transfer rates are penalized. A plate thickness of 100 μm and a gap between plates of 50 μm is needed to obtain a hydraulic diameter and porosity equivalent to the 0.3 mm spheres used in previous experiments. This could not be achieved with the material and technology available to the laboratory. Instead, the parallel plate design used 540 μm thick, 15 mm wide, and 90 mm long gadolinium strips. To maintain a 36% porosity the gap was set at 300 μm.

Parallel plate geometries introduce some considerations which may be less of a concern with spheres:

- Plate orientation relative to the magnetic field has an impact on the performance through the demagnetizing field.
- Plate size, geometrical shape and orientation have an impact on eddy currents and magnetic forces.
- Plate alignment needs high accuracy to avoid preferential flow among the parallel gaps and flow maldistribution.
- Given the high alternating forces acting on the plates the assembly needs to be structurally sound and not susceptible to fatigue.

The regenerator geometry used in this work is illustrated in Figure 5-4. It consists of a scaffolding structure to maintain plate position and alignment during operation, while allowing for simple installation of the plates in the regenerator shell. Two circular end pieces with the same diameter as the regenerator shell inner cavity support each group of plates. Perforations of 300 μm diameter allow for fluid flow. On the inner face, 300 x 300 μm tabs protruding 500 μm and 500 μm apart are used as guides for the plates. Four intermediate discs with equivalent perforations and tab pattern are used for the inner sections, this time on both sides. The end pieces and intermediate ones are held together by two spacers featuring perforations for locating pins plus an additional hole for a connecting rod. The assembly results in five layers each holding 14 plates. The structure is made out of nylon and the locating pins and connecting rod are of stainless steel. By

removing one or more intermediate discs and using shorter connecting rods 4 or fewer modules can be tested. The 5 module regenerator is 80 mm long and has similar mass (60 g) and porosity (36%) of the previously tested spheres regenerators. Each plate has a length of 15 mm and a width ranging from 10.8 to 15.5 mm depending on the location (the plates fit a circular cross-section).

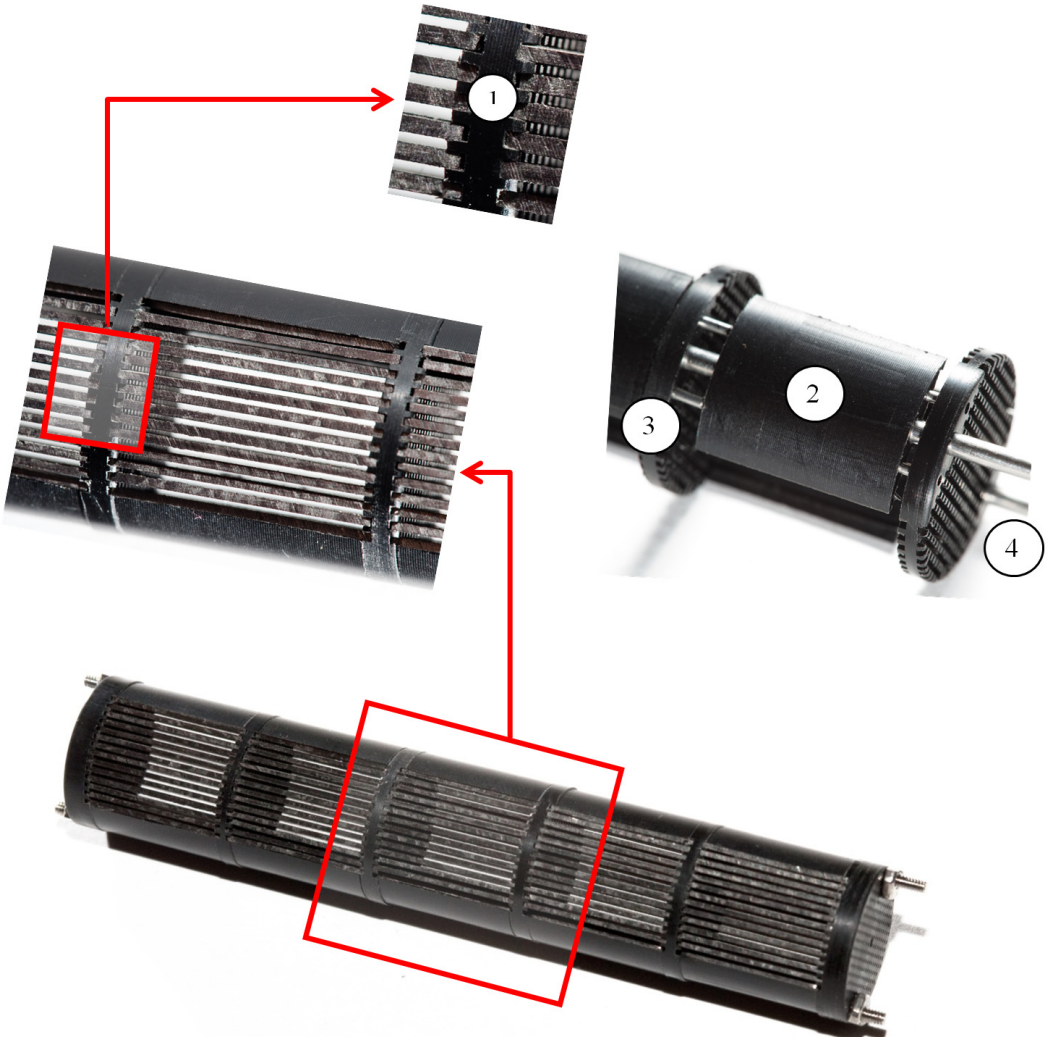

Figure 5-4. Parallel plate regenerator assembly. Details are shown of 1) tabs, 2) spacers, 3) locating pins, and 4) connecting rods.

Table 5-1. Parallel plate configuration regenerator testing parameter space

Parameter	Range	Units
Heat rejection temperature	17, 22, 27, 32	ºC
Operating frequency	0.5, 1, 2	Hz
Utilization (1)	0.33, 0.53, 0.81	-
Thermal load	0, 10	W

Table 5-1 summarizes the experimental conditions. They are different from Table 3-2 because the parameter space is not suitable for this configuration. Indeed, the results differ substantially from previous tests performed with gadolinium spheres.

Results for T_H = 22 °C are presented in Figure 5-5. Temperature span is contoured against frequency and utilization with no applied thermal load. The major differences with respect to the spherical particles are lower temperature spans and a strong temperature span dependency on frequency. The reason for this behavior is the larger hydraulic diameter in the parallel plate geometry. This results in a small wetted surface area and a low convection coefficient. Since we are greatly relying on the conductive heat transfer rate in the fluid, blow duration (or mass flow rate) has a non-trivial impact on the regenerator effectiveness. In theory, operating very slowly, with a small displaced volume would result in the largest temperature span, however this leads to extremely low cooling power. In order to obtain a better performance thinner plates and narrower gaps are needed to create a smaller hydraulic diameter. Such regenerators are difficult to fabricate.

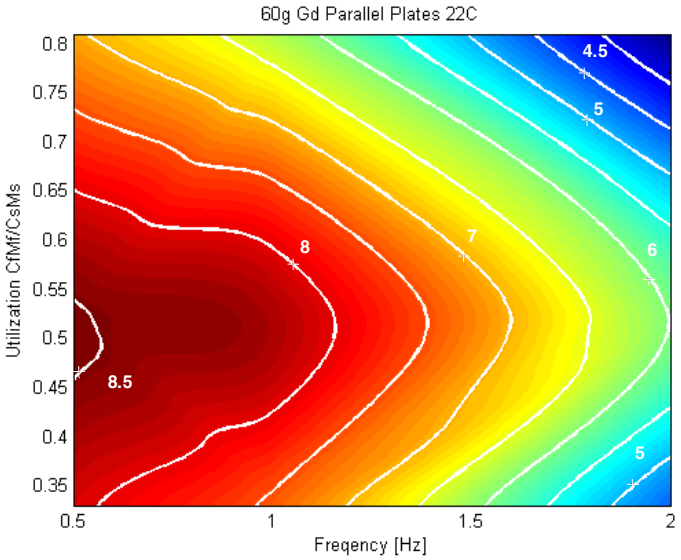

Figure 5-5. Parallel plate results for T_H = 22 °C. Temperature span is contoured against frequency and utilization with no applied thermal load.

As has been shown by other researchers both numerically [24] and experimentally [51], parallel plate performance can be severely affected by flow maldistribution. Figure 5-6 shows the impact imperfections plate alignment can have on cooling power; effective cooling performance requires a great level of precision for structures on the order of 200 μm or less.

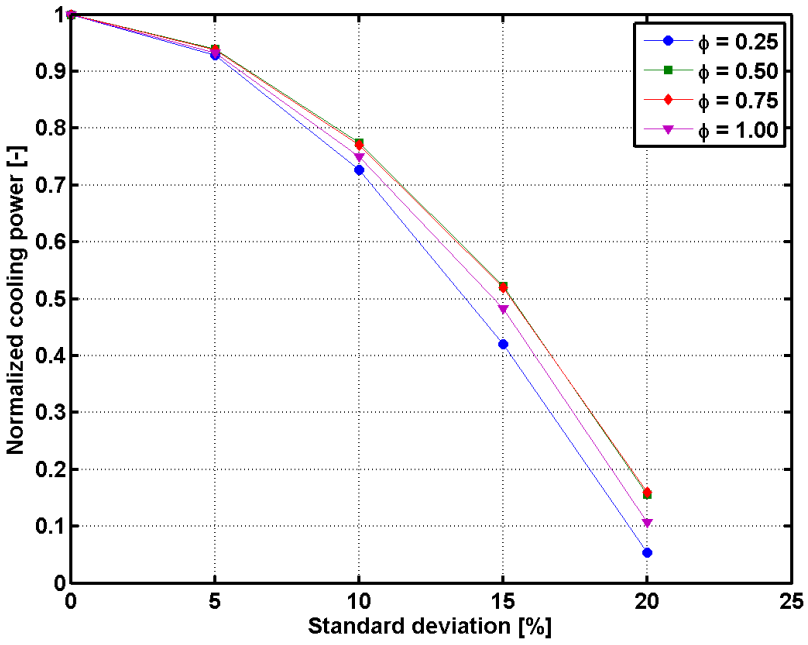

Figure 5-6. Effects of maldistribution of spacing in parallel plates AMR cooling capacity [24].

5.1.3 Is the PMMR meeting its objectives?

The PMMR successfully achieved what it was designed for. It performs well in terms of power densities and temperature span, while of simple and compact construction with convenient access to all components. It only requires few minutes for replacing the regenerators and the entire device can be assembled or disassembled within one hour. Operating up to 4 Hz allows reaching steady state in relatively short times (less than one hour for most tests). Device performance characterization for a single regenerator was done by mapping over one hundred different operating points. No AMR performance has been published before in such a range of operating parameters and resolution. The PMMR has proven to perform with good repeatability, generally within 0.1 - 0.2 °C. Since its initial tests this device has operated as planned, testing many regenerators of

different matrix structure and composition, logging hundreds of hours with minimal maintenance.

It was also learned that the PMMR performance can be improved by refining its design. Specifically, cylinders with larger bores would help in reducing hydraulic viscous losses and flow channeling along the regenerator walls. Also, the magnetization waveform could be improved by broadening the demagnetization time (Figure 3-6), to look more like a sine wave. Finally the magnets could be designed to reduce the magnetic torques, improving the overall efficiency.

5.2 Modelling results

5.2.1 Validation

The objective of the model validation is to ensure that predicted performance is comparable to experimental data. Because of the simplified nature of the theoretical model, the main concern is that general trends and parameter sensitivities are captured. A more complete model validation with gadolinium properties has been reported [33].

Figure 5-7 shows the experimental data of net cooling power versus temperature span. Linear fits to the data show extrapolated results for maximum Q_c/no-span to maximum span/no-load. Figure 5-8 shows a similar plot using the model, where an ideal MCE scaling which would result in 75% of the peak MCE of Gd is used.

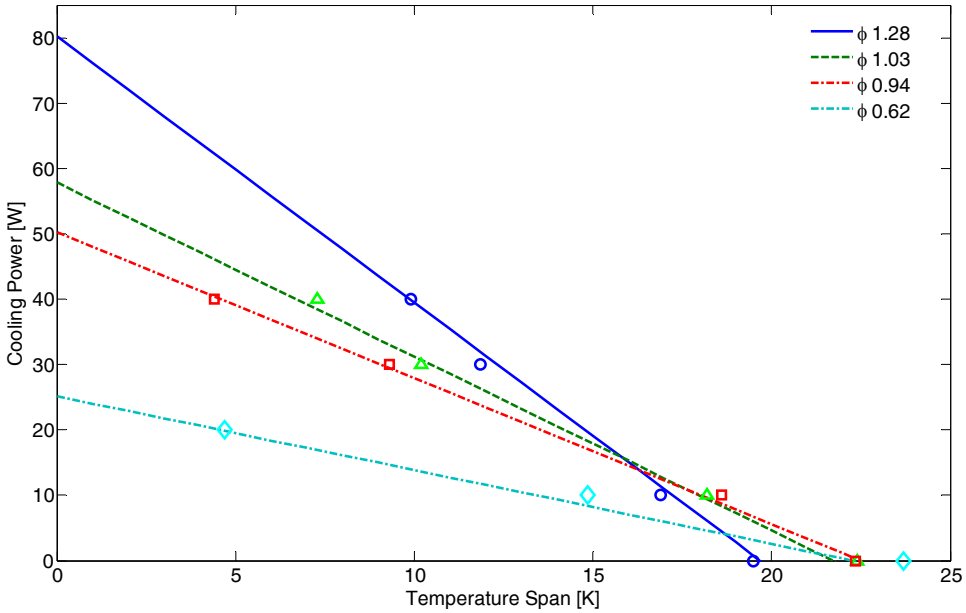

Figure 5-7. Extrapolated (lines) and experimental (markers) data of cooling versus temperature span.

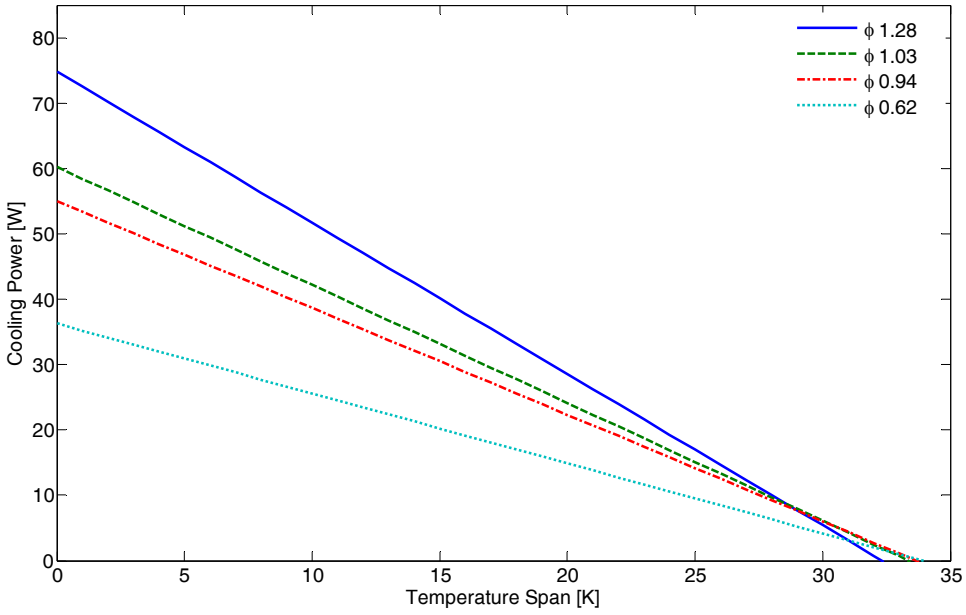

Figure 5-8. Model results of cooling versus temperature span, where the ideal MCE at 75% of Gd is used.

Based on the cooling power as a function of span comparison, the model does capture the experimental trends. If operating at zero temperature span the real refrigerant is closest to performing like the idealized material as the properties are relatively constant. Under such operating conditions (ΔT = 0) the chosen ideal refrigerant performance produces results similar to the experimental data. Lower utilizations tend to slightly overestimate cooling power for equivalent span, while the reverse is true for the higher utilizations. Thus the model shows less spread as utilization is varied from 0.62 to 1.28. In general, some degree of overestimation by the model is expected for several reasons. Firstly, the model assumes an ideal refrigerant, with an ideal MCE distribution and constant specific heat equal to gadolinium at zero field and the Curie temperature. In addition, it assumes a step wise cycle while the apparatus adopts a pseudo-sinusoidal wave form for the magnetization and fluid blow (this is partially incorporated by using RMS values). Conversely, the experimental apparatus could be underperforming because of flow channeling, air trapped in the system, void volumes, and other imperfections. Additionally, if the ideal refrigerant is chosen to perform similarly to the experimental device for $\Delta T = 0$, by intuition it should be less sensitive to the cooling load when $\Delta T \neq 0$. In other words the slope of the load/span line in the plot should not be as pronounced. This can be explained by the fact that gadolinium displays a caret shaped MCE rather than following an ideal linear distribution. It can be clearly observed that, while the trend of the curves in Figure 5-7 and Figure 5-8 follow the same pattern, the model is indeed less sensitive to thermal loads showing a maximum span (for Q_c = 0) of almost 35 °C compared to the actual device, with only 22 °C. It is interesting to observe that the impact of changing utilization follows the same trend in all three cases: larger utilizations allow larger cooling power, but the curves become steeper too, meaning that only lower temperature spans can be achieved. In the experimental case the curves cross over at about ΔT = 16 °C, while in the model this happens for ΔT = 30 °C. The difference in predicted temperature span is to be expected because of nature of the refrigerant used. This qualitative validation shows that the model captures the trends and the performance order of magnitude which is all it is needed at this stage since ideal refrigerants represent a target and not effective performance.

5.2.2 Optimization and Parametric Sweep.

This section presents the estimated cost, size, operating parameters, and efficiency of a dual Halbach cylinder magnetic refrigerator when total cost rate is the optimization objective function. Optimized results are determined for a range of values of the design variables $MCE_{ideal}/MCE_{Gd@295K}$ (scaled from 0.6 to 1.1, with 0.05 increments), and maximum device cooling power (70-400 W, 11 W increments). The results are presented as contour plots with a mesh resolution of 300 optimized points. Plots with four times the resolution (1200 optimized points) were also obtained, with no visible change in the contour plot. The solution is on average acquired in under a minute on a personal computer with a 2.3 GHz i7 Intel process and 8 Gb of RAM. It is worth noting that throughout the optimization sweep the pressure drop was the only binding constraint (with the exception of Q_c) and the upper and lower bounds of the *OF* variables were never active. Lagrange multipliers at the solution points are close to zero, suggesting that the optimization results are not strongly limited by the constraints; this is supported by the fact that if the pressure drop limit is removed the solution does not change significantly, favoring slightly higher aspect ratio regenerators with a minor increase in cost. Higher pressure drops are undesirable because of the efficiency loss, therefore a capital cost saving (from higher specific exergetic cooling) would be hampered by a higher operating cost. Regenerator matrix structure plays a critical role in this regard, maximizing heat transfer while minimizing viscous losses. For instance the optimization process showed that if the regenerator was to operate with a pressure drop 50% lower than the 300 μm spheres while maintaining the same heat transfer, we would see approximately 20% savings in both capital and operating cost.

Figure 5-9 illustrates the cost of the magnets and of the refrigerant. The plots display similar trends and intuitively the system grows larger and more expensive to satisfy larger cooling demand, while larger MCE has an inverse effect, helping the power density, and thus reducing size and cost. For the given variable ranges the cost of the magnets spans from $100 to $ 800 and $50 to $250 for the refrigerant.

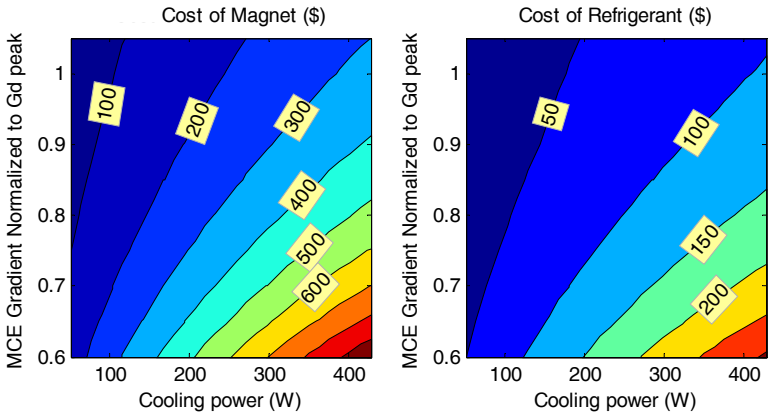

Figure 5-9. Capital cost of magnets and refrigerant.

Figure 5-10 (left) shows the cost of refrigeration on a hourly base assuming a life cycle of 10 years and a duty cycle of 0.35. The optimized cost shows a similar trend as the previous plots with values ranging between 0.4 and 2.4¢/h. Figure 5-10 (right) shows the weighting of the capital to operating costs. For high MCE and low cooling demand, capital cost is < 1.5 times the operating cost, while it grows 2 - 2.5 times for low MCE and high cooling demand. Also, cost ratio is less sensitive to cooling demand as this grows larger.

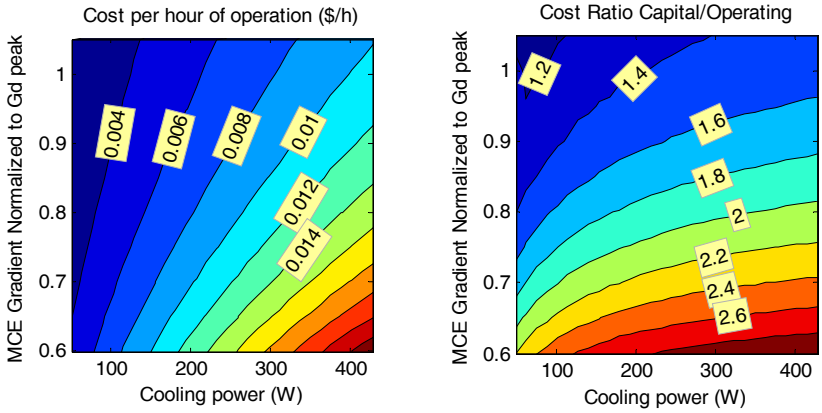

Figure 5-10. Ratio of capital/operating cost rate and cost per hour of operation.

Looking at the cylinder geometry (Figure 5-11), the magnet length shows virtually no sensitivity to cooling demand above 200 W. Regenerator length ranges from a minimum of 90 mm to 120 mm. The magnet outer diameter is sensitive to both magnetocaloric

properties and cooling demand, ranging from 40 mm to 120 mm, while the inner diameter ranges from 20 mm to 50 mm, following a similar sensitivity pattern as the outer diameter. Although not reported in any of the figures, the regenerator aspect ratio (*L/D*) is insensitive to MCE (likely because it is more strongly coupled with the heat transport, rather than MCE), while it varies from 5.5 to 2.5 for cooling demands between 70 and 400 W.

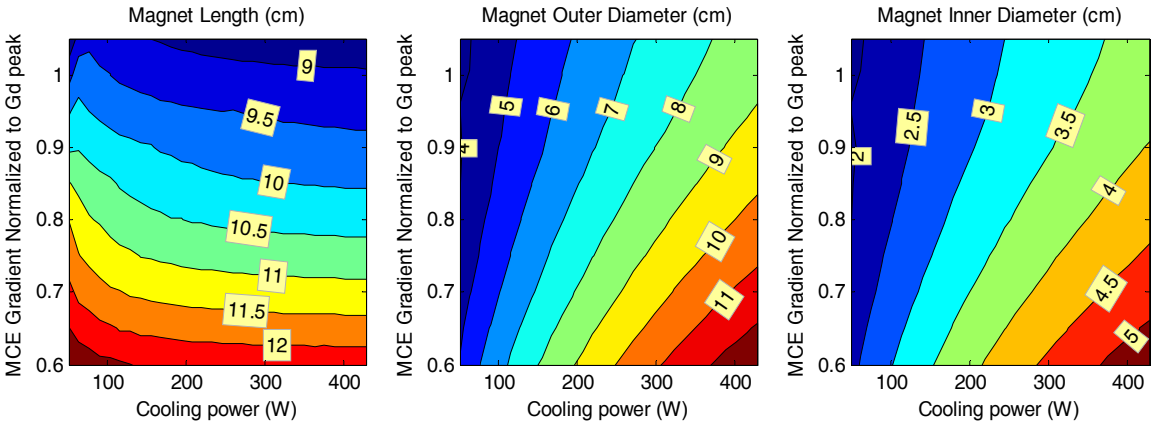

Figure 5-11. Optimization results for magnet geometry: length, outer diameter and inner diameter.

Peak magnetic field, frequency, and utilization values show some interesting and somewhat unexpected results in Figure 5-12. The optimization routine suggests that the field should not be maximized, but rather set around 1 T with no more than 15% increase if high cooling demand and low MCE is chosen. This result is quite remarkable because the device magnetization cycle is sinusoidal and not stepwise, thus the effective field change is even lower (RMS rather than peak value). Maximizing the peak magnetic field would create a more efficient cycle and higher cooling capacity, however it seems that a lower field creates a better balance between operating cost and capital cost. The figure also shows that the optimized frequency is not binding, ranging between 3 and 4.5 Hz; interestingly, lower frequencies are preferred for the higher cooling demands. Finally utilization seems to be optimized for relatively low values, between 0.3 and 0.6. This is due to the large imposed temperature span (ΔT = 50 °C). Higher cooling powers increase the optimal utilization with associated reduction in optimized operating frequency in this range (3 Hz vs 4.5 Hz) Also, utilization is seen to be insensitive to the magnetocaloric

properties of the refrigerant although currently available refrigerants would likely deviate somewhat from this result, as temperature perturbations induced by the fluid would affect performance more significantly.

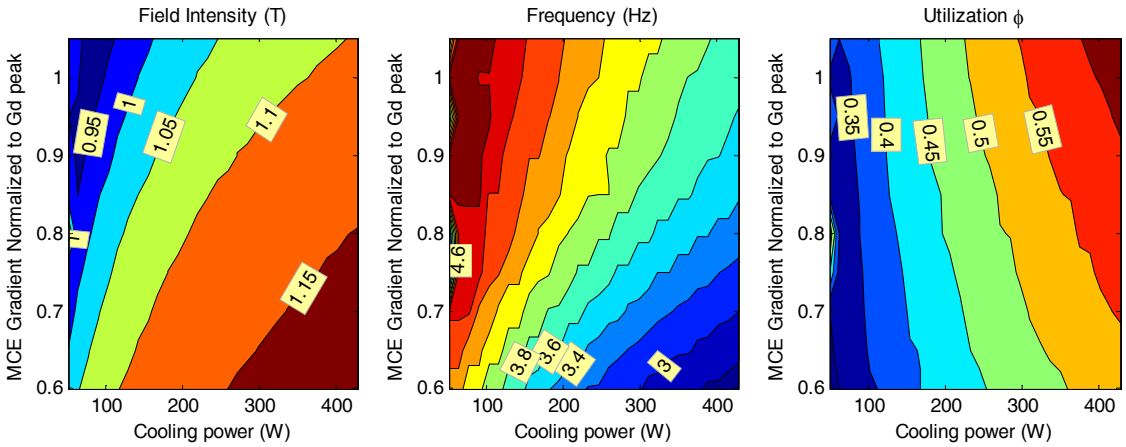

Figure 5-12. Optimized results for maximum field intensity, frequency, and utilization.

Figure 5-13 (left) illustrates the expected efficiencies of the optimized system (when operating at the maximum rated cooling power). As expected both higher MCE and rated cooling power promote higher efficiencies. Smaller systems (below 200 W) have a COP not larger than 3.5 while higher capacity systems show COPs up to 5.

Figure 5-12 (center) shows that specific exergetic cooling is mostly sensitive to the refrigerant MCE, while it is does not depend on cooling power as the device's cooling capacity grows larger than 200 W. The specific exergetic cooling is found to range between 0.5 WT^{-1} cm^{-3} and 1.5 WT^{-1} cm^{-3}. Total cost of cooling follows a similar trend (Figure 12 – right) ranging between 2.5 $\$W^{-1}$ and 1 $\$W^{-1}$ (Figure 5-13, right).

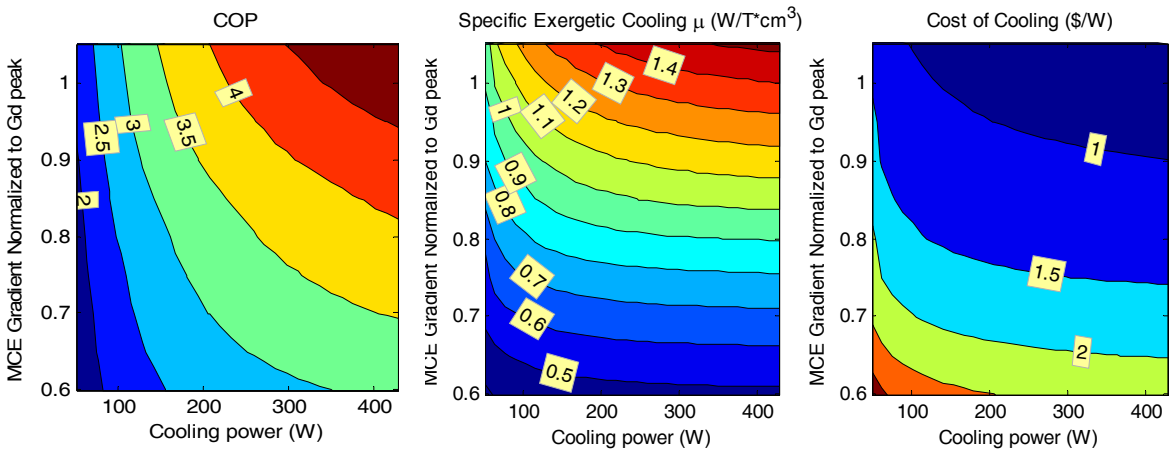

Figure 5-13. Optimization results for COP specific exergetic cooling and cost of cooling.

It is worth noting that if the cost of refrigerant is reduced to 20 $\$kg^{-1}$ from 150 $\$kg^{-1}$ the results are almost the same for this particular device configuration. In this case, there is a 25% reduction in specific exergetic cooling and a slightly higher COP resulting in approximately to 20% improvement in cost of cooling.

These results are in good agreement with the optimization results obtained by Bjørk et al [29]. He estimated the minimum total cost for magnet and refrigerant for a number of regenerator configurations. He considered both Gadolinium and an idealized material with constant ΔT_{ad} (with peak adiabatic temperature change to be the same as Gd) in parallel plates and 300 μm sphere regenerators. Operating conditions are set to 100 W of cooling capacity and 20 °C temperature span. Using the ideal material properties and spheres as the matrix geometry for the regenerator, Bjørk suggested a total cost of $7. The model presented here, under the same conditions, estimates a cost of $15. If we take into account that in the dual Halbach cylinder the magnet is actively used only for 50% of the cycle, while the model used by Bjørk is based on 100% of the cycle, the results are strikingly close. It is interesting to observe that if the model takes into account the operating cost, the optimized capital cost shifts from $15 to $35 and the COP improves from 1 to 4, while the operating frequency changes from 10 Hz to 2.5 Hz. Bjørk commented in his article that his model did not find an optimum for frequency, which means that in the parameter space explored, the cost of the device monotonically decreases with cycle frequency. However, if operating cost is accounted for, viscous

losses degrade the efficiency to a degree that the overall (capital + operating) cost is negatively affected by it and an optimum can be found, well below the 10 Hz.

5.2.3 Optimization Model Benefits

The optimization model is a flexible tool that can display sensitivities and trends of a broad range of parameters. Results can be used to estimate competitiveness or what improvements are needed to make it possible.

For instance Rowe [27] suggested that for a cooling capacity of 70 W when operating between 7.4 °C and 54.4 °C, a specific exergetic cooling power ranging between 0.4 and 1 $WT^{-1}cm^{-3}$ is needed for cost of cooling to be less than 2 $\$W^{-1}$ (if a dual nested Halbach configuration is to be used). The results in Figure 5-13 show that this should be possible if an ideal refrigerant with a scaling to Gd peak of approximately 0.85 is to be used. Such an MCE does not seem unrealistic.

Additionally the model can easily be modified to fit specific conditions, i.e. the conditions of Bjørk et al., such as cooling demand, temperature span, cost of magnet and refrigerant can be matched, and the operating cost can be set to zero. It was shown earlier how the device efficiency can affect the design parameters and the capital cost optimization, taking a broader view of the results presented by Bjørk. Sensitivity to other design parameters can also be performed, such as observing the effect of varying the specific heat of the refrigerant, the thermal conductivity, temperature span, or the duty cycle. Outcomes can be manipulated by varying the cost of the materials, or the lifecycle of the product, shifting the weight of the capital or operating cost, favoring a more expensive but more efficient solution or viceversa.

In general, if a specific performance or cost is desired, a simulation tailored to the purpose can be performed in just a few minutes. Sensitivity charts can be used to estimate target parameter values and feasibility. The ability to perform such evaluations with ease makes this method effective and unique. As a comparison, Evans [23] recently presented a cost optimization for large air conditioning systems (175 kW) using superconducting magnets. A genetic algorithm was used with volumetric cooling capacity and COP as the objectives of the optimization. Temperature span was set to 28 °C with the high field

fixed at 2 T. In total 850 designs were simulated. The model parameter sweep required days to solve on a cluster. Investigating for a range of temperature spans and field intensity can be extremely time consuming using this model. An analytical model, requiring lean computational power, can be a more effective tool for such applications.

While the results of the proposed method are specific to the PMMR configuration, they can be extrapolated to other design approaches. For instance device configurations and performance metrics such as Λ_{cool} can be used as scaling criteria. In the future, it would be valuable to be able to extend solutions to other device configuration natively.

5.3 Summary

This Chapter presented the key findings of this research. Firstly, the results of the experimental characterization of the PMMR were shown for both regenerators using spheres and parallel plates. Then the regenerator data was used to qualitatively validate the performance model. Finally the optimization results were presented.

The packed sphere regenerator produced a much larger pressure drop than the parallel plate approach, however the performance in terms of useful cooling power was also far superior. Cooling power up to 50 W was observed when operating at 4 Hz and temperatures spans up to 29 °C. While Appendix II and III present the findings more in depth, this Chapter only shows results relevant for the model validation, with heat rejection temperature set at 22 °C.

The model validation results were then presented, and finally optimization solutions were displayed in the form of contour plots, where each optimized design point meets a specific scenario for cooling power and MCE. The sensitivity analysis shows some interesting trends. A relatively low field (1 T) is preferred due to the large cost of the magnet. Utilization is in the expected range, and the operating frequency is generally limited below 4 Hz, because of the viscous losses. The device cost is in general penalized by the cost of the magnet, however it is important to recognize that the chosen device configuration is characterized by a very low Λ_{cool}, and therefore such result is not a surprise.

The experimental and model results demonstrate that the objectives of the research were successfully met. A prototype device operating as specified was built and characterized, and a predictive mathematical tool to be used as a design guide was successfully developed.

Chapter 6

Conclusion and Recommendations

This thesis presented the development of a novel MR prototype and a mathematical tool identifying preferred characteristics for minimum cost of cooling.

A novel MR is described. The device is compact, simple, and modular. Compared to many other MR devices, it is easy to operate and capable of high operating frequencies. Using 110 g of gadolinium as a refrigerant, the device produced a maximum temperature span under no thermal load of 29 °C, and 10 °C under 50 W. For most operating conditions the COP ranged between 0.8 and 0 for temperature spans between 0 and 29 °C, while a maximum value of 1.6 is found when operating at 1.4 Hz with a utilization of 1.28. A maximum operating frequency of 4 Hz was dictated by the large pressure drop in the regenerators. Most of the efficiency loss was found in the drive system for the magnets and fluid displacer. Using a single, refrigerant the maximum specific exergetic cooling power is found to be 0.085 $WT^{-1}cm^{-3}$, when operating with a utilization of 1.03, frequency of 4 Hz, and T_H set at 22 °C.

An experimental investigation of device performance using parallel plate AMRs is described. The objective is to characterize a regenerator with significantly different hydraulic properties than a bed of packed spheres, with limited heat transfer but much reduced viscous losses. The plates are 0.54 mm thick, with a spacing of 0.3 mm to maintain a porosity similar to the backed spheres. In general, it is found that the largest temperature spans are obtained at the lowest frequencies and that the cooling power is significantly smaller than the case of spheres. This is attributed to the dimensions of the plates and their spacing. Plates with a thickness of 0.1 mm and a spacing of 0.05 mm are needed if heat transfer characteristics similar to those obtained when using spheres are to be obtained. Temperature span sensitivity to utilization and rejection temperatures are shown with maximum no-load spans found with utilization of ~0.5. Maximum spans for the configuration and conditions explored were ~12 °C. While the poor experimental result performance is due to the large hydraulic diameter of the structure, in general the

challenge with parallel plate geometry is that their performance is heavily affected by flow maldistribution. This requires a very high manufacturing precision on already extremely small mechanical structures.

An optimization model of a dual Halbach cylinder magnetic refrigerator was developed using a simplified analytical method to evaluate the AMR performance. The objective function is the total cost rate based on a 10 year life cycle. The constraints are set to be minimum cooling power, maximum pressure drop, and maximum peak field. The performance model is first validated against extrapolated experimental data. Results show that, under the given constraints and configuration, cost limiting factors are the permanent magnet size and pressure drop, while, surprisingly, power requirements are achieved with a relatively low magnetic field, operating frequency, and utilization factor. Among all results, it is found that if cost rate is to be maximized, the target magnetic field should not be higher than 1.15 T, operating frequency no more than 4.5 Hz and utilization not larger than 0.6 and that the optimal cost rate ranges between 0.4 and 2.4 ¢/h. Finally, even if a constraint of 0.7 MPa is removed, the optimization model generally avoids solutions operating at higher pressure drop because a higher operating cost due to lower efficiency occurs.

Two novel contributions to the field of active magnetic regenerative refrigeration are described, an experimental device and a mathematical model. The PMMR can characterize regenerators to an unmatched parameter range and resolution, effectively and with ease. The mathematical model is flexible and effective tool for evaluating performance, design impacts and cost sensitivity.

6.1 Future work and Recommendations

Future work includes further refinements of the tool presented and further experimental and theoretical investigations on the AMR.

Improvement of the design of the PMMR

The PMMR I is a good machine, yet vast improvements can be done to augment its performance. In terms of performance Figure 5-2 shows that there is a lot of room for improving efficiency. This can be done by 1) reducing the torque necessary to rotate the

magnet 2) increasing the cooling per cycle, and 3) reducing the viscous losses, 4) improving motor efficiency.

Torques can be improved by optimizing the Halbach cylinders. Mostly this is done by minimizing the stray field interactions between the inner and outer cylinder. The cylinders could be designed with a larger gap and the outer ones longer than the inner ones. Further torque cancellation could be done by other mechanical means, such as a flywheel, a spring-loaded mechanism, or another magnetic system counteracting the residue torque.

Cooling power per cycle can be augmented by improving the field waveform. The inner and outer magnet field intensities could be more closely matched to minimize the low field condition. The PMMR has a low field of about 150 mT, taking this value to close to 0 T could significantly improve the performance. Increasing the maximum field would also contribute positively. This can be done by using more exotic rare earth compounds with higher magnetic remanence. Also using a larger number of segments would allow generating a field closer to an ideal Halbach cylinder. Modifying the magnetization waveform from squared sine to sine would eliminate the very narrow demagnetization part of the cycle effectively improving the heat transfer during the cold blow. This could have a crucial effect on the cycle performance and of primary interest for further developments of this configuration.

Viscous losses are for the most part caused by the regenerator pressure drop, a device with a larger bore and regenerator larger cross sectional area would allow more refrigerant per cycle, thus more cooling per cycle. A pump-distribution valve system could also potentially be more efficient than and hydraulic cylinder.

Optimization routine further developments

Often, when performing optimizations on large parameter spaces and complex physics, it is convenient to first attempt a simplified search, to give a global view, and then apply a more refined and resource intensive study to a much narrower domain. The optimization routine presented in this research is effective in rapidly scanning a very large domain, while a more detailed model could then be used to obtain more accurate

estimates in the target design and operating parameter values. In order to give predictions of real devices the model needs to implement real refrigerant properties, or at least target refrigerant properties that can be realistically manufactured. This would dramatically slow down the optimization model, and that is why such a model is suggested to be used to refine the study presented in this thesis. Burdyny validated the model using real second order refrigerants against the experimental results from the AMRTA and PMMR. It is suggested to use this model, which has the ability of shaping real thermodynamic material properties, for the next step in the optimization modeling.

Further work in the MR technology development

The main two challenges in the AMR performance are the development of a satisfactory temperature span and pressure drop. These depend on both regenerator composition and matrix topology. Given the current refrigerant performance, layering seems to be a necessity for reaching sufficiently large temperature spans. Experimental and model results should focus in finding the most effective way of implementing layering and predicting how this can be successfully tailored to specific applications. While beds of packed spheres seem to be effective for AMR prototyping, matrices with superior thermo-hydraulic performance need to be researched for increasing MR power densities.

References

[1] Gschneidner Jr., K. A., Pecharsky, V. K., Thirty years of near room temperature magnetic cooling: Where we are today and future prospects, International Journal of Refrigeration, vol. 31, pp. 945-961, 2008.

[2] Gschneidner, K.A., and Pecharsky, V.K., *Intermetallic Compounds:* Vol. 3, *Principles and Practise.* John Wiley, pp. 519, 2002.

[3] Grössinger R., Haas M., Turtelli S., Magnetocaloric versus thermoelectric effect – new systems for thermal applications, *Forth IIF-IIR International Conference on Magnetic Refrigeration at Room Temperature*, Baoutou, pp. 15-29, 2010.

[4] Rowe, A., Active Magnetic Regenerators: Performance in the Vicinity of Para Ferromagnetic Second Order Phase Transition, *Ph.D. Thesis, University of Victoria*, Victoria 2002.

[5] Yu, B.F., Gao, Q., Zhang, B., Meng, X.Z., Chen, Z., Review on Research of Room Temperature Magnetic Refrigeration, *International Journal of Refrigeration*, vol. 26, pp 622-636, 2003.

[6] Barclay J., 1985, Low-temperature magnetic refrigerator, US patent, patent number 4,507,927.

[7] Yu, B., Liu, M., Egolf, P. W. & Kitanovski, A. A review of magnetic refrigerator and heat pump prototypes built before the year 2010, *International Journal of Refrigeration* vol. 33, pp. 1029-1060 (2010).

[8] Gschneidner, K.A., and Pecharsky, V.K., Tsokol, A. O., Recent Developments in Magnetocaloric Materials, *Rep. Prog. Phys.* 68 1479-1539, 2005.

[9] Rowe, A., Tura, A., Experimental investigation of a three-material layered active magnetic regenerator, *International Journal of Refrigeration*, vol. 29, Issue 8, pp 1286-1293, 2006.

[10] Green, G., Chafe, J., Stevens, J., Humphrey, J., A Gadolinium-Terbium Active Magnetic Regenerator, in *Advances in Cryogenic Engineering*, vol.35, pp. 1165, 1990.

[11] Zimm, C., Johnson, J., Murphy, R.W., Test Results on a 50 K Magnetic Refrigerator, in *Advances in Cryogenic Engineering*, vol. 41, pp. 1675, 1996.

[12] Zimm, C., Jastrab, A., Sternberg, A., Pecharsky, V., Gschneidner, K., Osborne, M., Anderson, I., Description and Performance of a Near-Room Temperature Magnetic Refrigerator, in *Advances in Cryogenic Engineering*, vol. 43, pp. 1759, 1998.

[13] Tura, A., 2005, Active Magnetic Regenerator Experimental Optimization, *MaSc Thesis*, University of Victoria, Victoria, 2005.

[14] Tura, A., Roszmann, J., Rowe, A., Cryogenic Active Magnetic Regenerator Test Apparatus, *CEC-ICMC Proceedings*, Keystone, Colorado, 2005.

[15] Coulumb, D., The IIR and the Environmental Challenges Facing the Refrigeration Sector, *Proceedings of IIR International Conference on Magnetic Refrigeration at Room Temperature*, Opening Session, Portoroz, Slovenia, pp. 3-5, 2007

[16] Russek, S., Auringer, J., Boeder, A., Chell, J., Jacobs, S., Zimm, C., The Performance of a Rotary Magnetic Refrigerator with Layered Beds, *Proceedings of IIR International Conference on Magnetic Refrigeration at Room Temperature*, Baotou, China, 2010.

[17] Jacobs, S., Auringer, J., Boeder, A., J., Chell, Komorowski, L., Leonard, J.,Russek, S., Zimm, C., The Performance of a large-scale rotary magnetic refrigerator, *Proceedings of IIR International Conference on Magnetic Refrigeration at Room Temperature*, Grenoble, France, pp. 421-428, 2012.

[18] Hirano, N., Nagaya, S., Okamura, T., Kawanami, T, Wanda, H., Development of Room Temperature Refrigerator –Overall Plan-, *Proceedings of IIR International Conference on Magnetic Refrigeration at Room Temperature*, Portoroz, Slovenia, April 11-13 2007, pp. 281-287.

[19] Hirano, N., S. Nagaya, M. Takahashi, T. Kuriyama, K. Ito, and S. Nomura, Development of magnetic refrigerator for room temperature application, in *Advances in Cryogenic Engineeering*, vol. 47, pp.1027-1034, 2002.

[20] Bahl, C.R.H., Engelbrecht, K., Eriksen, D., Lozano, J.A., Bjørk, R., Geyti, J., Nielsen, K.K., Smith, A., Pryds, N.,Development and experimental results from a 1 kW Prototype AMR, *Proceedings of IIR International Conference on Magnetic Refrigeration at Room Temperature*, Grenoble, France, pp. 53-60, 2012.

[21] Bahl, C.R.H., Magnet design at DTU: Challenges in AMR magnet design, DTU-UFSC workshop 'Identifying Ways to Increase the Efficiency of Magnetocaloric Devices', Florianopolis, Brazil, 2013.

[22] Coey, J.M.D., Industrial applications of permanent magnetism, *Physica Scripta*, vol T66, pp 60-69, 1996.

[23] Evans, B.M., West, D.L., Mallow, A., Abdelaziz, O., Scaling and optimization of magnetic refrigeration for commercial building HVAC systems greater than 175 kW in capacity, *Proceedings of IIR International Conference on Magnetic Refrigeration at Room Temperature*, Grenoble, France, pp. 349-356, 2012.

[24] Nielsen, K. K., Bahl, C. R. H., and Engelbrecht, K., The effect of flow maldistribution in heterogeneous parallel-plate active magnetic regenerators, *J. Phys. D: Appl. Phys.* 46 105002, 2013.

[25] Peksoy O., Rowe A., Demagnetizing effects in active magnetic regenerators, *Journal of Magnetism and Magnetic Materials* 288, pp 424–432, 2005.

[26] Peksoy O., Tura, A., Rowe A, Shimmed active magnetic regenerator for use in thermodynamic devices, *Patent US 20100107654 A1*.

[27] Rowe, A., Configuration and performance analysis of magnetic refrigerators, *International Journal of Refrigeration*, vol. **34,** pp 169-177, 2011.

[28] Bjørk, R., Bahl, C.R.H., Smith, A., Pryds, N., Review and comparison of magnet designs for magnetic refrigeration, *International Journal of Refrigeration*, vol. 33, Issue 3, pp. 437-448, 2009.

[29] Russek, S.L., Zimm, C., Potential for cost effective magnetocaloric air conditioning systems, *Proceedings of IIR International Conference on Magnetic Refrigeration at Room Temperature*, Montreoux, Switzerland, pp. 59-68, 2005.

[30] Kitanovski, A., Egolf, P.W., Application of magnetic refrigeration and its assessment, *Journal of Magnetism and Magnetic Materials*, vol. 321, Issue 7, pp. 777-781, 2009.

[31] Bjørk, R., Smith, A., Bahl, C.R.H., Pryds N., 2011, Determining the minimum mass and cost of a magnetic refrigerator, *International Journal of Refrigeration*, vol. 34, Issue 8, pp. 1805-1816, 2011.

[32] Gschneidner, K.A., and Pecharsky, V.K., Tsokol, A. O., Recent Developments in Magnetocaloric Materials, *Rep. Prog. Phys.* 68 1479-1539, 2005.

[33] Burdyny, T., Simplified Modeling of Active Magnetic Regenerators, *MaSc Thesis*, University of Victoria, Victoria, 2012.

[34] Engelbrecht, K., Bahl, C. R. H., Evaluating the effect of magnetocaloric properties on magnetic refrigeration performance, *J. Appl. Phys*. 108: 123918, 2010.

[35] Hall, J.L., Reid, C.E., Spearing, I.G., and Barclay, J.A., Thermodynamic Considerations for the Design of Active Magnetic Regenerative Refrigerators, in *Advances in Cryogenic Engineering*, vol. 41, pp. 1653, 1996.

[36] Dikeos, J. and Rowe, A., Validation of an Active Magnetic Regenerator (AMR) Test Apparatus Model, *International Journal of Refrigeration*, vol. 36, Issue 3, pp. 921-931, 2013.

[37] Li, P., Gong, M., Yao, G., Wu, J., A practical model for analysis of active magnetic regenerative refrigerators for room temperature applications, *International Journal of Refrigeration*, vol. 29, Issue 8, pp. 1259-1266, 2006.

[38] Bjørk, R., Designing a magnet for magnetic refrigeration, *Ph.D. Thesis, Risø*, *DTU*, Copenhagen 2010.

[39] Ní Mhíocháin T.R. , Weaire D., McMurry S.M., Coey J.M.D., Analysis of torque in nested magnetic cylinders, *J. Appl. Phys.,* 86: 6412-6425,1999.

[40] Franco, V., Blazquez, J.S., Ingale, B., Conde, A., The Magnetocaloric Effect and Magnetic Refrigeration Near RoomTemperature: Materials and Models, *Annual Review of Materials Research*, Volume: 42 Pages: 305-342, 2012.

[41] Rowe A., Thermodynamics of active magnetic regenerators: Part I*, Cryogenics*, 52 (2-3): 111-118, 2012.

[42] Rowe, A., Thermodynamics of active magnetic regenerators: Part II, *Cryogenics*, 52 (2-3): 119-128, 2012.

[43] Burdyny, T., Rowe A., 2013, Simplified modeling of active magnetic regenerators, *International Journal of Refrigeration,* vol 36, Issue 3, pp. 932-940, 2013.

[44] Rowe, A. M., Barclay, J. A., Ideal magnetocaloric effect for active magnetic regenerators, *Journal of Applied Physics* , vol.93, no.3, pp.1672,1676, 2003.

[45] Kaviany, M., 1995, Principles of Heat Transfer in Porous Media, Springer.

[46] Schmidt F.W. and Wilmott A.J., 1981, Thermal energy storage and regeneration, Hemisphere, Washington DC.

[47] Embraco compressor technical information, isobutane compressor line -50 Hz- HBP applications .

[48] Tura, A., Rowe, A., Permanent magnet magnetic refrigerator design and experimental characterization, *International Journal of Refrigeration*, 34(3):628-639, 2011.

[49] Tura, A., Nelsen, K.K., Rowe, A., Experimental and modelling results of a parallel-plate based active magnetic regenerator, *International Journal of Refrigeration*, vol. 35, pp. 1518-1527, 2012.

[50] Rowe, A., Performance metrics for active magnetic refrigerators, *3rd IIF-IIR Conference on Magnetic Refrigeration at Room Temperature*, Des Moines, Iowa, 2009.

[51] Zimm, C., Auringer, J., Boeder, A., Chell, J., Russek, S., Sternberg, A., Design and initial performance of a magnetic refrigerator with rotating permanent magnet, *Proceedings of IIR International Conference on Magnetic Refrigeration at Room Temperature*, Portoroz, Slovenia, pp. 341-347, 2007.

Appendix I
List of Up-to-Present Published Magnetic Refrigerators

	Name and location	*Date of announcement*	*Type and max. frequency (Hz)*	*Max. cooling Power (W)*	*Max. ΔT (K)*	*Max. magnetic field strength (T)*	*Magnetocaloric regenerator material*
1	Brown (1976, 1978) NASA, USA	1976	Reciprocating, Styrling/	/	47	Supercond.7	1 mm Gd plates, 20% ethyl alcohol- water
2	Kirol and Dacus (1987) Idaho National Engineering Laboratory, USA	1987	Rotating type, Ericsson cycle 0.5 Hz	/	11	Permanent 0.9 T	125 Gd plates 76 mm, spacing 127 mm, Water
3	Green et al. (1990) US NAVY, USA	1990	Reciprocating, 0.02 Hz	/	24	Supercond.7	GdeTb metal ribbons, Nitrogen gas
4	Zimm et al. (1998) AMES Ast. Corp. A., USA	1997	Reciprocating	600	38	Supercond. 5	Gd spheres 0.15- 0.3 mm
5	Bohigas et al. (2000) Mater. Science Institute, Barcelona, Spain	2000	Rotary 0.8 Hz	/	5	Permanent 0.9	Gd as ribbon on plastic disk, olive oil
6	Okamura et al. (2005) Tokyo Inst. Tech Chubu Electric Power, Japan	2000	Reciprocating	100	21	Supercond. 4	Gd spheres
7	Rowe and Barclay (2002) Univ. Victoria, Victoria, Canada	2001	Reciprocating, 0.8 Hz	2	14	Supercond 2	Gd & Gd1 xTbx layered beds of grains, Helium
8	Zimm et al. (2003, 2005, 2006), Ast. Corp. A., Madison, Wisconsin, USA	2001	Rotary 4 Hz	50	25	Permanent 1.5	Gd, GdEr spheres, 0.25-0.5 mm, water
10	Blumenfeld et al. (2002) Los Alamos Natl. Lab. New Mexico, USA	2002	Charging- discharging a coil, no moving parts	3	15	Supercond 1.7	Gd powder.
11	Okamura et al. (2005) Tok.Inst.Tech. Chubu Electric Japan	2003	Rotary (rotation of magnets) 0.4 Hz	60	8	Permanent 0.77	Gd1-xDyx layered alloys, spheres 0.6 mm, 1 kg, water
12	Clot et al. (2003) Lab. d'Electrontechnique Grenoble, France	2003	Reciprocating 0.5 Hz	8.8	4	Permanent 0.8	Gd foils, 1 mm with gaps for water, 0.1mm
13	Richard et al. (2004) Univ. Quebec, U Univ. Victoria, Canada	2004	Reciprocating	2	14	Supercond 2	Gd-R alloys layered beds of grains
14	Rowe et al. (2005, 2006) Univ. Victoria Canada	2004	Reciprocating 1 Hz	10	50	Supercond 2	Gd-R layered alloys, Helium
15	Rowe and Rowe Univ. Victoria Canada	2005	Reciprocating 1 Hz	/	86	Supercond 5	Gd-R layered alloys, Tb, Helium
16	Shir et al. (2005) George Washington Univ., Ashburn, Virginia, USA	2005	Reciprocating	/	5	Permanent 2	Gd powder
17	Okamura et al. (2007) Tokyo I. Tech., Chubu Electric Power, Japan	2005	Rotary	110	10	Permanent 0.77	Gd alloys MnAsSb alloys, and Gd packedbeds Water

	Name and location	*Date of announcement*	*Type and max. frequency (Hz)*	*Max. cooling Power (W)*	*Max. ΔT (K)*	*Max. magnetic field strength (T)*	*Magnetocaloric regenerator material*
18	Vasile and Mu¨ ller (2005, 2006) INSA, Cooltech Applications Strasbourg, France	2005	Rotary	360	10	Permanent 2.4	Gd plates, water
19	Yu et al. (2005) School of Energy and Power Engineering, Xi'an Jiatong University Xi'an, China	2005	Reciprocating	18.7	3	Electro-magnet (water cooled) 2.18	Gd 0.3mmand Gd5Si2Ge2 particles, water
20	Kawanami et al. (2005) Graduate School of Engineering, Hokkaido University, Japan	2005	Reciprocating, 0.02 Hz	/	10	Permanent 1.0	Gd, 63% vol.- fraction, distilled water
21	Yao et al. (2006) Technical Institute of Physics and Chemistry, Beijing, China	2006	Reciprocating 1 Hz	51	42	Permanent 1.5	Gd particles, helium
22	Egolf et al. (2006aec) University of Applied Sc.of Western Switzerland, Switzerland	2006	Rotary 0.8	-	-	Permanent 0.8	Gd particles, air
23	O Okamura et al. (2005, 2007) Tokyo Inst. Tech., Chubu Electric Power, Japan	2006	Rotary 0.5 Hz	560	8	Permanent 1.1	Gd foils, water
24	Huang et al. (2006, 2007) Baotou Research Institute of Rare Earth, China	2006	Reciprocating	50	18	Permanent 1.5	Gd 750 g and $LaFe_{10.97}Co_{0.78}Si_{1.05}B_{0.2}$ 200 g, alkalescent water solution, Ph = 10
25	Zimm et al. (2007) Astronautics Corp. America Madison, Wisconsin, USA	2007	Rotary 4 Hz	220	12	Permanent 1.5	Gd plates, water
26	Tura and Rowe (2007) Univ. Victoria Victoria, Canada	2007	Rotary 4 Hz	/	13.2	Permanent 1.47	Gd flakes, 0.6 mm, water
27	Buchelnikov et al. (2007) Chelyabinsk State University Russia	2007	Rotary 10 Hz	40	/	Permanent 1	Gd, NiMnGa alloys
28	Petersen et al. (2007) Risø National Laboratory, Denmark	2007	Reciprocating <1 Hz	/	8.7	Permanent 1.2	Gd plates, 1 mm
29	Muller et al. (2007) INSA, Cooltech Applications Strasbourg, France	2007	Rotary magnet	/	/	Permanent 1.3	Gd, water
30	Chen et al. (2007) School of Materials Science and Engineering, Sichuan University Chengdu, China	2007	Rotary magnet 0.7 Hz	40	11.5	Permanent 1.5	Gd particles, 0.5 mm, 1 kg, water

	Name and location	*Date of announcement*	*Type and max. frequency (Hz)*	*Max. cooling Power (W)*	*Max. ΔT (K)*	*Max. magnetic field strength (T)*	*Magnetocaloric regenerator material*
31	Nakamura et al. (2008) Graduate School of Engr, Hokkaido University in Japan	2008	Reciprocating	/	/	Permanent 2	Gd particles, 33.4 g, water or air
32	Hirano et al. (2009) Hokkaido Industrial Research Institute, Japan	2009	Reciprocating	/	~2	Permanent 2.3	LaFeSi-type material, air
33	Zheng et al. (2009) South China University of Technology, Chian	2009	Reciprocating	/	/	Permanent 1.5	Gd
34	Bour et al. (2009), Cooltech Applications, France	2009	Reciprocating 1 Hz	/	16.1	Permanent 1.1	Gd plates, 0.6 mm, water
35	Coelho et al. (2009) Universidade Estadual de Campinas, Brazil	2009	Rotary 0.85	/	11	Electro-magn. 2.3	Gd pins, ethyl alcohol
36	Dupuis et al. (2009) Grenoble Electrcal Engineering Laboratory, France	2009	Reciprocating 1 Hz	/	7.8	Permanent 0.8	Gd sheets, 1 mm
37	Kim and Jeong (2009) Korea Advanced Institute of Science and Technology	2009	Reciprocating 1Hz	/	16	Permanent 1.58	Gd particles, 325 -500 mm, Helium
38	Pryds et al. (2009) Risø DTU, Denmark	2009	Reciprocating	/	/	Permanent 1.5	La0.67Ca0.33xSrxMnO3 plates, water and ethanol mixt
39	Sari et al. (2009) IGT in University of Applied Sciences of Western Switzerland, Switzerland	2009	Reciprocating	/	/	Permanent 2	LaFe11Co0.9Si1.1 and Gd, air
40	Tagliafico et al. (2009) University of Genoa, Genoa, Italy	2009	Reciprocating <0.2 Hz	/	/	Permanent 1.5	Gd, 300 mm, water
41	Tura and Rowe (2009) University of Victoria, Victoria, Canada	2009	Rotary 4 Hz	50	29	Permanent 1.47	Gd spheres, 300 mm
41	Tusek et al. (2009) University of Ljubljana, Slovenia	2009	Rotary 4 Hz``	/	~7	Permanent 1.4	Gd plates, 0.3 mm, 600 g, distillated water
42	Russek et al (2010) Ast. Corp. A., Madison, Wisconsin, USA	2010	Rotary 4 Hz``	840	19	Permanent 1.5	Gd spheres, 900 g
43	Trevizoli et al (20011) Federal University of Santa Caterina, Brazil	2011	Reciprocating 0.14	4	4.2	Permanent 1.7	Gd plates, 150 g
44	Jacob et al (2012) Ast. Corp. A., Madison, Wisconsin, USA	2012	Rotary 4 Hz``	2049	~	Permanent 1.5	LaFeH alloys spheres,
45	Bahl et al, (2012) Risø National Laboratory, Denmark	2012	Rotary 2.5 Hz	1010	25	Permanent 1.4	Gd spheres, 2800 g
46	Arnold et al (2012), University of Victoria, Victoria, Canada	2012	Rotary 0.8 Hz	100	32	Permanent 1.45	Gd spheres, 620 g

Appendix II
Permanent Magnet Magnetic Refrigerator Design and Experimental Characterization

INTERNATIONAL JOURNAL OF REFRIGERATION XXX (2011) 1–12

available at www.sciencedirect.com

ScienceDirect

journal homepage: www.elsevier.com/locate/ijrefrig

Permanent magnet magnetic refrigerator design and experimental characterization

*A. Tura**, *A. Rowe*

Department of Mechanical Engineering, Institute for Integrated Energy Systems, University of Victoria, 3800 Finnerty Rd, Victoria, B.C. V8W 3P6, Canada

ARTICLE INFO

Article history:
Received 29 October 2010
Received in revised form
15 December 2010
Accepted 15 December 2010
Available online xxx

Keywords:
Magnetic refrigerator
Magnet
Magnetic field
Gadolinium
Regenerator
Curie
Cop

ABSTRACT

Magnetic refrigeration (MR) using permanent magnets is being investigated for near-room temperature applications. An MR prototype is described and results using gadolinium as refrigerant are presented. Important design features are simple sealing, compactness, high operating frequencies, and ease of use. Using a total of 110 g of refrigerant, the device produces a maximum temperature span under no thermal load of 29 °C, and 10 °C under 50 W. The overall COP determined by using the power to the drive motor is between 0.3 and 0.8 under most operating conditions and temperature spans. The maximum COP measured is 1.6 with a span of 2.5 °C when operating at 1.4 Hz and utilization of 1.28. If the inefficiency of the motor is removed the maximum COP is 2.2, and, when the magnet drive losses are excluded, the maximum COP becomes 10. The peak specific exergetic cooling power is 0.085 W T^{-1} cm^{-3}.

Conception d'un réfrigérateur magnétique à aimant permanent et caractérisation expérimentale

Mots clés : Réfrigérateur magnétique ; Aimant ; Champ magnétique ; Gadolinium ; Régénérateur ; Curie ; COP

1. Introduction

During the past decade a number of MR prototypes using permanent magnets have been reported in the literature (Yu et al., 2010). Only a few of these have reported an extensive range of experimental results. These include the Tokyo Institute of Technology's rotating magnet refrigerator (Chubu Electric Power Co.) (Okamura et al., 2006), and Astronautics Corporation's (ACA) second (Zimm et al., 2006) and third generation magnetic refrigerators (Zimm et al., 2007).

The second generation (ACA) magnetic refrigerator represented the first attempt to develop a machine that had the look and feel of a compact refrigerator rather than a large and complex laboratory apparatus. The device, presented the first

* *Corresponding author*. Tel.: +1 250 721 7295; fax: +1 250 721 6051.
E-mail address: atura@uvic.ca (A. Tura).

0140-7007/$ – see front matter © 2010 Elsevier Ltd and IIR. All rights reserved.
doi:10.1016/j.ijrefrig.2010.12.009

Nomenclature

Acronyms

AMR(R)	active magnetic regenerator (refrigerator)
MCE	magnetocaloric effect (adiabatic temperature change)
MR	magnetic refrigerator
PMMR	permanent magnet magnetic refrigerator

Symbols

A	cross sectional area/surface area
B	magnetic flux density
c	heat capacity
D	diameter
H	magnetic field intensity
h	heat transfer coefficient
I	current
k	thermal conductivity
L	inductance/Length
M	magnetization
m	mass/mass magnetization
p	pressure
Q	energy flux/heat transfer
r	radius
Re	Reynold's number
S	stroke
T	temperature
t	time
W	work

Greek

α	porosity
β	balance/isothermal compressibility
Φ	utilization
φ	fluid thermal capacity
μ	viscosity/magnetic permeability
ρ	density
τ	period

Subscripts

ad	adiabatic
B	blow
C	cold
$Curie$	curie point
d	demagnetizing/displacer
f	fluid
H	hot
$high$	high
i	inner
low	low
M	magnetic
max	maximum
min	minimum
r	magnetic remanence
ref	reference value
o	outer
P	pressure/particle
rev	reversible
irr	irreversible
s	solid
x	location

time in 2001, consisted of a disc housing the refrigerant (a wheel) rotating through a gap in a static, C-shaped, permanent magnet. The field in the gap was 1.5 T. As the regenerators move in and out of the gap, they undergo magnetization and demagnetization. The magnetic wheel had a capacity of approximately 180 g of refrigerant distributed in six regenerators. The refrigerator produced cooling powers up to 50 W and a no-load temperature span up to 25 C, operating up 4 Hz. References (Zimm et al., 2006) and (Engelbrecht, 2008) provide additional detail.

Chubu developed a machine with a cooling capacity of 500 W and a COP of 3 or greater (Okamura et al., 2007) purportedly for air conditioning applications. This was their second generation machine after a proof of concept reciprocating device was previously built and tested (Hirano et al., 2002). In 2005, the initial rotary magnetic refrigeration system based on moving permanent magnets and stationary regenerators was developed. The machine produced a cooling power of 60 W. Through redesigning the magnets, magnetic yoke, and regenerator flow path, they finally obtained a cooling capacity of 540 W and a COP of 1.8 over a 0.2 K temperature span. This refrigerator consisted of four regenerators each with a mass of 1 kg, and a peak magnetic field generator capable of 1.1 T. The operating frequency was 0.5 Hz.

Astronautics Corporation built their third generation refrigerator in 2007 (Zimm et al., 2007). This design uses a rotating permanent magnet and twelve stationary active regenerators. The choice of a rotating magnet simplifies the heat transfer liquid sealing and flow control. The machine produced a cooling power up to 220 W with large COP (up to 13) for no temperature span; however, the efficiency measurements did not incorporate the mechanical inefficiencies of motors and pumps. Recently a cooling power of 840 W at zero span and 400 W at a span of 10 °C using 0.9 kg of Gd was reported (Russek et al., 2010). Also 400 W on a span of 13.4 °C was obtained using regenerator beds made of five layers of LaFeSiH. A review of these and other devices can be found in several review articles (Yu et al., 2010; Gschneidner and Pecharsky, 2008), reporting up to 41 prototypes so far published.

2. AMR design

A large number of parameters affect the behavior and the performance of an AMR (Table 1) (Hall et al., 1996). If a good thermal design is realized, an important operating parameter in determining performance is utilization, which is the thermal capacity ratio between the fluid displaced in the regenerator and the total thermal mass of the solid. With a single material, a reference utilization can be defined using:

$$\Phi \equiv \frac{m_f c_f}{M_s c_s} \tag{1}$$

where m_f is the fluid mass blown over one cycle, c_f the fluid specific heat, M_s is the mass of a single regenerator mass and c_s

Please cite this article in press as: Tura, A., Rowe, A., Permanent magnet magnetic refrigerator design and experimental characterization, International Journal of Refrigeration (2011), doi:10.1016/j.ijrefrig.2010.12.009

Table 1 – Variables in an AMR system.

Geometric	Magnetic	Thermofluid/ Operational
Porosity	Field intensity	Heat transfer fluid
Regenerator shape	AMR material	Utilization, Φ
Regenerator aspect ratio	Field distribution	Frequency
Matrix geometry		Pressure (for gaseous heat transfer fluid)
		Heat sink temperature
		Regenerator composition
		Phasing and magnetization-fluid flux waveform

the refrigerant specific heat in the demagnetized state and at the Curie temperature T_{Curie}. By fixing the desired range of utilizations the relative sizing of the fluid flow system and regenerators is determined. A designer can begin device sizing from here by setting the mass of refrigerant to be used. With a particular configuration in mind for both the magnet and device, an estimate of total cost can be determined (Rowe, 2011).

Current magnet refrigeration prototypes are not competitive with conventional technology: temperature spans and cooling powers are too low and, as a result, costs are too high.Some ways to improve MR performance are:

1. Find better refrigerants with larger MCE;
2. Develop better materials for permanent magnets (larger B_r/H_c);
3. Develop devices to operate at higher frequencies: higher frequencies can mean larger cooling power. This would require improved regenerator matrix geometries to reduce pressure drop while maintaining porosity and heat transfer with low axial conduction and eddy current losses.
4. Optimizing the properties along a regenerator by using different alloys: This strategy follows the same logic of point 1, however it does not necessarily imply new materials. A layered regenerator has trade-offs in terms of cooling power and temperature span. The optimal number of layers, composition, and geometry need to be tailored to a specific design conditions (Tura, 2005).
5. Improving control strategies to optimize operational parameters to match power demand without penalizing efficiency.

The PMMR design described here addresses points 3–5. Frequencies as high as 5 Hz are possible depending upon the matrix structure, amount of material, and the volume of fluid displaced. The regenerators can be easily changed and may consist of one or more materials. Parameters such as frequency and utilization can be varied to investigate preferred operating strategies. The following section provides a complete description of the device, followed by experimental results using gadolinium as a refrigerant.

2.1. Design objectives

Although high performance with low cost is desirable, at this stage of development, there are other drivers governing the design of a laboratory apparatus. The following aspects are also important considerations:

1. Compact with small field generators and refrigerant mass;
2. Capable of high operating frequencies;
3. Ease of access to refrigerant for replacement and inspection;
4. Easy to instrument;
5. Small hydraulic dead volume (Jacobs, 2009) between regenerators and heat exchangers; and,
6. Modularity, to simplify components upgrades.

In this design a strong emphasis is placed on the magnet and refrigerant mass and volume as these are among the main contributors to cost. The ability to operate at high frequencies is necessary for achieving high power densities. Finally, testing a variety of regenerator matrix compositions and geometries implies replacing the refrigerant frequently. Thus a design that allows easy access to the regenerators is desirable. A design solution that satisfies such objectives is a rotary type of device with moving permanent magnets and stationary regenerators.

2.2. Design options

The magnetic refrigerants available to a designer will ultimately decide if AMR refrigerators can become commercially successful. And, with this in mind, new alloys are being synthesized and characterized (Gschneidner and Pecharsky, 2008). However, given a specified refrigerant or choice of refrigerants, the performance of an AMR refrigerator will depend upon good mechanical design choices, effective regenerator design, and optimized operating parameters.

The mechanical design of AMR systems is governed by two main decisions: (1) the method of creating the required field-flow waveforms, and (2) the type of magnet. Items 1 and 2 are closely related and will impact the resulting forces that the structure must be designed to accommodate. Once the drive system configuration has been determined, there are three sub-systems to design: the magnet, regenerator, and fluid flow/heat transfer system.

The device concept is illustrated in Fig. 1. Two active magnetic regenerators (1) are connected by a fluid transfer loop (water–glycol mix) with oscillating flow. A cold heat exchanger (2) separates the two AMRs, and two hot heat exchangers (3) reject heat from the system. Each AMR bed is alternatively magnetized and demagnetized by a Halbach array (4), where an inside magnet rotates with respect to the outside one. The AMR cycles are synchronized such that they operate in opposite phases. An electric motor (5) drives the inner magnets by means of a timing belt. The fluid can be pulsed through the hydraulic system by means of a pump coupled with a rotary valve or a reciprocating fluid displacer (6) operated by the magnet drive system by means of a crank mechanism (7). An accumulator (8) maintains the operating pressure. A valve (9), allows for filling and pressurizing.

2.3. Magnet

The field generator geometry of choice is a cylindrical nested Halbach array (Fig. 2). Each array has a transverse field in the bore (radial direction) so that when the arrays are rotated with

Please cite this article in press as: Tura, A., Rowe, A., Permanent magnet magnetic refrigerator design and experimental characterization, International Journal of Refrigeration (2011), doi:10.1016/j.ijrefrig.2010.12.009

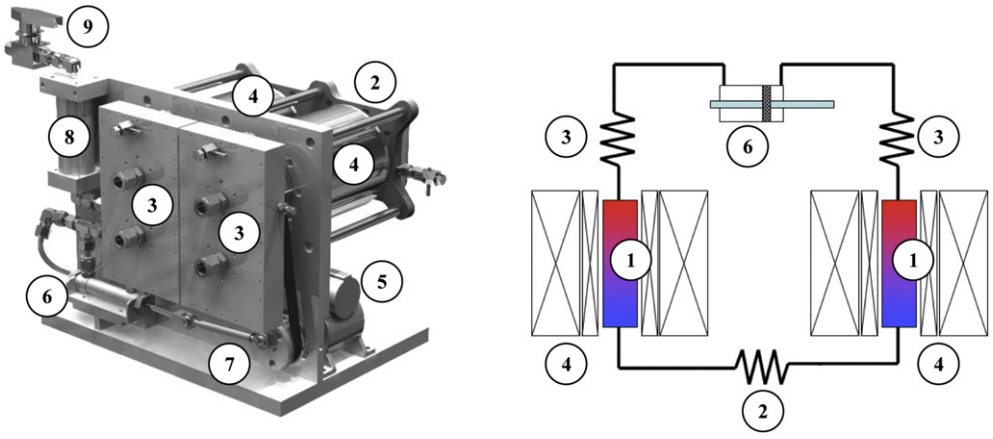

Fig. 1 – The permanent magnet magnetic refrigerator and its hydraulic schematics. (1) AMRs (displayed only in the schematic), (2) Cold heat exchanger, (3) Hot heat exchangers, (4) Halbach cylinders, (5) DC gearmotor, (6) Hydraulic displacer, (7) Crank mechanism, (8) Accumulator, (9) Valve.

respect to each other the field in the inner bore varies as the vector sum of the two fields. Such a configuration allows for high maximum field intensity and a simple mechanism for magnetizing and demagnetizing. Detailed descriptions of Halbach cylinders are available in the literature (Coey, 2002; Bjork et al., 2008). Since the regenerator is stationary no dynamic sealing is required, in addition, only the inner magnet needs to be rotated which is only a fraction of the mass of the entire field generator.

A disadvantage of the nested Halbach design is the magnetization waveform, which is not symmetric between high and low fields. Another issue that arises is that inner bore diameter needs to be relatively small for a large magnetic flux (1 T or more), otherwise the Halbach cylinders might become too large and expensive. Thus regenerators with a high aspect ratio regenerator are favored (length/diameter), which imposes constraints on the regenerator geometry so as to manage viscous losses. In addition the rotation of the inner array with respect to the outer one might require an uneven torque because of the ferromagnetic properties of the refrigerant and the edge effects on the magnets (Bjørk et al., 2010). Coupling two nested arrays in opposite magnetization phase helps balance the torques reducing the required input power.

2.4. *Field generator design*

The Halbach array design is constrained by the maximum field intensity (driven by the magnetic material coercitivity), volume of the cavity, and manufacturing cost. Based on extrapolation of previous experimental results (Tura, 2005) zero-span cooling powers on the order of 200 W could in theory be obtained with a refrigerant volume of 50 cm^3 and an operating frequency of 3–4 Hz. For a specific regenerator diameter, maximum field of 1.5 T, and magnetic material properties (NdFeB), an ideal Halbach array obeys the following equation (Mhiochain et al., 1999):

$$H = \frac{B_r}{\mu_0} \ln\left(\frac{D_o}{D_i}\right) \quad (2)$$

where H is the magnetic Field, B_r is the remanence of the permanent magnet, μ_0 is the magnetic permeability of free space, D_o is the outer diameter, and D_i the inner diameter. Thus, the designer is left with choosing only the length, L, to fully define the field generator geometry. Weight, cost, and manufacturability, led to a Halbach with $D_o/L \sim 1$ for the outer arrays. An ideal Halbach cylinder has a continuously varying polarization direction as function of angle, however for

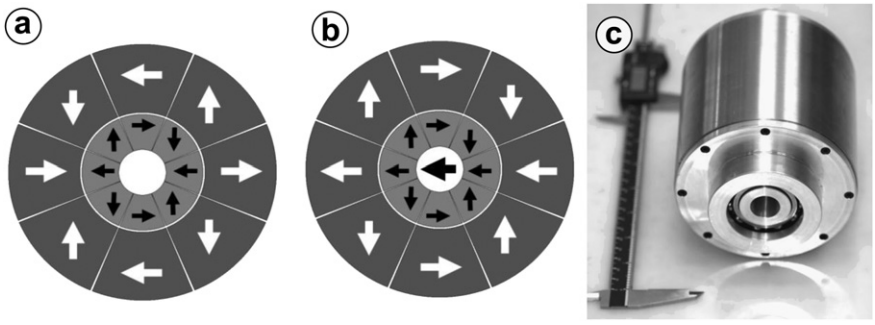

Fig. 2 – Nested Halbach arrays. Each cylinder displays a magnetic field in the bore that is not axial but transversal aligned with the North and South poles. a) If the nested arrays are counter aligned (S–n, N–s) then the inner bore sees almost no field b) if they are aligned (N–n, S–s) then the inner bore sees the sum of the fields. This case is very similar as having a single solid array. c) shows the inner and outer cylinders assembled with the bearings installed to allow relative rotation. Inner bore is also visible, that is where the refrigerant needs to be located.

Please cite this article in press as: Tura, A., Rowe, A., Permanent magnet magnetic refrigerator design and experimental characterization, International Journal of Refrigeration (2011), doi:10.1016/j.ijrefrig.2010.12.009

practical purposes an 8 segment array with uniform magnetization in each section is used.

A 3-D analysis of the design using COMSOL was found to be in good agreement with the maximum experimentally measured field of 1.47 T. Experimental magnetic field measurements were performed with a three-axis Lakeshore mmz-2536-uh probe, and a 460 3-Channel Gauss meter. Fig. 3a shows that the experimental and numerical magnetic field intensity in the bore of each of the arrays is in agreement. Fig. 3b illustrates the numerical results of the magnetization waveform 60 mm inside the nested assembly along the axis of symmetry obtained when rotating the inner array through 360°. The plot shows a comparison for arrays composed of 4, 8, and 16 elements and a pure cosine wave. From 4 to 8 segments the maximum magnetization is improved by 45%, while from 8 to 16 only 7%. In addition, all of the nested array waveforms deviate substantially from the sinusoidal, especially in the low field range, showing a narrow cusp in the low field state.

When assembled in the device the two outer Halbach cylinders are positioned so that the field in the bore points toward the other cylinder. The inner magnets are mounted on bearings and they are synchronously rotated by a single timing belt in the same direction. The field strength in the cavities is in opposite phase.

2.5. *Hydraulic system design*

Oscillating fluid flow can be created with either a pump-rotary valve combination or a fluid displacer. The pump-rotary valve solution provides lower vibration, and potentially lower friction losses. It also allows for unidirectional fluid flow in the system outside the regenerators depending on where the valving can be located. However, it is more difficult to accurately control the amount of fluid blown per cycle and ensuring a constant utilization when speed is varied. For this reason the current configuration uses a fluid displacer for pumping the heat transfer fluid. A cylinder with a double acting rod, 19.05 mm bore diameter (0.75 in), and 25.4 mm stroke (1 in), allows the maximum fluid displaced to be 6.5 cm^3. Larger volume displacements (up to 15–20 cm^3) can be obtained by replacing the current cylinder with a larger diameter or longer stroke.

Both warm and cold heat exchangers are designed for low pressure drop, void space outside the regenerators, and to create a compact apparatus. They are constructed of aluminum, with milled flow channels. The warm heat exchangers interact with a fluid stream connected to a recirculating chiller which ensures a controllable heat rejection temperature between 40 and −20 °C. The design uses parallel flow channels for reduced pressure drop. Table 2 summarizes heat exchanger design specifications.

Fig. 4 illustrates the heat exchangers, the regenerator support and the regenerator shell assembly, and a view of the flow channel path. The shaded areas are the volumes where there is fluid. Two G-10 tubes of 16 mm inner diameter and 1.5 mm wall thickness housing the regenerator matrix connect the hot heat exchangers to the cold one. The material was chosen for its low thermal conductivity, electrical properties, strength, machinability, and availability. The tube clearance from the inner rotating magnet is of approximately 1 mm. The dead volume between each regenerator and the heat exchangers is approximately 1 cm^3 (value varies slightly, depending on the chosen regenerator length), therefore the total fluid volume in the cold region between the regenerators is 12 cm^3 (including the cold heat exchanger). Approximately 20 cm^3 are available for the refrigerant inside each tube.

The hydraulic system design includes the following aspects:

- A check valve mechanism at the cold end of the regenerator to ensure unidirectional flow in the cold heat exchanger.
- A bypass circuit for tuning utilization balance between hot and cold blow.
- A buffer volume that compensates for loss of pressure due to leaks during operation.
- Low pressure drop throughout the hydraulic system.

Installing a check valve at each end of the regenerator converts the flow outside the regenerator from oscillating to unidirectional. This is desirable for better heat exchanger effectiveness. It also reduces performance loss due to dead volumes. In our design we implemented a valving system only at the cold side, as the fluid–fluid heat exchanger at the hot side ensures a satisfactory heat transfer ever with an alternating flow. Fig. 5 shows the working mechanism in the cold

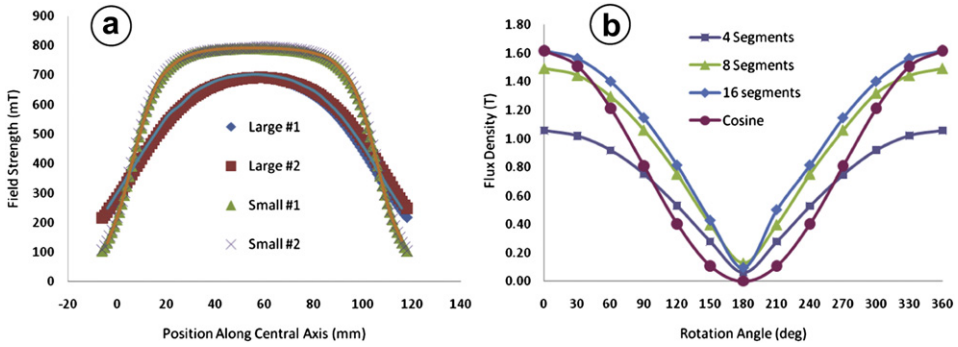

Fig. 3 – 3D simulations and experimental of the Halbach array fields. a) Field intensity along the central axis for each of the array. Numerical and experimental values are compared. The continuous lines without markers are the numerical results. Large stands for outer cylinder, while small for inner cylinder. b) Numerical evaluation of the field intensity at 60 mm on the central axis when the inner and outer arrays are assembled. The field is shown for a full rotation of 360. The plot shows a comparison for arrays composed of 4, 8, and 16 elements. The waveforms are compared to a pure cosine wave.

Please cite this article in press as: Tura, A., Rowe, A., Permanent magnet magnetic refrigerator design and experimental characterization, International Journal of Refrigeration (2011), doi:10.1016/j.ijrefrig.2010.12.009

Table 2 – Heat exchangers table of properties.

Property	Cold HEX	Hot HEX	Units
Channels	Parallel flow	Parallel flow	
Flow	Pulsating unidirectional	Pulsating bidirectional	
Wetted area	63	245	cm^2
Volume	5	32	cm^3

heat exchanger. Component 1 is the valves and heat exchanger housing, made out of 17.5 mm thick acrylic (clear and thermally insulating). Location 1a and 1b are alternatively the inlet and outlet from the regenerators. For the represented configuration 1a is the inlet and 1b is the outlet. 2 and 3 are the nylon disc check valves, which are allowed to slide in the manifold. 4 is the heat exchanger which is made from aluminum plate with fins milled in an upper and lower region. With fluid blowing from 1a to 1b, the valves are pushed up, with 2 sealing the upper channel and 3 opening the end of the lower channel. Heat transfer fluid flows from left to right only in the lower region of the heat exchanger. By reversing the blow the valves are pushed down and the fluid flow is in the upper region from right to left. The clear acrylic housing allows for inspecting the valve activity and detecting possible air trapped in the channels during filling and purging.

Typically a refrigerant like gadolinium displays a lower specific heat when in the magnetized state and in the neighborhood of its transition temperature. For instance for gadolinium, the specific heat peaks at 381 J kg^{-1} K^{-1} at approximately 292 K and 0 T, while it is only 290 J kg^{-1} K^{-1} at 2 T at the same temperature. For first order phase transition materials such effect can be even more pronounced. Consequently if the same amount of fluid is pulsed in both directions the regenerator operates under unbalanced conditions (Rowe, 2002). Allowing part of fluid to recirculate from the cold to the warm side bypassing the regenerator is a way to thermally balance it. The effectiveness of this solution depends upon materials and operating conditions. The PMMR was designed to accommodate a hydraulic circuit that allows a controlled amount of fluid to bypass the regenerator (Fig. 6). A port at each of the regenerator ends allow for partial fluid extraction and injection. Check valves ensure unidirectional flow from cold to hot end, a needle valve is used to adjust bypassed flow, and a positive displacement flowmeter is used to measure the volume flow rate in the bypass loop.

Additional hydraulic components are needed for fluid filling, purging, and maintaining a desired positive pressure of 2–3 bar to avoid cavitation when operating at higher frequencies (2–4 Hz). The system is first evacuated by using a positive displacement vacuum pump. Then it is filled with a water–glycol mixture injected in the system at 0.3 MPa. Four bleed valves (one at each end of the two regenerators, in the heat exchangers) are used for purging possible air trapped in the system during filling. An accumulator (Fig. 1, component 8) helps to maintain the absolute fluid pressure to a set value via a check valve. It consists in a simple acrylic vessel of approximately 80 cm^3 partially filled with the heat transfer fluid, in direct contact with pressurized air.

2.6. *Regenerator matrix geometry and composition*

A regenerator is a porous matrix that allows fluid to flow through. Geometries performing with large heat transfer need a large wetted surface, small hydraulic diameter, and small solid structures to minimize thermal gradients within them. Ideal porosity depends on the fluid and solid thermal mass. For water–glycol and gadolinium alloys a porosity ranging between 30 and 40% is desirable. In addition, custom matrix structures can be expensive to manufacture, especially if not mass-produced, which is a large financial constraint on choice

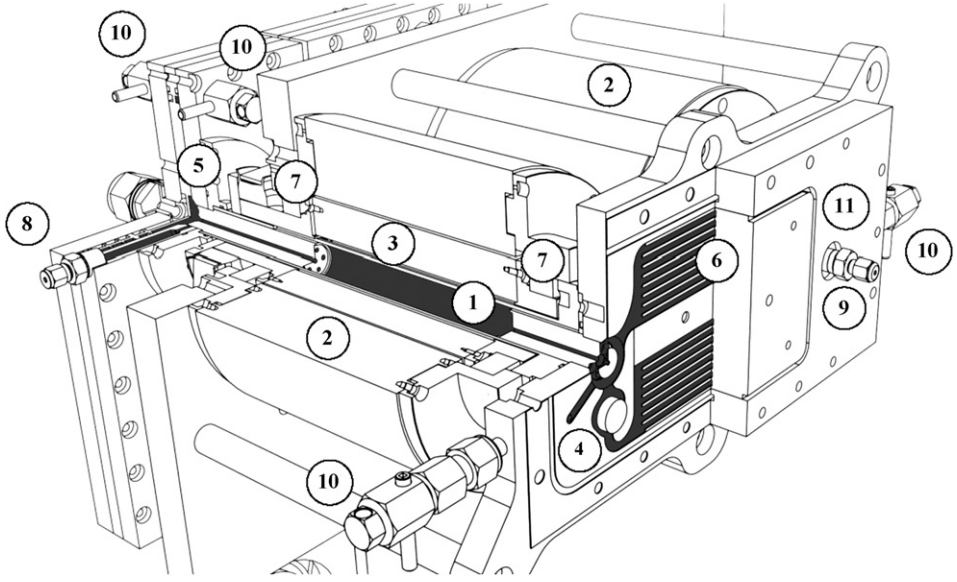

Fig. 4 – PMMR core details. 1: regenerator shell housing. 2: Outer, fixed Halbach array. 3: Inner, rotating array. 4: Check valve. 5: Hot heat exchanger. 6: Cold heat exchanger. 7: bearings. 8: warm side thermocouple feedthrough. 9: Cold side thermocouple feedthrough. 10: Bleed valves. 11: cold heat exchanger housing. The shaded areas are wetted by the heat transfer fluid.

Please cite this article in press as: Tura, A., Rowe, A., Permanent magnet magnetic refrigerator design and experimental characterization, International Journal of Refrigeration (2011), doi:10.1016/j.ijrefrig.2010.12.009

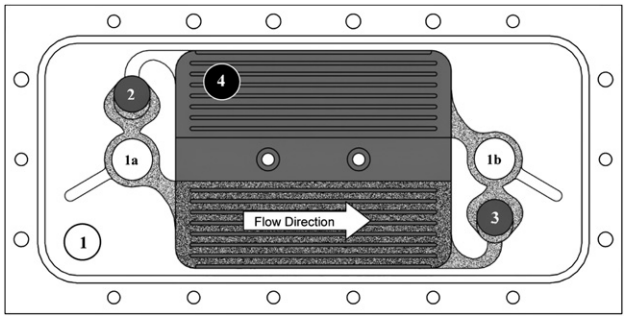

Fig. 5 – Cold heat exchanger design. 1: Acrylic housing. 4: heat exchanger. 2 and 3: check valves. 1a: inlet from the regenerator. 1b: outlet. The granular region represents the fluid in motion from 1a to 1b.

of matrix. Small diameter spheres are often used as they are available in a useful size range (0.1–1 mm), and they can easily fill arbitrary geometrical volumes. In addition, they respond homogeneously to an external force (no moments), they allow minimal eddy currents because of their small size and point contacts, which also leads to low conductive losses along the regenerator. Heat transfer and pressure drop performance can be tuned by selecting a specific sphere diameter.

For initial tests gadolinium spheres of 0.3 mm diameter are used. Gadolinium is a good prototype refrigerant because its magnetocaloric properties and thermal properties are well known, its T_{curie} is opportunely placed for near-room temperature applications (≈23 °C), and it offers a relatively large MCE (≈2.5 K T^{-1}) with no hysteresis and therefore suitable for high frequency applications. Gadolinium performance is often considered the benchmark to which other materials are compared. The 0.3 mm diameter is the largest readily available for testing, larger diameter may be desirable for reducing the hydraulic losses.

2.7. *Instrumentation*

A Labview data acquisition system is used for signal conditioning and logging. Measured properties are temperatures at the hot and cold ends of the regenerators, pressure of the fluid, operating frequency, displacer stroke, applied thermal load, and power to drive the DC motor. The four temperature readings are obtained by means of type E thermocouples with exposed tips. An Omega PX 603 thin film pressure transducer is used to measure the pressure at one of the inlets of the displacer. It ranges 0–2 MPa (0–300 psi) with a 0–5 V output. Operating frequency and magnet orientation can be measured using a rotary encoder installed on a secondary shaft of the motor; however, it was not operational at the time and a strobe light is used instead. An Omega linear potentiometer installed in parallel with the displacer measures stroke. Thermal load to the refrigerator is provided by 2 Kapton flexible electric heaters each of 65 cm^2 (10 in^2), and 25 W capacity (50 W total). They are wired in series and powered by a Xantrex LXQ 20-3 DC power supply. A Tektronic A622 m is used to measure the current drawn by the DC motor. It can measure AC/DC currents from 50 mA to 100 A peak over a frequency range of DC to 100 kHz. It provides 10 mV/Amp or 100 mV/Amp output. The bypass flowmeter is an Omega FDP 2001 – A positive displacement with a 0–2 LPM range. All transducers feed into an NI SCXI 1000. Finally, the hot temperature sink is thermally controlled by an RTE 740 Neslab recirculating chiller. It can operate in a temperature range between −40 °C and 200 °C depending on the nature of the fluid. It has a cooling power of 800 W at 20 °C, a heating power of 800 W. Table 3 summarizes the specifications of the prototype.

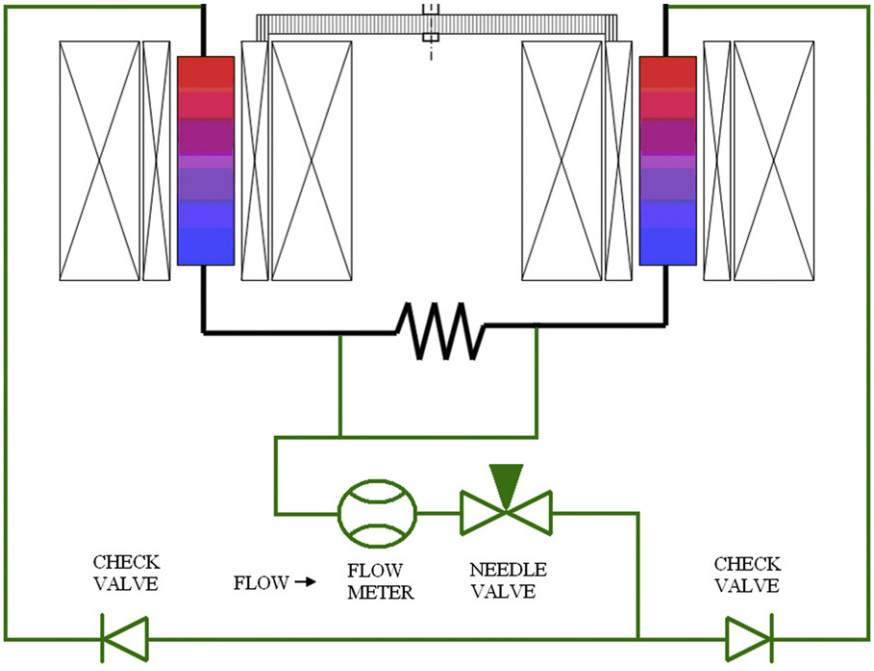

Fig. 6 – Hydraulic circuit of the fluid bypass. It allows matching the pulsed fluid thermal mass in each blow, compensating the matrix thermal capacity change.

Please cite this article in press as: Tura, A., Rowe, A., Permanent magnet magnetic refrigerator design and experimental characterization, International Journal of Refrigeration (2011), doi:10.1016/j.ijrefrig.2010.12.009

Table 3 – PMMR specifications.

Property	Range	Units
Magnetic field (average over regenerator volume)	0.1–1.4	T
Operating frequency	0–5	Hz
Heat transfer fluid	Water–glycol (80-20%)	
Max fluid displacement/cycle	6.5	cm^3
Heat rejection temperature	0–45	°C
Max thermal load	50	W
Available regenerator volume (each)	20	cm^3
Regenerator diameter	16	mm
Available regenerator length	110	mm
Regenerator properties for current tests:		
Volume	10.8	cm^3
Length	55	mm
Mass	55	g
Porosity	36%	
Composition	Gadolinium, metal	
Geometry	Spheres, diameter 0.3	mm

3. Experimental characterization

The experimental characterization of the device consists in measuring performance under a range of values for operating frequency, fluid mass displaced per cycle (utilization), and heat rejection temperatures. Performance is expressed in terms of temperature span, cooling power, and coefficient of performance (COP). We are interested in the measurement of the temperature at the hot and cold side of each regenerator under an imposed thermal load, and mechanical power input, when periodic steady-state has been reached. Input power is used with the above variables to determine efficiency. Periodic steady-state is assumed to be achieved when the recorded temperature span is unchanged over a period of 120 s. A peak-hold function is designed in Labview that resets a counter when a larger temperature span is recorded. Accuracy of approximately 0.5 °C is obtained. The PMMR performance is mapped over the parameter space summarized in the Table 4.

Given the definition of utilization in Eq. (1), it can be varied by setting a different stroke on the displacer; therefore, for this specific device configuration, stroke length, displaced fluid volume, or utilization are interchangeable parameters. Table 5 shows the relationship between each of these parameters.

Tests are performed with the following procedure: (1) with a set operating frequency and displacer stroke, the first data point is obtained for the highest heat rejection temperature ($T_H = 32$ °C) and no heat load input; (2) Subsequent data points are obtained for the same T_H, and thermal loads of 20, 30 and 40 W; (3) Similar tests are then performed for a progressively decreasing heat rejection temperature (27, 22, and 17 °C); (4) This test subset is repeated for the next frequency case; (5) Finally the same tests are repeated for all other stroke lengths. In total, this results in approximately 120 tests for mapping the performance over the desired parameters. Not all points could be measured either because the pressure drop was too high or because the imposed thermal load would exceed the cooling power of the unit, resulting in a negative temperature span. For this work no fluid bypass is used.

Table 4 – PMMR parameter space.

Parameter	Range	Units
Heat rejection temperature	17, 22, 27, 32	°C
Operating frequency	2, 4	Hz
Utilization	0.62, 0.94, 1.03, 1.28	
Thermal load	0, 20, 30, 40	W

Table 5 – Stroke, volume displaced, and utilization relationship using a reference specific heat for Gd of 381 $J\,kg^{-1}\,K^{-1}$.

Stroke [mm]	Volume [cm^3]	Utilization
12.20	3.10	0.62
18.75	4.75	0.94
20.30	5.15	1.03
25.40	6.40	1.28

3.1. *Operating ranges and limitations*

For the regenerator matrix, the main factor limiting the utilization and frequency is the pressure drop. This is due to the high aspect ratio of the regenerator and the small diameter of the spheres. The maximum utilization of 1.28 can only be used at 2 Hz or less. At 4 Hz, the pressure drop is approximately 2 bar for the lowest utilization tested (0.62) and grows rapidly as utilization increases (with a pressure drop of over 6 bar with a utilization of 1.03). In addition, the gearmotor is rated to operate up to 5 Hz at 130 V. However, only 4 Hz is obtainable with the current 120 V and 4.5 A power supply.

4. Results

Fig. 7 illustrates the experimental results when the heat rejection temperature T_H is set at 32 and 22 °C and operating frequency is of 2 or 4 Hz. The contour plots represent the temperature span obtained as function of the thermal load (horizontal axis) and utilization (vertical axis). The trend looks similar among all plots, where temperature spans tend to be larger with lower utilizations for small thermal loads, while high utilizations deliver larger cooling power. In addition, higher frequency increases the cooling power and reduces the sensitivity to the thermal load, while the temperature span is somewhat insensitive to frequency for no heat load. For example, when operating at 2 Hz with a utilization of 0.62 and heat rejection temperature of 22 °C, the unit cannot provide more than 30 W of cooling. Instead, if operating at 4 Hz, the device delivers a positive temperature span with a 50 W load. Such behavior suggests that the device would benefit from variable speed and/or flow rates to control the temperature in the refrigerated area.

Please cite this article in press as: Tura, A., Rowe, A., Permanent magnet magnetic refrigerator design and experimental characterization, International Journal of Refrigeration (2011), doi:10.1016/j.ijrefrig.2010.12.009

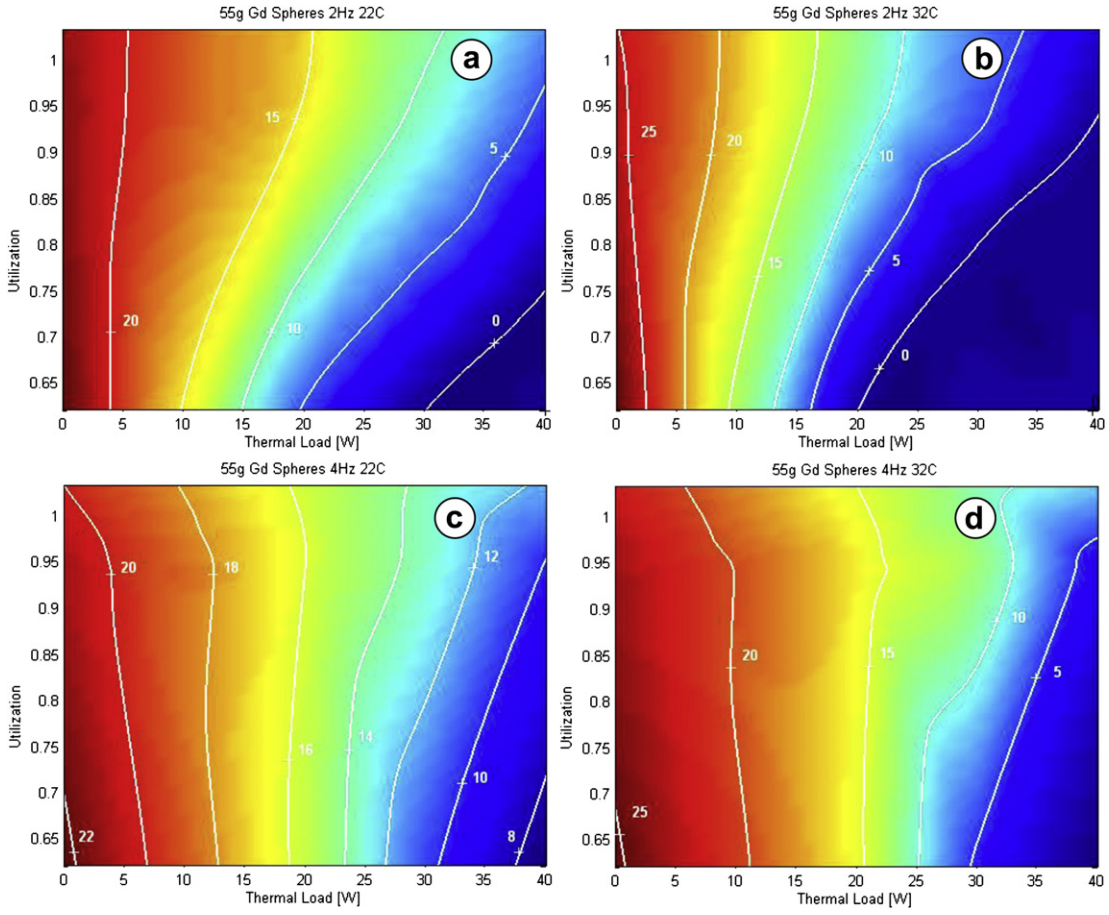

Fig. 7 – Temperature span as function of thermal load and utilization. a) 2 Hz with heat rejection temperature of 22 °C, b) 2 Hz with heat rejection temperature of 32 °C, c) 4 Hz with heat rejection temperature of 22 °C, d) 4 Hz with heat rejection temperature of 32 °C.

When operating at a heat rejection temperature close to the Curie temperature (22 °C) the refrigerator shows a reduced sensitivity to the heat load when compared to the case with T_H of 32 °C. This can be clearly seen in Fig. 8, which illustrates the impact of heat rejection temperature and cooling power on temperature span when operating at 4 Hz and utilization of 0.62. A similar behavior, where the temperature span is more sensitive to thermal load when operating with a heat rejection temperature above the Curie point, was already found in previous experiments with lower utilizations (Tura, 2005). This is somewhat intuitive since a reduction in temperature span allows for a larger adiabatic temperature change if T_H is equal or lower than T_{Curie} at all times (positive feedback), while this is not necessarily true if both T_H and T_C are above T_{Curie}. This is a direct consequence of the characteristic caret-shaped MCE dependence to temperature. The largest no-load temperature span is 29 °C obtained when operating with a utilization of 0.62 and a heat rejection temperature T_H of 32 °C.

4.1. *Power consumption*

By measuring the voltage and current to the gearmotor it is possible to evaluate the overall power consumption of the refrigerator. While the voltage is considered constant, the current drawn over a cycle strongly depends on the highly uneven torque caused by the hydraulic cylinder and the magnetic forces of the Halbach arrays (Fig. 9). By knowing the input power and thermal load per cycle, it is possible to evaluate the overall COP of the device. For the existing parameter space and temperature spans between 0 and 29 °C the COPs range between 0.8 and 0 while a maximum value of 1.6 is found when operating at 1.4 Hz with a utilization of 1.28. At this peak COP the PMMR had a cooling power of 50 W and a temperature span of 2.5 °C. Under same operating conditions the COP is 2.2 if motor is assumed 100% efficient and 10 if also the magnet drive power is omitted. By changing frequency from 2 to 4 Hz the input power increases by 120%–150%; therefore operating at higher frequencies with the same regenerator matrix boosts power at the expense of the COP. This trend is shown in Fig. 10. The plot illustrates cooling power and COP as function of operating frequency and utilization. Size of data point is proportional to utilization (listed in the circle.) For the 2 Hz series the utilization values are 0.62, 1.03, 1.28, while for the 4 Hz are 0.62, 0.94, and 1.28. All data points refer to a temperature span of 10 °C.

In order to determine the potential for improved performance it is useful to know how the power is distributed among the PMMR sub-systems. Such a breakdown identifies

Please cite this article in press as: Tura, A., Rowe, A., Permanent magnet magnetic refrigerator design and experimental characterization, International Journal of Refrigeration (2011), doi:10.1016/j.ijrefrig.2010.12.009

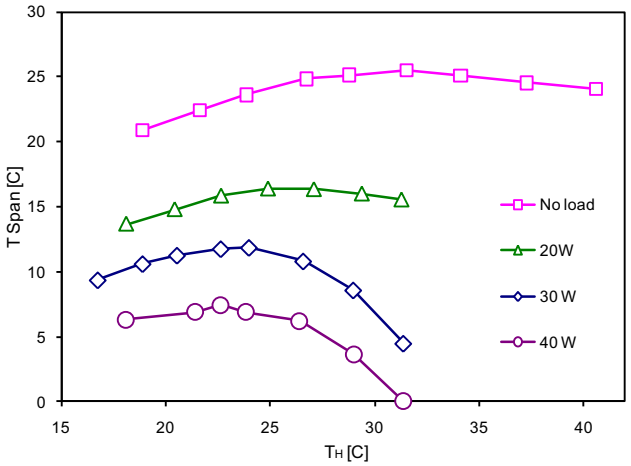

Fig. 8 – Temperature span vs heat rejection temperature (T_H) for 55 g spheres of 300 μm diameter, for 0, 20, 30 and 40 W. Tests were performed at 4 Hz and utilization of 0.62.

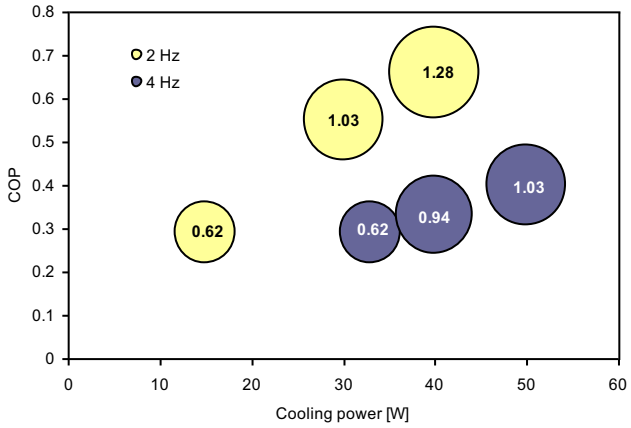

Fig. 10 – Cooling power and COP as function of operating frequency and utilization. Size of data point is proportional to utilization. All data points refer to a temperature span of 10 °C.

which components impact the refrigerator efficiency the most. For this purpose, the motor drive power was measured in a number of configurations:

1. The motor is disconnected from the PMMR (turns freely), power draw is measured for a number of frequencies.
2. The motor is only connected to the magnet drive – power draw is measured for a number of frequencies.
3. Power draw is measured when the refrigerator is fully functional, with all components connected (magnet drive + hydraulic pumping).

The power to drive the hydraulic system plus the cycle work is obtained by subtracting measurements obtained in 3 from the measurement in 2. The validity of this approach needs to be corroborated by mechanically measuring the torque required to operate the device. The current measurement includes the power required for the motor, which might operate at different efficiencies in each of the scenarios 1, 2, and 3. If that is the case a simple additive estimate as the above may be inaccurate. Fig. 11 illustrates the power input breakdown. *Base* is the power to run the gearmotor freely; *mechanical* is the power required to rotate the magnets with no fluid flow (i.e. mechanical losses only, determined by subtracting (1) from (2)); *cycle* is the power required to drive the displacer mechanism and the magnetic work. All data refers to a utilization of 0.62.

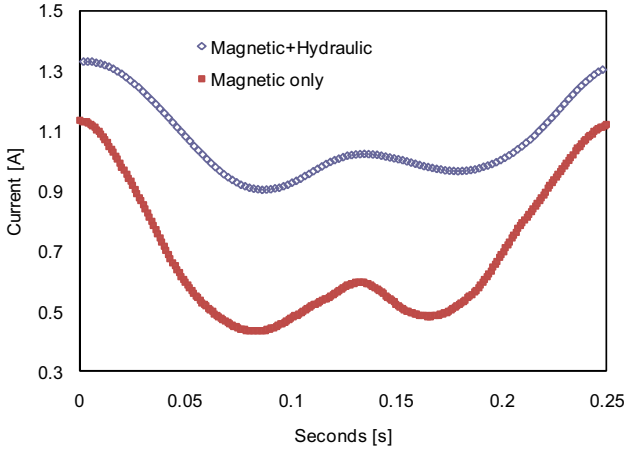

Fig. 9 – Current drawn by the motor over a cycle, operating conditions are 4 Hz, utilization of 1.03 and heat rejection temperature of 22 °C.

To create the plots additional tests were performed at 3 Hz. As can be seen, motor and mechanical losses are relatively large, consuming over 70% of the total power input. A significant fraction of the mechanical loss is due to a manufacturing imperfection in one of the Halbach arrays creating an unbalanced magnetic force. The base power, consuming approximately 30%, is also relatively large. A properly sized motor with a more efficient gearbox could reduce base losses significantly. Finally, the cycle power could be further reduced using a better regenerator geometry with lower pressure drop. If the above issues are addressed, it should be possible to obtain system COPs approximately three times larger. These results indicate that the power required to drive the actual thermodynamic cycle is a small fraction of the total.

4.2. *Exergetic performance*

A measure of the useful cooling produced by a refrigerator is the exergetic-equivalent cooling power, Ex_Q (Rowe, 2011):

$$Ex_Q = Q_c\left(\frac{T_H}{T_c} - 1\right) \tag{3}$$

When expressed in terms of unit applied field and refrigerant volume we obtain the specific exergetic cooling power:

$$\mu = \frac{(1-\alpha)Ex_Q}{B_0 V} \tag{4}$$

where B_o is the magnetic field intensity expressed in Tesla, V the total refrigerant volume in cm^3, and α the matrix porosity. Fig. 12 illustrates the exergetic-equivalent cooling power for a range of operating conditions. Lines connect point

Please cite this article in press as: Tura, A., Rowe, A., Permanent magnet magnetic refrigerator design and experimental characterization, International Journal of Refrigeration (2011), doi:10.1016/j.ijrefrig.2010.12.009

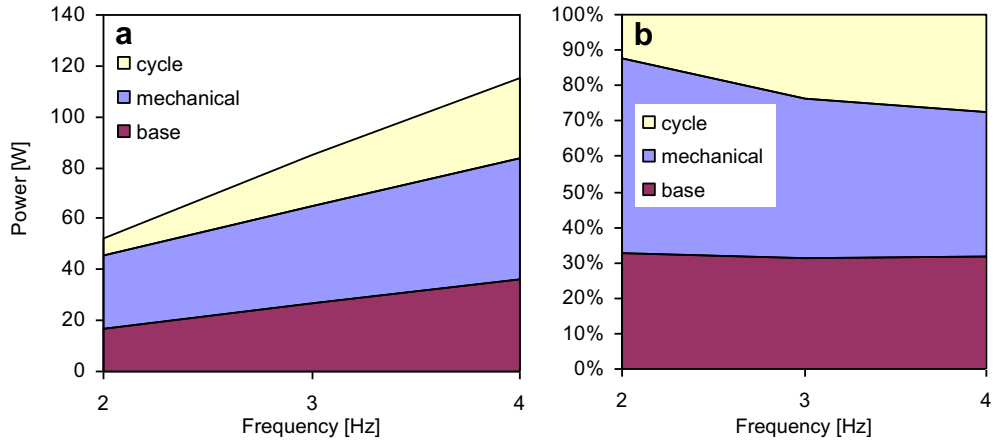

Fig. 11 – Power input with a utilization of 0.62 for 2, 3 and 4 Hz. a) shows the absolute individual contributions by each of the mechanical sub-systems with a utilization of 0.62 for 2, 3 and 4 Hz, while b) shows the relative contributions.

operating with same frequency and cooling load, but different heat rejection temperatures. All results are for utilization of 1.09. Best results are obtained, as expected when operating at 4 Hz rather than 2 Hz. Specific exergetic cooling power μ can be obtained by multiplying the values by the constant 0.0513 T^{-1} cm^{-3} (reciprocal of the product of the mean high field by the effective regenerator volume). The maximum value found within the tests performed is 0.085 W T^{-1} cm^{-3}.

4.3. *Regenerative losses*

It is generally assumed that with suitably sized particles the Biot number is low and the temperature of the particles is uniform throughout their volume. However, this may not be true when operating at high frequencies with a large utilization, and the heat transfer losses due to internal gradients could impose limitations on the regenerator performance. This means that there is an upper limit for the operating frequency beyond which there is no gain in cooling power. Based on the estimated Fourier and Biot numbers, and using the results from (Engelbrecht et al., 2006), the thermal effectiveness of the PMMR regenerators are ~90% or better. Therefore with 0.3 mm diameter gadolinium spheres temperature gradients inside the refrigerant do not constitute a limitation to the heat transfer at the current operating frequencies.

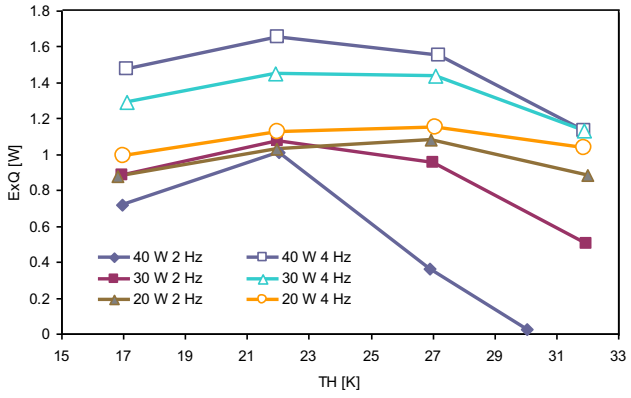

Fig. 12 – Exergetic-equivalent cooling power for a range of operating conditions. Lines connect point operating with same parameters at different heat rejection temperatures. All results are for utilization of 1.09.

5. Conclusions

A novel MR is described. The device met the objectives of a compact, simple construction, modular and easy to operate design, capable of high operating frequencies. Using 110 g of gadolinium as a refrigerant, the device produced a maximum temperature span under no thermal load of 29 °C, and 10 °C under 50 W. For most operating conditions the COP ranged between 0.8 and 0 for temperature spans between 0 and 29 °C, while a maximum value of 1.6 is found when operating at 1.4 Hz with a utilization of 1.28. A maximum operating frequency of 4 Hz was dictated by the large pressure drop in the regenerators. Most of the efficiency loss was found in the drive system for the magnets and fluid displacer. Using a single, refrigerant the maximum specific exergetic cooling power is found to be 0.085 W T^{-1} cm^{-3}, when operating with a utilization of 1.03, frequency of 4 Hz, and T_H set at 22 °C.

REFERENCES

Bjork, R., Bahl, C.R.H., Smith, A., Pryds, N., 2008. Optimization and improvement of Halbach cylinder design. J. Appl. Phys. 104 (013910).

Bjørk, R., Smith, A., Bahl, C.R.H., 2010. Analysis of the magnetic field, force, and torque for two-dimensional Halbach cylinders. J. Magn. Magn. Mater. 322, 133–141.

Coey, J.M.D., 2002. Permanent magnet applications. J. Magn. Magn. Mater. 248, 441–456.

Engelbrecht, K.A., 2008. Numerical Model of an Active Magnetic Regenerator Refrigerator with Experimental Validation.

Engelbrecht, K.L., Nellis, G.F., Klein, S.A., 2006. The effect of internal temperature gradients on regenerator matrix performance. J. Heat Transfer 128, 1060–1069.

Please cite this article in press as: Tura, A., Rowe, A., Permanent magnet magnetic refrigerator design and experimental characterization, International Journal of Refrigeration (2011), doi:10.1016/j.ijrefrig.2010.12.009

Gschneidner Jr., K.A., Pecharsky, V.K., 2008. Thirty years of near room temperature magnetic cooling: where we are today and future prospects. Int. J. Refrigeration 31, 945–961.

Hall, J.L., Reid, C.E., Spearing, I.G., Barclay, J.A., 1996. Thermodynanic considerations for the design of active magnetic regenerative refrigerators. Adv. Cryog. Eng. 41.

Hirano, N., Nagaya, S., Takahashi, M., Kuriyama, T., Ito, K., Nomura, S., 2002. Development of magnetic refrigerator for room temperature application. In: Preceedings of the Cryogenic Engineering Conference Ser, 613.

Jacobs, S., 2009. Modeling and optimal design of a multilayer active magnetic refrigeration system, Preceedings of the Third International Conference on Magnetic Refrigeration at Room Temperature.

Mhiochain, T.R.N., Weaire, D., McMurry, S.M., Coey, J.M.D., 1999. Analysis of torque in nested magnetic cylinders. J. Appl. Phys. 86, 6412–6424.

Okamura, T., Yamada, K., Hirano, N., Nagaya, S., 2006. Performance of a room-temperature rotary magnetic refrigerator. Int. J. Refrigeration 29, 1327–1331.

Okamura, T., Rachi, R., Hiramo, N., Naraya, S., 2007. Improvement of 100W Class Room Temperature Magnetic Refrigeration, Preceedings of the Second International Conference on Magnetic Refrigeration at Room Temperature.

Rowe, A.M., 2002. Active Magnetic Regenerators: Performance in the Vicinity of Para-Ferromagnetic Second Order Phase Transitions.

Rowe, A., 2011. Configuration and performance analysis of magnetic refrigerators. Int. J. Refrigeration 34, 169–177.

Russek, S., Auringer, J., Boeder, A., Chell, J., Jacobs, S., Zimm, C., 2010. The Performance of a Rotary Magnet Magnetic Refrigerator with Layered Beds, Preceedings of the Fourth International Conference on Magnetic Refrigeration at Room Temperature, Baotou, China, 339–349.

Tura, A., 2005. Active Magnetic Regenerator Experimental Optimization.

Yu, B., Liu, M., Egolf, P.W., Kitanovski, A., 2010. A review of magnetic refrigerator and heat pump prototypes built before the year 2010. Int. J. Refrigeration 33, 1029–1060.

Zimm, C., Boeder, A., Chell, J., Sternberg, A., Fujita, A., Fujieda, S., et al., 2006. Design and performance of a permanent-magnet rotary refrigerator. Int. J. Refrigeration 29, 1302–1306.

Zimm, C., Boeder, A., Chell, J., Sternberg, A., Fujita, A., Fujieda, S., 2007. Design and Initial Performance of a Magnetic Refrigerator with Rotating Permanent Magnet, Preceedings of the Second International Conference on Magnetic Refrigeration at Room Temperature, Portoroz, Slovenia, 341–347.

Please cite this article in press as: Tura, A., Rowe, A., Permanent magnet magnetic refrigerator design and experimental characterization, International Journal of Refrigeration (2011), doi:10.1016/j.ijrefrig.2010.12.009

Appendix III
Experimental and Modeling Results of a Parallel-Plate based Active Magnetic Regenerator

Available online at www.sciencedirect.com

SciVerse ScienceDirect

journal homepage: www.elsevier.com/locate/ijrefrig

Experimental and modeling results of a parallel plate-based active magnetic regenerator

A. Tura [a,*], K.K. Nielsen [b,c], A. Rowe [a]

[a] Department of Mechanical Engineering, Institute of Integrated Energy Systems, University of Victoria, PO Box 3055 STN CSC, Victoria, BC, Canada

[b] Department of Mechanical Engineering, Technical University of Denmark, Produktionstorvet, Building 425, Room 020, DK-2800 Kgs. Lyngby, Denmark

[c] Fuel Cells and Solid State Chemistry Division, Risø National Laboratory for Sustainable Energy, Technical University of Denmark, Frederiksborgvej 399, DK-4000 Roskilde, Denmark

ARTICLE INFO

Article history:
Received 22 November 2011
Received in revised form
10 January 2012
Accepted 19 April 2012
Available online 8 May 2012

Keywords:
Gadolinium
Magnetocaloric effect
Active magnetic regenerator
Demagnetization
Magnetic refrigerator
Magnetic field

ABSTRACT

The performance of a permanent magnet magnetic refrigerator (PMMR) using gadolinium parallel plates is described. The configuration and operating parameters are described in detail. Experimental results are compared to simulations using an established two-dimensional model of an active magnetic regenerator (AMR). In particular, the effect of geometric demagnetization in the regenerator is included in a simplified manner. The model and experimental data are in good agreement while the effect of demagnetization is seen to degrade the performance. It is concluded from the experiments that both thinner plates and channels are needed in order to obtain both temperature spans and cooling powers comparable to those obtained with packed spheres.

Régénérateur actif magnétique alternatif aux plaques parallèles : résultats expérimentaux et de modélisation

Mots clés : Gadolinium ; Effet magnétocalorique ; Régénérateur actif magnétique ; Désaimantation ; Réfrigérateur magnétique ; Champ magnétique

1. Introduction

The active magnetic regenerator (AMR) cycle is an alternative to conventional refrigeration with a potential for higher efficiencies using solid-state refrigerants with zero ozone-depleting potential (Gschneidner and Pecharsky, 2008). There exists a range of technological and fundamental scientific challenges to be overcome before commercially

* *Corresponding author*. Tel.: +1 250 721 7295; fax: +1 250 721 6051.
E-mail address: atura@uvic.ca (A. Tura).

0140-7007/$ – see front matter © 2012 Elsevier Ltd and IIR. All rights reserved.
doi:10.1016/j.ijrefrig.2012.04.016

viable magnetic refrigerators may come to market (Rowe, 2011). These challenges include the development and tailoring of magnetocaloric materials, efficient device design and the design of the thermal regenerator, which is the core of the magnetic refrigerator. This component is made of one or several magnetocaloric materials and acts through the magnetocaloric effect as an active refrigerant. The AMR cycle is described in detail in numerous publications; see e.g. Pecharsky and Gschneidner (1999).

In an AMR the magnetocaloric material acts as a thermal regenerator, which means that a temperature gradient is maintained between the hot and cold end of the refrigerator. The periodic interaction between the aqueous heat transfer fluid and the solid magnetocaloric material creates this gradient. The thermal efficiency of the regenerator is crucial for the overall performance of the regenerator. Packed spheres have been widely used as solid refrigerant since they are fairly easy to come by and they have proven to provide superior heat transfer properties. However, the pressure drop in the heat transfer fluid across the regenerator bed can be a limiting factor for this geometry. Parallel plates have been suggested as a good alternative since they, theoretically, provide good heat transfer characteristics while maintaining a small pressure drop.

In this paper a previously published permanent magnet magnetic refrigerator (PMMR) (Tura and Rowe, 2011) is tested using parallel plates. Details of the configuration and experimental results are presented in Section 2. In Section 3 a two-dimensional numerical AMR model, also previously published, is applied to the experimental test cases and the results of the model are compared to those of the experiment. The effect of geometric demagnetization on the AMR performance is investigated in a simple way by combining the AMR model and an established magnetostatic model of the magnetic field in a stack of flat ferromagnetic plates. In Sections 4 and 5 the results are concluded and suggestions for future work are provided.

2. AMR prototype setup

The PMMR was developed as an apparatus for testing the performance of AMRs using various refrigerants, geometries and compositions. A detailed description of the device tested with Gd spheres as refrigerant can be found in Tura and Rowe (2011). The objective is to optimize the regenerator in terms of performance and heat transfer effectiveness paying a minimal hydraulic loss penalty. Specifically looking at the impact of the regenerator geometry, there is always a tradeoff between heat transfer effectiveness and viscous losses. For instance when using 0.3 mm diameter gadolinium spheres in regenerators of 55 g, 36% porosity, enclosed in a cylindrical volume of 16 mm diameter and 55 mm length, pressure drop of 10 atm or larger could be observed when operating at 4 Hz. Such viscous losses are unacceptable because they cause a severe limitation to high operating frequencies and mass flow rates, which are required to achieve the power densities needed to develop a commercially viable device (Rowe, 2011).

A geometry that can be operated at much higher frequencies and fluid flow rates is a parallel plate type of regenerator. Flat plates are stacked together with equally spaced gaps necessary for the fluid to flow and exchange heat with the solid medium. Parallel plates can be one order of magnitude better in terms of viscous losses than spheres; however, surface area and heat transfer rates are penalized. While testing relatively small spheres for regenerator matrix gave an insight into one end of the spectrum of possible geometries, a parallel plate approach represents another extreme. Combined, data for these two configurations can provide further insights into AMR design, material selection and model validation.

2.1. *Regenerator design*

A plate thickness of 100 μm and a gap between plates of 50 μm would be required to obtain a hydraulic diameter and porosity equivalent to the 0.3 mm spheres used in previous experiments. This could not be achieved with the material and technology available to the laboratory. Instead, the parallel plate design used 540 μm thick, 15 mm wide and 90 mm long gadolinium strips (Fig. 1). To maintain a 36% porosity the gap was set at 300 μm.

Parallel plate geometries introduce some considerations, which may be less of a concern with spheres:

- Plate orientation relative to the magnetic field has an impact on the performance through the demagnetizing field.
- Plate size, geometrical shape and orientation have an impact on eddy currents and magnetic forces.
- Plate alignment needs high accuracy to avoid preferential flow among the parallel gaps and flow maldistribution.
- Given the high alternating forces acting on the plates the assembly needs to be structurally sound and not susceptible to fatigue.

The regenerator geometry used in this work is illustrated in Fig. 2. It consists of a scaffolding structure to maintain plate position and alignment during operation, while allowing for simple installation of the plates in the regenerator shell. The scaffolding is a modular design with the following characteristics. Two circular end pieces with the same diameter as the regenerator shell inner cavity support each group of plates; 300 μm diameter perforations allow the flow through them. On the inner face 300 × 300 μm tabs protruding 500 μm and 500 μm apart are used as guides for the plates. Four intermediate discs with equivalent perforations and tab pattern are used for the inner sections, this time on both sides. The end pieces and intermediate ones are held together by two spacers featuring perforations for locating pins plus an additional hole for a connecting rod. The assembly results in five layers each holding 14 plates. The structure is made out of nylon and the locating pins and connecting rod are of stainless steel. By removing one or more intermediate discs and using shorter connecting rods four or fewer modules can be tested. The five-module regenerator is 80 mm long and has similar mass (60 g) and porosity (36%) of the previously tested spheres regenerators. Each plate has a length of 15 mm and a width ranging from 10.8 to 15.5 mm depending on the location (the plates fit a cylindrical cross-section).

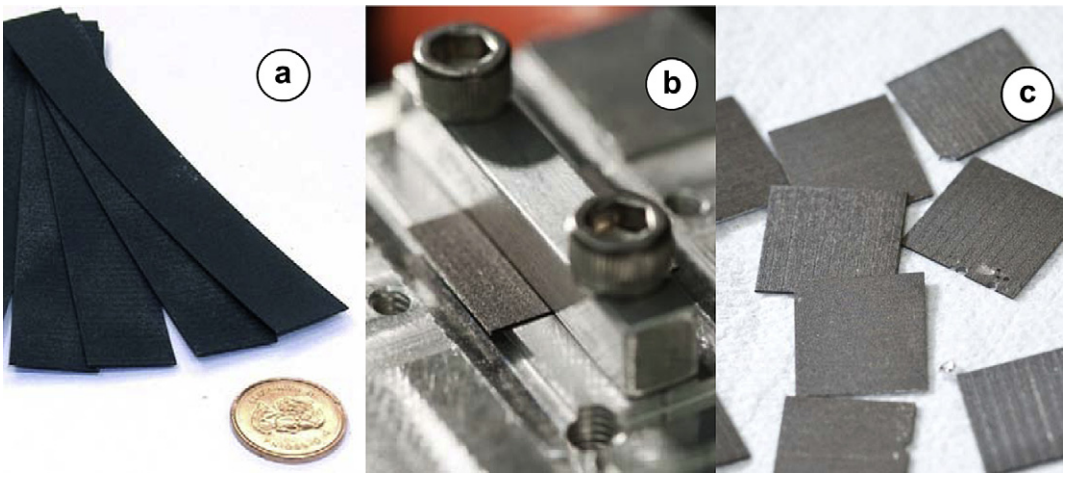

Fig. 1 – Gadolinium strips. Figure on the far left (a) represents the supplied material, the central one (b) the cutting jig, and the far right one (c) the final plates.

Fig. 3 illustrates how the regenerator is installed in the magnetic refrigerator. Labels (1) and (2) are the hot and cold heat exchangers, (3) and (4) are the outer fixed and the inner rotating Halbach arrays. As the inner cylinders rotate the inner cavity sees a field intensity change from approximately 0.1 T to 1.47 T. Labels (5) and (6) are nylon spacers, required to both mechanically constrain the regenerators (7) and to minimize the dead volume between the regenerators and the heat exchangers. The shading labeled as (8) represents the normalized maximum field strength, which tapers off toward the ends of the Halbach cylinders. The regenerators are installed in the inner region, where the field is the most intense. The regenerators are positioned slightly to the left (closer to the warm side) to favor maximum field intensity swing on the cold side. The net field changes in magnitude and direction with the magnet rotation, as shown in Fig. 4. Each arrow shows the field direction for 30° incremental rotation of the inner Halbach cylinder. The field is parallel to the horizontal plane at maximum and minimum intensity (0° and 180° of rotation). If we desire to minimize geometrical demagnetization in the gadolinium plates when the field is maximum, then we need to position the plates horizontally. It might be preferable to orient the plates normal to the maximum field so that the low field magnetization is minimized; however, this will not be investigated in this work.

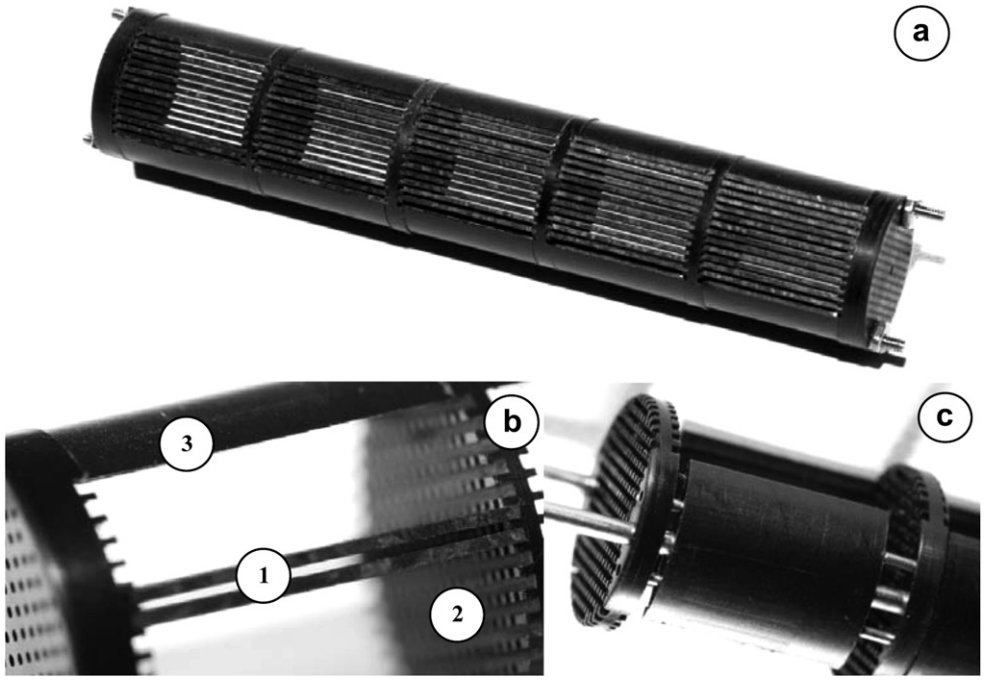

Fig. 2 – Gadolinium installation and scaffolding. (a) Illustrates the complete assembly, (b) shows two plates (1) inserted in the scaffolding (2), held together by spacers (3), while (c) illustrates the connecting rods and the spacer locating pins.

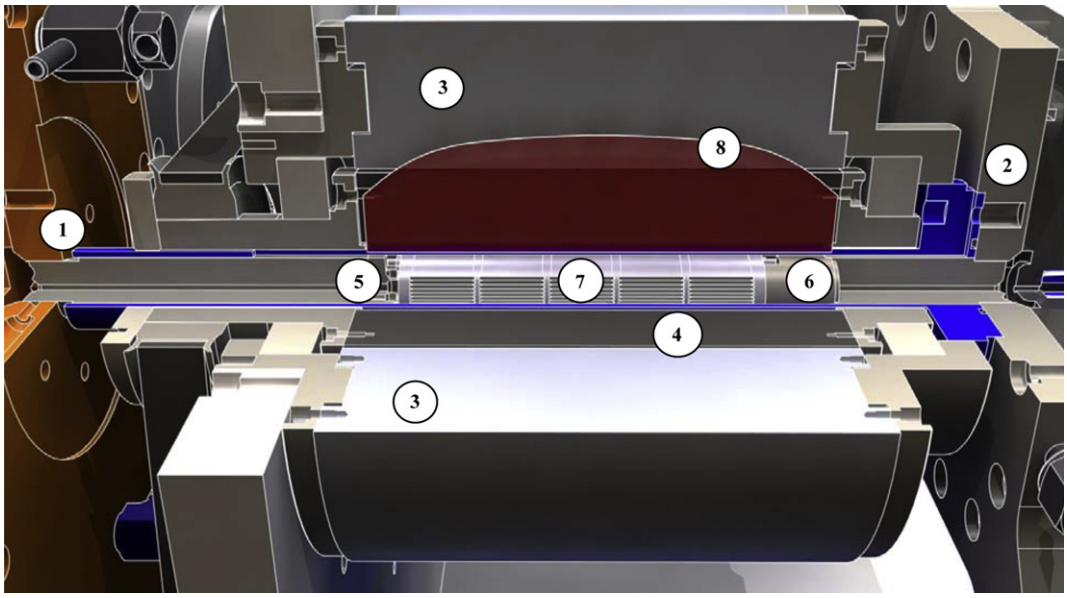

Fig. 3 – PMMR cut out. (1) Hot heat exchanger, (2) cold heat exchanger, (3) fixed outer Halbach cylinder, (4) rotating inner Halbach cylinder, (5) warm side regenerator spacer, (6) cold side regenerator spacer, (7) regenerator, (8) magnetic field distribution.

2.2. *Experimental characterization*

The experimental characterization of the device consists of testing its performance over a range of values for operating frequency, utilization (or fluid mass displaced per cycle) and heat rejection temperatures. Utilization is the thermal capacity ratio between the fluid displaced in the regenerator and the total thermal mass of the solid:

$$\Phi \equiv \frac{m_f c_f}{m_s c_s} \quad (1)$$

where m_f is the fluid mass blown over one cycle, c_f the fluid specific heat, m_s is the mass of one regenerator and c_s the refrigerant specific heat in the demagnetized state and at the Curie temperature T_{Curie}. Utilization, in this device, can be changed by varying the displacer stroke; therefore, an equivalence exists between utilization, stroke, or volume displaced as shown in Table 1.

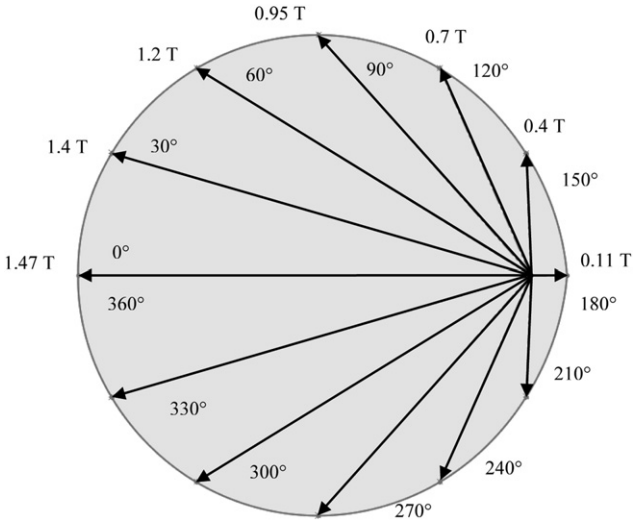

Fig. 4 – Vectorial magnetic field distribution over a range inner Halbach cylinder rotation angles. Cylinder end effects are not taken into account.

Performance can be expressed in terms of temperature span, cooling power and coefficient of performance. Here, only no-load temperature span will be considered. We are interested in the measurement of the temperature at the hot and cold side of each regenerator, imposed thermal load and mechanical power input when a periodic flow for a specific operating regime has been reached. The PMMR performance was mapped over the parameter space summarized in Table 2, to match previous experiments performed with gadolinium spheres.

Tests were performed with the following procedure. With a set operating frequency and displacer stroke, the first data point is obtained for the highest heat rejection temperature ($T_H = 32\,^{\circ}C$) and no heat load input. The subsequent data points are obtained for the same T_H, and thermal loads of 10 and 0 W, respectively. Similar tests are then performed for a progressively decreasing heat rejection temperature (27, 22 and 17 °C). This test subset is repeated for the next frequency

Table 1 – Stroke, volume displaced and utilization relationship using a reference specific heat for Gd of 371 J kg^{-1} K^{-1}.

Stroke (mm)	Volume (cm^3)	Utilization (–)
12.20	3.10	0.62
18.75	4.75	0.94
20.30	5.15	1.03
25.40	6.40	1.28

Table 2 – PMMR parameter space.

Parameter	Range
Heat rejection temperature (°C)	17, 22, 27, 32
Operating frequency (Hz)	0.5, 1, 2
Utilization (1)	0.33, 0.53, 0.81
Thermal load (W)	0, 10

case. Finally the same tests are repeated for all other stroke lengths. Therefore approximately 70 tests were performed for mapping the performance over the desired parameters space.

Fig. 5 illustrates the experimental data when the heat rejection temperature T_H is set at 17, 22, 27 and 32 °C. The contour plots represent the temperature span obtained as function of the operating frequency (horizontal axis) and utilization (vertical axis). All plots are obtained for no-load tests, which means that the only cooling loads are the thermal losses of the system. The trend looks similar among all plots, where the temperature spans tend to be larger for utilizations in the range of 0.5 and at the lowest frequencies. However the cooling power is very low under such operating conditions and overall never exceeded 10 W, which was obtained when operating above 1 Hz. A maximum temperature span of 12 °C was obtained for an operating frequency of 0.5 Hz, utilization of 0.35, with a heat rejection temperature of 27 °C.

The results differ substantially from previous tests performed with gadolinium spheres. The major deviations are the much poorer performance due to the low frequency and low heat transfer, and the strong temperature span dependency on frequency. The reason of this dependency is to be found in the much larger hydraulic diameter in the parallel plate geometry. Given the laminar nature of the flow, it can be expected that the convective component of the heat transfer is limited. Since we are greatly relying on the conductive heat transfer rate in the fluid, blow duration (or mass flow rate) has a non-trivial impact on the regenerator effectiveness. In theory, operating very slowly, with a small displaced volume would result in the largest temperature span, however this configuration leads to extremely low cooling power. In order to obtain a better performance thinner plates and narrower gaps are needed to create a smaller hydraulic diameter.

3. Modeling results

A numerical AMR model is used to simulate the experiments presented in the previous section. The model was presented

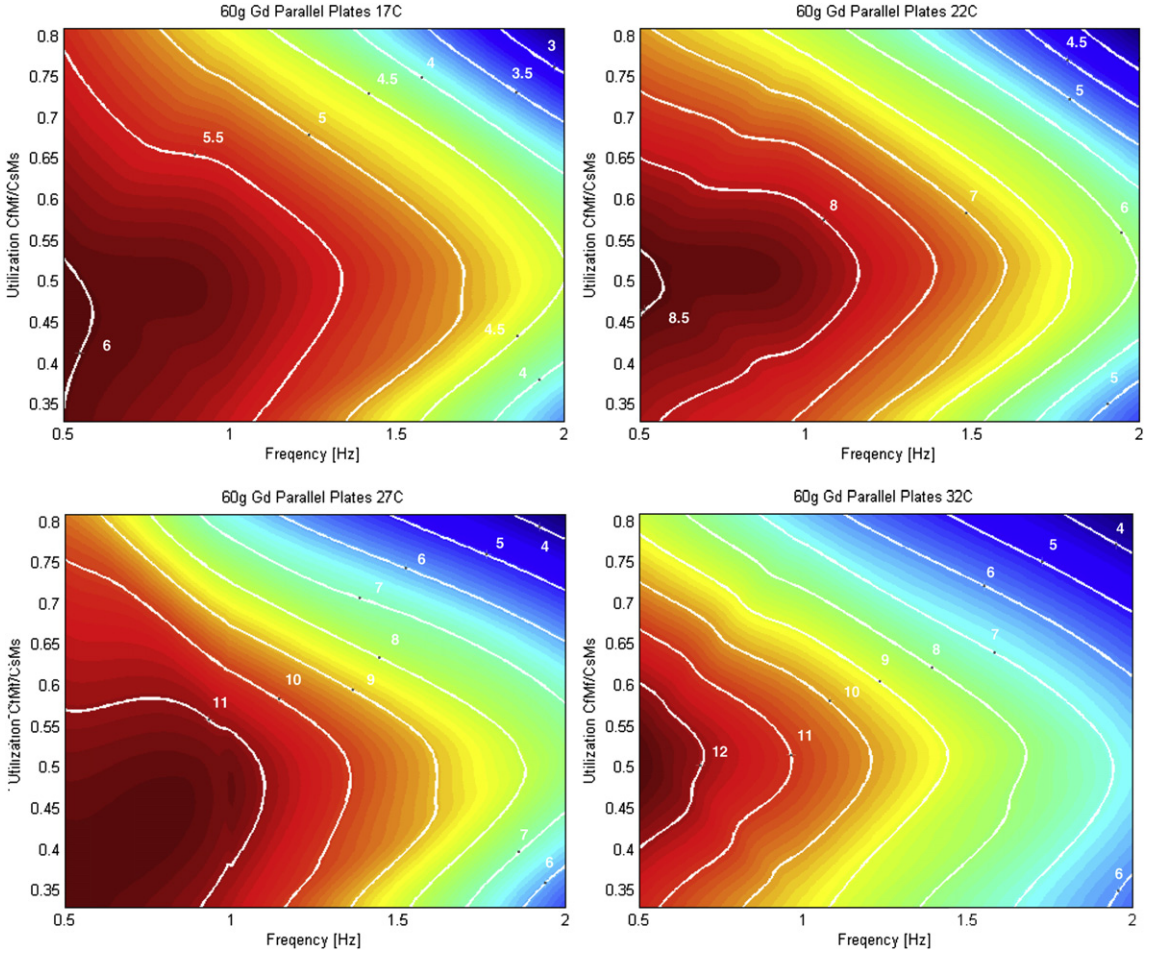

Fig. 5 – No-load temperature spans as function of frequency and utilization. Each plot refers to a different heat rejection temperature, from 17 °C to 32 °C.

in detail in Nielsen et al. (2009a). In the following the model is briefly described. Following this the adaption of the experimental fluid velocity and magnetic field profiles are discussed. Special emphasis is put on the effect of the demagnetizing field. An established magnetostatic model of this field in a stack of rectangular plates is applied in order to probe the average internal field experienced in the parallel plate regenerator during operation.

3.1. Description of the AMR model

The numerical model presented here was first published by Petersen et al. (2008a) and later modified and converted from being a Comsol-based (www.comsol.com) finite element model into a second order finite difference model implemented in Fortran (Nielsen et al., 2009a). The model solves a set of coupled partial differential equations that describe the heat transfer by conduction (in both the solid and the fluid) as well as the convection in the fluid. These are given by

$$\frac{\partial T_f}{\partial t} = \frac{k_f}{c_f \rho_f}\nabla^2 T_f - u\frac{\partial T_f}{\partial x} \tag{2}$$

$$\frac{\partial T_s}{\partial t} = \frac{k_s}{c_s \rho_s}\nabla^2 T_s + \frac{1}{c_s \rho_s} Q_{MCE} \tag{3}$$

where T, t, k, c, ρ and u are the temperature, time, thermal conductivity, specific heat, mass density and fluid velocity, respectively. The subscripts f and s denote fluid and solid domains, respectively. The volumetric magnetocaloric effect is implemented through the term Q_{MCE}. The domains on which Eqs. (2) and (3) are solved are coupled through a continuous boundary condition at the interface between the two domains. The model assumes symmetry in a way that only half a fluid channel and half a solid magnetocaloric material plate are modeled.

The domain is discretized using the finite difference approach combined with the Alternate Direction Implicit temporal integration scheme, as described in detail in Nielsen et al. (2009a). The convection term is defined using the upwind scheme. The velocity profile, $u(y)$, is assumed to be the solution of an incompressible, fully developed laminar flow, which can be expressed analytically as

$$u = \frac{3}{2}\tilde{u}\left(\frac{y^2}{H_f^2} - 1\right) \tag{4}$$

with $\tilde{u}$ being the mean fluid velocity and H_f denoting the thickness of the fluid channel. This solution was obtained using the non-slip boundary condition on the fluid–solid interface and symmetry on the boundary denoting the middle of the fluid channel. The temporal variation of the mean fluid velocity is shown in Fig. 6.

The magnetocaloric effect source term, Q_{MCE} is defined as

$$Q_{MCE} = f\left(H^{new}, H^{old}, T^{new}, T^{old}\right) \tag{5}$$

where $f(H^{new}, H^{old}, T^{new}, T^{old})$ is a function that returns the magnetocaloric effect based on either a look-up table of experimental data or through the usage of e.g. the mean field model and H denotes the norm of the magnetic field. The variation of the applied magnetic field is shown in Fig. 6.

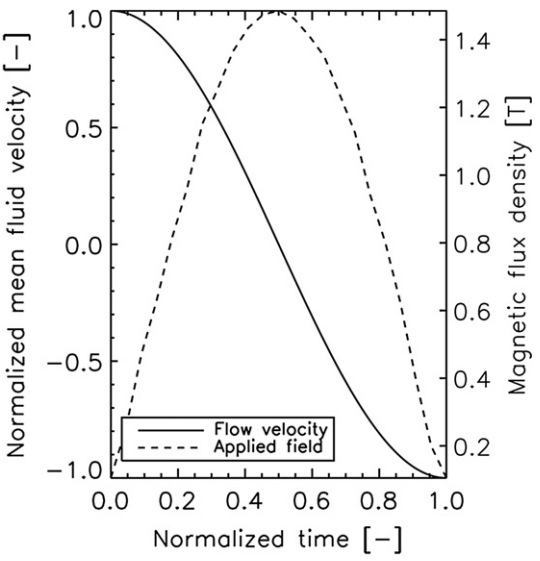

Fig. 6 – The mean fluid velocity and applied magnetic field as functions of time through one complete AMR cycle.

The AMR cycle is solved by integrating Eq. (1) in time steps of 0.1 ms, applying the cosine velocity profile and the magnetic field shown in Fig. 6. The steady state of the solution is reached when the relative changes in the cooling power (q_C) and rejected heat (q_H) are both less than 10^{-4} between two consecutive AMR cycles. The maximum temperature span and cooling power are determined by fixing the hot temperature and applied zero heat load at the cold end.

3.2. Magnetocaloric data

The adiabatic temperature change and the specific heat of a magnetocaloric material are generally functions of magnetic field, H, and temperature, T. It has been argued that proper materials data should be used whenever modeling an actual experiment as opposed to using a theoretical data set, like e.g. a mean field model (Nielsen et al., 2009b). In the present case commercial grade gadolinium was used and the magnetocaloric properties published in Dankov et al. (1998) were obtained through private communication w. V.K. Pecharsky. The data were published as a function of applied field. Assuming equilibrium at each measurement the magnetization of the sample may be assumed to be constant and homogeneous. This combined with the rectangular shape of the sample make the simplified Aharoni (1998) demagnetization correction valid and this was thus applied to obtain the magnetocaloric data as a function of internal magnetic field as described in Bahl and Nielsen (2009). The mass density was set to 7900 $kg\,m^{-3}$ and the thermal conductivity to 10.5 $W\,m^{-1}\cdot K^{-1}$ see Table 3 for more information.

3.3. Demagnetization model

It is well known that when applying a magnetic field to a magnetic material the field inside the sample, **H**, is generally not equal to the applied field. The reason for this is the effect

Table 3 – Relevant materials data for the gadolinium used as regenerator material and the heat transfer fluid assumed to be water.

Domain	Mass density ($kg\,m^{-3}$)	Specific heat, c ($J\,kg^{-1}\,K^{-1}$)	Thermal conductivity, k ($W\,m^{-2}\,K^{-1}$)	Thickness, H (mm)
Heat transfer fluid	1000	4200	0.6	0.3
Regenerator	7900	371	10.5	0.55

of demagnetization, which is a boundary effect that can be interpreted as a result of accumulated magnetic surface charge on the sample. It is conventional to write the internal magnetic field as

$$\mathbf{H} = \mathbf{H}_{\text{appl}} + \mathbf{H}_{\text{dem}} \tag{6}$$

with the applied and demagnetizing fields denoted by $\mathbf{H}_{\text{appl}}$ and $\mathbf{H}_{\text{dem}}$, respectively. Several approaches have been followed in order to calculate the demagnetizing field. However, it should be kept in mind that it will generally be a function of the magnetization, $\mathbf{M}(\mathbf{H},T)$, which in turn is a function of internal magnetic field and temperature. Thus, if the magnetization is not constant an iterative approach for the solution of Eq. (6) must be followed. A range of special cases in terms of calculation of the demagnetizing field have been studied in the literature—see e.g. Joseph and Schloemann (1965), Brug and Wolf (1985), Osborn (1945), Beleggia and De Graef (2003), Peksoy and Rowe (2005), Tandon et al. (2004a), Smith et al. (2010). In the simplest case of constant magnetization the norm of the demagnetizing field may be expressed as (Bahl and Nielsen, 2009)

$$\mathbf{H}_{\text{dem}} = -NM \tag{7}$$

where N is the average demagnetization factor (and is determined through only the geometry of the sample and orientation of the magnetic field lines) and M is the norm of the magnetization throughout the sample. The average demagnetization factor may be calculated analytically for some geometries (see e.g. Aharoni (1998) or Smith et al. (2010) for the case of flat plates or Osborn (1945) for the case of ellipsoids).

In the present case the demagnetizing field of a stack of rectangular prisms, or flat plates, is of interest. The demagnetizing field is as mentioned of geometric, thermal and material-specific nature. The geometric part is, in this specific case, coupled to the aspect ratio of the plates, along which axis the external magnetic field is applied, the number of plates and their spacing.

Generally, the system modeled here poses a non-uniform temperature distribution and thus non-uniform magnetization. Thus, Eq. (7) is generally not valid and the coupling between Eqs. (1) and (6) becomes non-linear and should be solved by iteration. The model for solving Eq. (6) is described in detail in Smith et al. (2010) and Christensen et al. (in press).

It is currently not feasible to directly couple the AMR model and that of the demagnetizing field in a stack of flat plates. The latter model is much too computer-intensive at present. However, the demagnetization model has been applied to the cases of various hot-side temperatures and the approximate temperature spans obtained assuming the applied magnetic field profile. In this way a set of corrected magnetic field profiles, as a function of time, have been obtained and applied in the AMR model. In this way the AMR model is run twice for each case—one where the applied field measured in the permanent magnet array is assumed and one where the average internal field derived from the demagnetization model is applied (taking into account the approximate temperature span of the given case).

4. Results and discussion

In the following experimental and modeling results are compared. First, the effect of demagnetization on the particular experimental system is discussed. Second, zero heat load temperature spans at a range of operating parameters are presented and discussed.

4.1. *The effect of demagnetization*

The demagnetization model presented in Christensen et al. (in press) was applied to the specific geometry as discussed in Section 2. When the magnets are rotated the applied field is perpendicular to the xy cross-section when the field is at its maximum and minimum (angles 0° and 180° in Fig. 7, respectively) thus minimizing the demagnetizing field. The applied magnetic field is perpendicular to the xz plane halfway between the maximum and minimum values of the magnetic field norm thus maximizing the demagnetizing field here. The spatial average of the resulting temporal internal field profiles are given in Fig. 7. It is apparent from the figure that the demagnetizing field reduces the internal field compared to the applied field (which is to be expected) and that as the hot-side temperature is lowered the field strength is decreased, which is due to the fact that the magnetocaloric material is (partially) in its ferromagnetic state. This combined with a rather large geometrical demagnetization (at angles 90° and 270°, respectively) makes the internal magnetic field become significantly lower than the applied magnetic field. It may thus be concluded that the internal magnetic field deviates the most from the applied magnetic field when this is halfway between its two extremes.

4.2. *Comparison between experiment and model*

A range of operational parameters were varied and the resulting steady-state, no-load temperature spans obtained. The PMMR device was run at the AMR cycle frequencies 0.5, 1.0 and 2.0 Hz and at two different fluid movement lengths corresponding to two different values of the utilization defined in Eq. (1). The hot-side temperature was varied between 290 and 305 K.

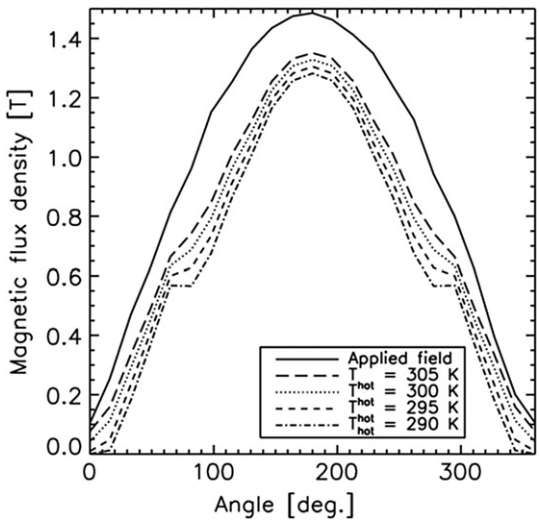

Fig. 7 – The magnetic field distribution profile and the average internal field as a function of various hot-side temperatures with an imposed temperature span of 10 K in each case calculated using the demagnetization model.

In Fig. 8 the results are plotted. The general trend is clear that the zero-load temperature span increases with increasing hot-side temperature. However, above a hot-side temperature of 300 K the trend of temperature span is slightly decreasing. This response was also observed in Rowe and Tura (2006, 2007). It is generally seen, from the experimental data, that a lower utilization and a lower operating frequency yield the larger no-load temperature span. This is a trend also clearly observed model-wise in, e.g., Nielsen et al. (2010). That the largest temperature spans appear at the lowest frequencies is simply due to the fact that the number of transfer units ($\mathrm{NTU} = hA/\dot{m}c_f$) is larger at smaller frequencies and thus the regenerator is more efficient (Dragutinovic and Baclic, 1998).

The reason why the low utilization yields the higher temperature span is due to the fact that less heat transfer fluid is moved through the system, which has two implications: the fluid velocity is lower, which improves the heat transfer and the temperature gradient across the regenerator in the flow direction is not moved as much as in the case of the higher utilization. Again, this behavior is well supported in literature (Tura and Rowe, 2009; Bahl et al., 2009).

The model results generally follow the trends of the experimental results. However, in some cases deviations are seen—especially at the lowest utilization and an operating frequency of 2 Hz. Here the model predicts a somewhat

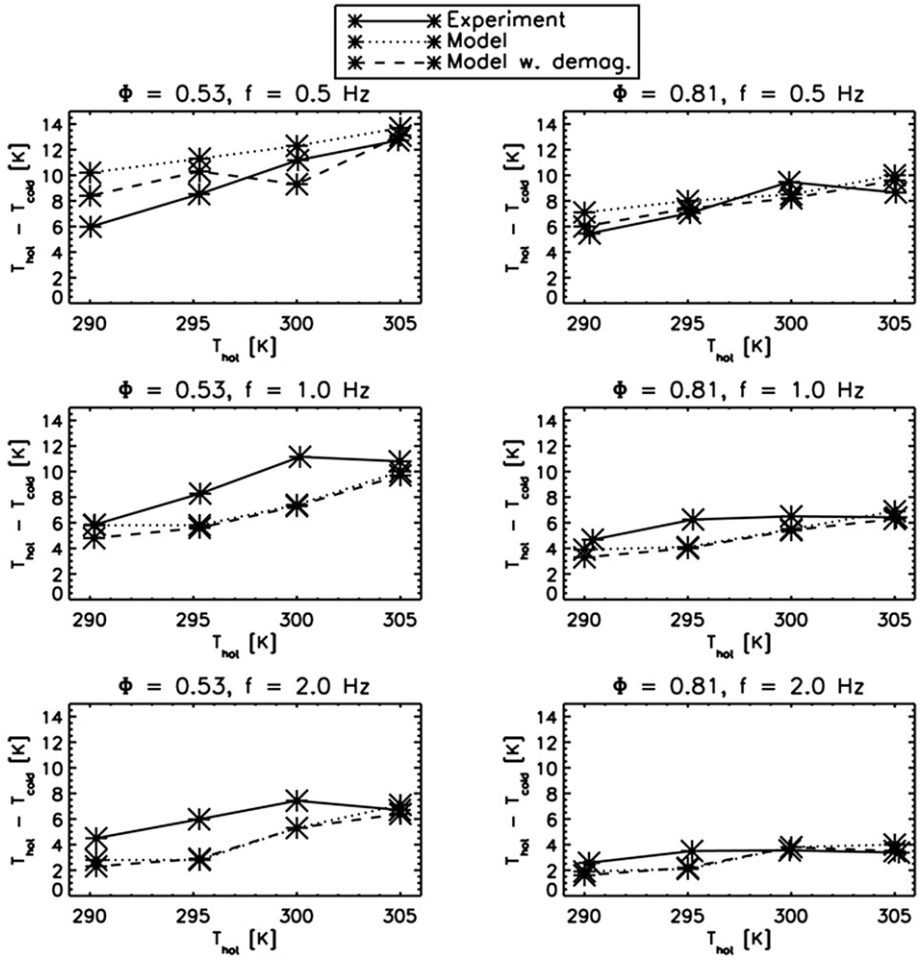

Fig. 8 – Results from PMMR with parallel plates and the corresponding modeling results.

smaller temperature span compared to that observed in the experiment. A possible explanation for this behavior is eddy-current dissipation due to the large conductive area presented by the plates. The rotating magnetic field induces eddy-currents in the plates, which act as a thermal source in the solid energy balance (Eq. (2)). The strength of this term increases with frequency. The impact on the energy balance will depend upon the magnitude relative to the other physical terms represented. As utilization decreases with a fixed frequency, the eddy-current dissipation term is expected to be more important. This is consistent with the results shown in Fig. 8. This highlights one of the advantages of a spherical particle bed, where point contacts and small particle size, reduce eddy-current dissipation.

Another reason for the slight inconsistency between the experimental and model data is the quality of the magnetocaloric effect properties (adiabatic temperature change and specific heat) input to the model. The gadolinium plates used in the experiment was not characterized, but rather an older Gd data set was used. This may lead to inconsistencies since the magnetocaloric properties of Gd can vary significantly depending on the purity and processing of the material (Dankov et al., 1998; Bahl and Nielsen, 2009).

Finally, another physical effect that is not currently resolved by the presented AMR model may cause deviations between experimental and predicted results. This is the effect of maldistribution of the flow due to inhomogeneous plate stacking. It has recently been found that in microchannel regenerators (as considered here) the regenerator effectiveness is very sensitive to the relative accuracy of the fluid channel thicknesses (Jensen et al., 2010, 2011).

It is generally not possible to quantify the impact of these effects at the current state of AMR modeling and is therefore a very important point to address in the future for improving the quality of AMR models and thereby improving their performance predictions.

Considering the effect of demagnetization the general trend is that the resulting temperature span is slightly lower than that obtained assuming the applied magnetic field profile. As expected, at the lower hot-side temperatures the deviation between applying the magnetic field profile and that corrected for demagnetization is largest. Here, the resulting internal field is lowered the most since the magnetocaloric material is in the ferromagnetic state.

5. Conclusions

An investigation into the performance of a parallel plate AMR is described. Experimental results are compared to a numerical model where the impacts of demagnetization are considered. In general, it is found that the largest temperature spans are obtained at the lowest frequencies and that the cooling power of the current setup is significantly smaller than when spheres of Gd are used. This is attributed to the dimensions of the plates and their spacing. As described in Section 2 plates with a thickness of 0.1 mm and a spacing of 0.05 mm are needed if heat transfer characteristics similar to those obtained when using spheres are to be obtained. Temperature span sensitivity to utilization and rejection temperatures are shown with maximum no-load spans found with utilization of ~0.5. Maximum spans for the configuration and conditions explored were ~12 K. Numerical results with and without demagnetization compare well to the experimental results with deviations in temperature span being more significant at lower utilizations.

Acknowledgments

K.K. Nielsen thanks the support of the Programme Commission on Energy and Environment (EnMi) (contract no. 2104-06-0032), which is part of the Danish Council for Strategic Research and the Danish Agency for Science, Technology and Innovation under the Danish Ministry for Science, Technology and Innovation. A. Tura and A. Rowe thank the Natural Sciences and Engineering Research Council of Canada for support as well as the H2Can Strategic Network.

REFERENCES

Aharoni, A., 1998. Demagnetizing factors for rectangular ferromagnetic prisms. J. Appl. Phys. 83 (6), 3432–3434.

Bahl, C.R.H., Nielsen, K.K., 2009. The effect of demagnetization on the magnetocaloric properties of gadolinium. J. Appl. Phys. 105, 013916.

Bahl, C.R.H., Petersen, T.F., Pryds, N., Smith, A., 2009. A Versatile magnetic refrigeration test device. Rev. Sci. Instrum. 79, 093906.

Beleggia, M., De Graef, M., 2003. On the computation of demagnetization tensor field for an arbitrary particle shape using a Fourier space approach. J. Magn. Mag. Mater. 263, L1–L9.

Brug, J.A., Wolf, W.P., 1985. Demagnetizing fields in magnetic measurements. I. Thin discs. J. Appl. Phys. 57 (10), 4685–4694.

Christensen, D.V., Nielsen, K.K., Bahl, C.R.H., Smith, A. Demagnetizing effects in stacked rectangular prisms. J. Phys. D: Appl. Phys., in press.

Dankov, S.Y., Tishin, A.M., Pecharsky, V.K., Gschneidner Jr., K.A., 1998. Magnetic phase transitions and the magnetothermal properties of gadolinium. Phys. Rev. 57 (6), 3478–3490.

Dragutinovic, G.D., Baclic, B.S., 1998. Operation of counterflow regenerators, v. 4. In: International Series on Developments in Heat Transfer, first ed. Computational Mechanics Publications.

Gschneidner Jr., K.A., Pecharsky, V.K., 2008. Thirty years of near room temperature magnetic cooling: where we are today and future prospects. Int. J. Refrigeration 31, 945–961.

Jensen, J.B., Engelbrecht, K., Bahl, C.R.H., Pryds, N., Nellis, G.F., Klein, S.A., Elmegaard, B., 2010. Modeling of parallel-plate regenerators with non-uniform plate distributions. Int. J. Heat Mass Transf. 53, 5065–5072.

Jensen, J.B., Bahl, C.R.H., Engelbrecht, K., Elmegaard, B., Pryds, N., 2011. Analysis of single blow effectiveness in non-uniform parallel plate regenerators. Int. J. Heat Mass Transf. 54, 4746–4751.

Joseph, R.I., Schloemann, E., 1965. Demagnetizing field in non-ellipsoidal bodies. J. Appl. Phys. 36 (5), 1579–1593.

Nielsen, K.K., Bahl, C.R.H., Smith, A., Bjørk, R., Pryds, N., Hattel, J., 2009a. Detailed numerical modeling of a linear parallel-plate active magnetic regenerator. Int. J. Refrigeration 32, 1478–1486.

Nielsen, K.K., Bahl, C.R.H., Smith, A., Pryds, N., Hattel, J., 2010. A comprehensive parameter study of an active magnetic

regenerator using a 2D numerical model. Int. J. Refrigeration 33, 753–764.
Nielsen, K.K., Pryds, N., Smith, A., Bahl, C.R.H., Hattel, J., 2009b. Two-dimensional numerical modeling of active magnetic regeneration, in: Egolf, P.W. (ed.), Proceedings of the Third International Conference on Magnetic Refrigeration at Room Temperature, International Institute of Refrigeration.
Osborn, J.A., 1945. Demagnetizing factors of the general ellipsoid. Phys. Rev. 67 (11-12), 351–357.
Pecharsky, V.K., Gschneidner Jr., K.A., 1999. Magnetocaloric effect and magnetic refrigeration. J. Magn. Mag. Mater. 200, 44–56.
Peksoy, O., Rowe, A., 2005. Demagnetizing effects in active magnetic regenerators. J. Magn. Mag. Mater. 288, 424–432.
Petersen, T.F., Pryds, N., Smith, A., Hattel, J., Schmidt, H., Knudsen, H.J.H., 2008a. Two-dimensional mathematical model of a reciprocating room-temperature active magnetic regenerator. Int. J. Refrigeration 32, 432–443.
Rowe, A., 2011. Configuration and performance analysis of magnetic refrigerators. Int. J. Refrigeration 34, 168–177.
Rowe, A., Tura, A., 2007. Active magnetic regenerator performance enhancement using passive magnetic materials. J. Magn. Mag. Mater. 320 (7), 1357–1363.
Rowe, A., Tura, A., 2006. Experimental investigation of a three-material layered active magnetic regenerator. Int. J. Refrigeration 29, 1286–1293.
Smith, A., Nielsen, K.K., Christensen, D.V., Bahl, C.R.H., Bjørk, R., Hattel, J., 2010. The demagnetizing field of a nonuniform rectangular prism. J. Appl. Phys. 107 (10), 103910–103918.
Tandon, S., Beleggia, M., Zhu, Y., De Graef, M., 2004a. On the computation of the demagnetization tensor for uniformly magnetized particles of arbitrary shape. Part I: analytical approach. J. Magn. Mag. Mater. 271, 9–26.
Tura, A., Rowe, A., 2011. Permanent magnet magnetic refrigerator design and experimental characterization. Int. J. Refrigeration 34, 628–639.
Tura, A., Rowe, A., 2009. Progress in the characterization and optimization of a permanent magnet magnetic refrigerator, in: Egolf, P.W. (ed.), Proceedings of the Third International Conference on Magnetic Refrigeration at Room Temperature, International Institute of Refrigeration.

Appendix IV
Dual Nested Halbach Magnetic Refrigerator Cost Optimization

Submitted to the International Journal of Refrigeration

Concentric Halbach Cylinder Magnetic Refrigerator Cost Optimization

A. Tura[1] and A. Rowe

[1]Department of Mechanical Engineering, Institute of Integrated Energy Systems

University of Victoria, PO Box 3055 STN CSC,

Victoria, BC, Canada

[1] To whom correspondence should be addressed:

A. Tura

Department of Mechanical Engineering

University of Victoria

Victoria, B.C., V8W 3P6

CANADA

Electronic mail: atura@uvic.ca

Tel.: 250-721-7295

Fax: 250- 721-6051

Abstract

Commercial magnetic refrigeration near room temperature faces technological challenges and high costs. Although several laboratory devices have been developed, no design is realistically close to the performance, reliability, and financial proposition of a vapor compression refrigerator.

This study examines the total cost of cooling provided by an idealized dual-regenerator concentric Halbach design. An optimization process, based on a simplified analytical model rather than a computationally intensive finite element model, is applied to geometrical and operational parameters, with the objective function minimizing capital and operating cost. Additionally, the model utilizes a refrigerant with ideal magnetocaloric (MCE) properties and constant specific heat. The model is first validated against extrapolated experimental data from an existing device, and then the optimization routine is applied to a range of cooling demand and MCE values. Results help in identifying target refrigerant properties, and refrigerator geometrical/operational parameters. Moreover, a sensitivity analysis demonstrates how the design variables affect the system performance.

Keywords: gadolinium, magnetocaloric effect, active magnetic regenerator, optimization, magnetic refrigerator, efficiency

Nomenclature

Acronyms

AMR(R)	Active Magnetic Regenerator (Refrigerator)
CRF	Capital Recovery Factor
CF	Duty Cycle
MCE	Magnetocaloric Effect (adiabatic temperature change)
MR	Magnetic Refrigerator
NTU	Heat Transfer Units
PMMR	Permanent Magnet Magnetic Refrigerator

Symbols

A	Cross sectional area/ Surface area
B	Magnetic flux density
C	cost
c	Heat capacity
D	Diameter
Ex	Exergetic
f	Frequency
H	Magnetic field intensity
h	Heat transfer coefficient
k	Non-dimensional conductance
L	Length
M	Magnetization
m	Mass
Nu	Nusselt number
P	Period fraction
P	Pressure
Q	Energy flux
R	Thermal mass ratio
r	Radius
RMS	Root mean square
Re	Reynold's number
T	Temperature

t	Time
u	velocity
V	Volume
W	Work
x	Spatial variable

Greek

α	Porosity
$\in$	Effectiveness
η	Efficiency
Λ	Figure of merit
Φ	Utilization
μ	Viscosity/ magnetic permeability/specific exergetic cooling
ρ	Density
τ	Period

Subscripts

ad	Adiabatic
b	Magnetic field dependent
C	Cold
cap	Capital
Curie	Curie point
e	Electricity
eff	Effective
f	Fluid
H	Hot
high	High
i	Inner
low	Low
mag	Magnet
M	Magnetic
max	Maximum
min	Minimum
r	Magnetic remanence

o	Outer
op	Operating
P	Pressure/ particle
s	Solid
w	wetted
x	Location

1. Introduction

Permanent magnet magnetic refrigerators (PMMRs) exploit the magnetocaloric properties (MCE) of certain materials to perform cooling. Both experimental and theoretical research has intensified in the last decade in hopes of finding more efficient and greener alternatives to conventional vapor compression cycles (Yu et al, 2010). However, currently magnetic refrigeration suffers from various technological challenges and high costs. In order to determine research priorities one should understand how the total cost of cooling varies with the device configuration, refrigerant properties and operating conditions. A number of numerical models (Nielsen et al.,2009) (Aprea et al, 2012) (Dikeos and Rowe, 2013) exploring performance of magnetic refrigeration cycles have been proposed, however assessing the cost of devices is a largely unexplored ground. Possibly the most significant publication in this direction is the work performed by Bjork (Bjork et al., 2011). Here an optimization analysis is presented, with the objective of estimating the minimum mass and cost of a magnetic refrigerator. The study conclusions are based only on capital cost minimization, thus the efficiency might be penalized. The method used a 2D numerical model to establish the temperature span and cooling power, while the geometry and magnetic field properties are based on an infinite length Halbach cylinder.

In a recent publication (Rowe, 2011), Rowe defined metrics for characterizing magnetic refrigerators (MRs) and identified targets to be met in order to make the technology commercially viable. Taking as a target market a system for household applications with a cooling capacity of 70 W when operating between 7.4 °C and 54.4 °C, he proposed that, in order to penetrate the market, it is needed to reach a specific exergetic cooling power ranging between 0.4 and 1 $WT^{-1}cm^{-3}$ and a cost of cooling less than 2 $\$W^{-1}$. This result does not include operating cost and assumes that a prescribed efficiency can be reached. By linking the device configuration to performance, one can determine both the capital and operating costs which together quantify the total cost of cooling for a

given application. One can do this calculation using a system model relating device geometry to performance of the device under arbitrary conditions.

The objective of this study is to determine the total cost of cooling for a dual-regenerator concentric Halbach configuration as well as optimal geometry and operating conditions, while also giving an insight of target refrigerant magnetocaloric properties. An optimization process to minimize total cost is applied to geometrical and operational parameters for cooling powers from 70 to 400 W and operating temperatures of T_C = 5 ºC and T_H = 55 ºC. Detailed performance models of magnetic refrigerators can be computationally intensive, thus it can be easily seen that mapping optimized point over a range of required cooling powers and refrigerant MCE properties with the given geometrical and operational parameters space may require powerful computational hardware and a long time to evaluate. Arguably a simple analytical solution, yet capable of estimating the device performance within an acceptable tolerance, could possibly allow capturing with confidence ideal design parameters in a matter of seconds or minutes on a modest computer.

2. Simplified Analytical Model

2.1. Governing equations

The idealized analytical model proposed in (Rowe, 2012) and further developed and validated in (Burdyny et al., 2012) is used to predict the performance of the MR. Following is a summary of the equations and assumptions used for the analysis, while a detailed derivation can be found in the original publications. The model replaces the coupled partial differential equations with a single one:

$$(m'_f c_p + m'_s c_b)\frac{\partial T}{\partial \tilde{t}} + \dot{m} c_p \frac{\partial T}{\partial \tilde{x}} - \frac{\partial T}{\partial \tilde{x}}\left(\kappa_{eff} A \frac{\partial T}{\partial \tilde{x}}\right) = -m'_s T \left(\frac{\partial M}{\partial T}\right)_H \frac{\partial \mu_0 H}{\partial \tilde{t}} \quad (1)$$

under the assumption that $T_f \cong T_s = T(x,t)$, valid for a high heat transfer coefficient, where m'_f is the mass of fluid per unit length of the regenerator entrained in the pores and m'_s is the mass of magnetocaloric material per unit length, M is the magnetization per unit mass, c is mass specific

heat, κ_{eff} is effective conductivity, including the solid and fluid terms, and A is the cross-sectional area of the regenerator.

Assuming the variation in MCE with temperature is constant, cooling power and input power are derived from the above governing equation combined with the expressions for magnetic work and losses (Rowe, 2012). If entrained fluid is taken in to account (R > 1), and a step-wise cycle is adopted, we have:

$$Q_c = \frac{m_s c_s}{\tau_c} U \left(\frac{\Delta T}{T} \right) T_{a0} \left(1 - \frac{p}{\sin p} \left(\frac{U}{\kappa} \frac{\Delta T}{T} \right)^{-1} \left(\frac{T_{a1}}{T_{a0}} - \cos(p) \right) \right) \tag{2}$$

$$W_M = \frac{m_s c_s}{\tau_c} \left(\frac{\Delta T}{T} \right) \left[\frac{R-1}{R} \left(\frac{\Delta T}{T} \right) \int_0^1 T dx + U \left(T_{a1} - T_{a0} \right) \right], \tag{3}$$

where

$$\int_0^1 T dx = \frac{1 - \cos(p)}{p \sin(p)} (-T_{a1} + T_{a0}), \text{ with } p \equiv \left(\frac{\Delta T}{T} \right) \left(\frac{1}{\kappa} \frac{R-1}{R} \right)^{\frac{1}{2}}. \tag{4}$$

(ΔT/T) is the variation in magnetocaloric effect with temperature, Ta0 and Ta1 are the temperatures at the ends of the regenerator at the final phase of the demagnetization process before the cold blow (T_{ax} is the temperature at a generic position x), and κ is the non-dimensional conductance. The non-dimensional parameter U is function of utilization Φ and thermal mass ratio R:

$$U \equiv \frac{\Phi}{R} \text{ with } \Phi \equiv \frac{\dot{m} c_p \tau_B}{m'_s L c_b}, \; R \equiv 1 + \frac{m'_f c_p}{m'_s c_b} \tag{5}$$

The boundary conditions T_{a0} and T_{a1} can be determined from:

$$T_C = \left(1 - \frac{U}{2} \frac{p \cos(p)}{\sin(p)} \right) T_{a0} + \frac{U}{2} \frac{p}{\sin(p)} T_{a1} \quad , \tag{6}$$

$$T_H = -\frac{U}{2} \frac{p}{\sin(p)} T_{a0} + \left(1 + \frac{U}{2} \frac{p \cos(p)}{\sin(p)} \right) T_{a1} \tag{7}$$

where T_C, and T_H are the average fluid temperatures at the cold and warm ends of the regenerator. The non-dimensional conductance κ is defined as:

$$\kappa = \frac{\tau_c}{m_s' L c_s} \frac{k_{eff} A}{L} \tag{8}$$

where effective conductivity, κ_{eff}, is divided into a static component, which takes into account the amount of solid and fluid in the regenerator, and a dispersive component, which accounts for the effects of fluid mixing (Kaviany, 1995).

Equations 2-4 assume the refrigerant behavior has an ideal magnetocaloric (MCE) profile (Rowe and Barclay, 2003), where the MCE is a linear function of temperature:

$$\Delta T_{MCE}(x) = \left(\frac{\Delta T}{T}\right) T(x). \tag{9}$$

In this study, the field dependence of the MCE is assumed to obey,

$$\Delta T_{MCE} = 3.675 H^{0.7} \tag{10}$$

which is consistent with a material like Gd near the Curie temperature (Grössinger et al, 2010). The choice of an ideal MCE is dictated by the interest in evaluating the upper bound of the possible scenarios. The matrix is treated as a bed of packed spheres of 0.3 mm diameter, which allows intimate contact between solid and fluid and it is well characterized in terms of heat transfer and viscous losses. Additional assumptions include a constant specific heat for both fluid and solid.

Having the temperature of the fluid matching the temperature of the solid implies infinite heat transfer. The impact of a finite heat transfer is included as parasitic heat leak through the regenerator. This accounts for the regenerator ineffectiveness, while maintaining a simple analytical approach. The parasitic heat loss Q_L is modeled as a function of the regenerator *NTU*. Using the Hausen model with infinite thermal mass for regenerator effectiveness, (Schmidt and Wilmott, 1981):

$$Q_L = (1-\in)\frac{2 m_d c_p}{\tau_c}(T_H - T_C) \qquad \text{with} \tag{11}$$

$$\in = \frac{NTU}{NTU + 2} \text{ and } NTU \equiv \frac{hA_w}{\dot{m}c_p} = \left(\frac{k_f}{D_h} Nu\right)\frac{A_w}{\dot{m}c_p} \tag{12}$$

where m_d is the fluid mass displaced per cycle and τ_c the cycle period, $\in$ the regenerator effectiveness. The Nu is evaluated by the Whitaker correlation (Kaviany, 1995) for the heat transfer coefficient:

$$Nu = 2 + \left(0.Re^{\frac{1}{2}} + 0.2Re^{\frac{2}{3}}\right)Pr^{0.4}, \text{ with } Re = \frac{\rho u_p}{\mu} \tag{13}$$

where ρ is fluid density, u_p pore velocity, and μ dynamic viscosity. Thermal losses due to imperfect insulation have been approximated to be a linear function of the temperature span (Equation 16), while losses due to eddy currents have been assumed to be negligible. Finally viscous losses are obtained applying the Ergun correlation for a packed bed of spheres.

For the nested Halbach configuration, the field intensity is assumed to scale with magnet size according to (Mhíocháin et al, 1999):

$$H = \frac{B_r}{\mu_0} \ln \frac{D_o}{D_i}, \tag{14}$$

where B_r is the magnet remanence, μ_0 the magnetic permeability in the vacuum, D_o the outer diameter and D_i the inner diameter of the cylinder. In addition, the effective volume available for the refrigerant is assumed to be limited to 85% of the magnet (field drop off toward the ends). Also, the useful volume is assumed to have a diameter 3 mm smaller than D_i to accommodate for a regenerator shell.

The cylinder size has an impact on the torque necessary for the system rotation, therefore an additional mechanical loss is added to the cycle. In accordance with Mhíocháin (1999) the torque in relatively long nested Halbach cylinders has been found to be, on first approximation, a cubic function of diameter only. Thus, based on experiments using our device, magnet torque is estimated using the following,

$$Torque = 300\ (Nm^{-2}) D_o^{\ 3}. \tag{15}$$

Although it is not possible to state with confidence if this is a realistic estimation (we observed great variability in torques based on manufacturing precision and other design parameters), the model results are not very sensitive to this parameter. Mechanical losses are also accounted for, and estimated to be 0.5 Nm. This value is also based on the existing laboratory apparatus measurements.

2.2. The Dual regenerator Halbach cylinder model: comparison with experimental data

The specific configuration analyzed is the device investigated in Tura et. al. (2011). The apparatus is comprised of two active magnetic regenerators (AMRs) connected by a fluid transfer loop (water-glycol) with oscillating flow created by a displacer. A cold heat exchanger separates the two AMRs and two hot heat exchangers reject heat from the system. The AMR beds are alternatively magnetized and demagnetized by two nested Halbach arrays, where an inside magnet rotates with respect to the outside one. The AMR cycles are synchronized such that they operate 180° out of phase. The geometrical and operational parameters are summarized in Table 1. The model results are compared to experimental data for a heat rejection temperature T_H of 22 °C and utilizations of 0.64, 0.94, 1.03 and 1.28. Utilization is evaluated using as reference heat capacity c_B from Gd peak value of 383 J $kg^{-1}K^{-1}$ at 0 T, while the thermal heat leak is approximated to be

$$Q_{amb} = 0.35\left[WK^{-1}\right]T_{span}, \tag{16}$$

where T_{span} is the span at which the system is operating. The constant of proportionality is obtained from a finite element thermal model of the device.

The effects of geometry on local field (demagnetization) are estimated with a three dimensional magnetostatic model assuming gadolinium properties and a linear temperature distribution between 300 K - 280 K. From this an averaged demagnetization value of 0.25 is used for the entire volume of the regenerator.

Figure 1 compares gadolinium MCE to three cases of ideal MCE where at 295 K, $\Delta T/T$ is 100%, 75%, and 50% of the Gd adiabatic temperature change for a 0-1.4 T field variation.

Table 1. PMMR specifications

Property	Range	Units
Magnetic field	0.1-1.4	T
Operating frequency	2	Hz
Utilization	0.62,0.84, 1.03, 1.28	[-]
Heat rejection temperature	22	°C
Additional model parameters:		
Magnetic field rms	0.66-1.1	T
Demagnetization	25%	[-]
Heat Leak proportionality constant	0.35	WK^{-1}
Regenerator properties:		
Volume	10.8	cm^3
Length	55	mm
Mass	55	g
Porosity	36%	[-]
Composition	Gadolinium, metal	[-]
Geometry	Spheres, diameter 300	µm

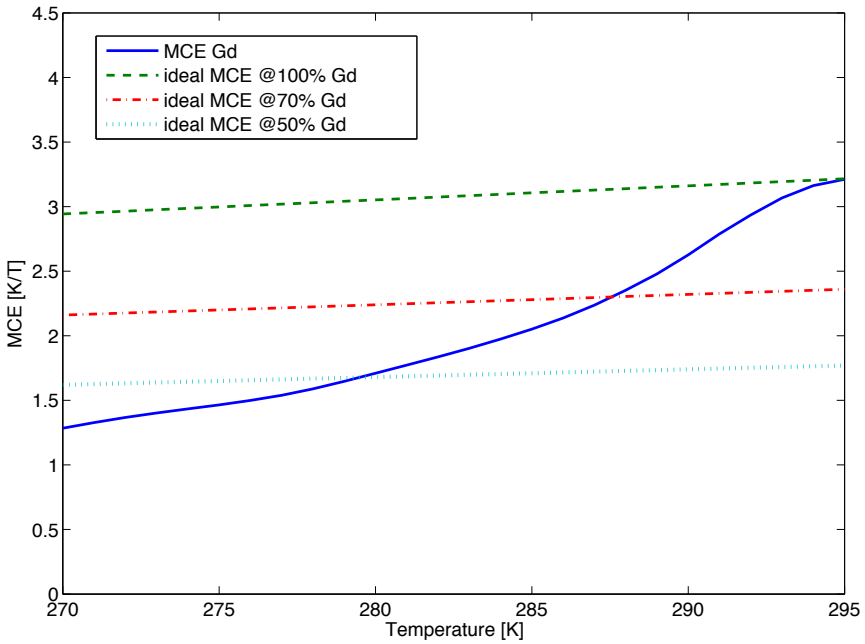

Figure 1: Gd MCE compared to idealized MCE for 100% , 70%, and 50% of Gd MCE @ 295 K

Figure 2 shows the experimental data of net cooling power versus temperature span. Linear fits to the data show extrapolated results for maximum Q_c/no-span to maximum span/no-load. Figure 3 shows a similar plot using the model, where the ideal MCE at 75% of Gd was arbitrarily chosen.

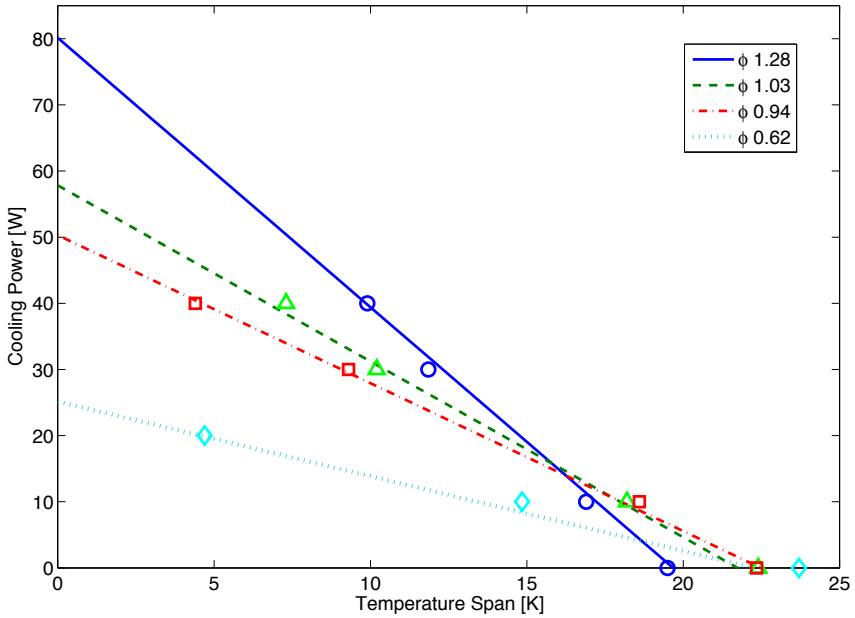

Figure 2: Extrapolated (lines) and experimental (markers) data of cooling versus temperature span.

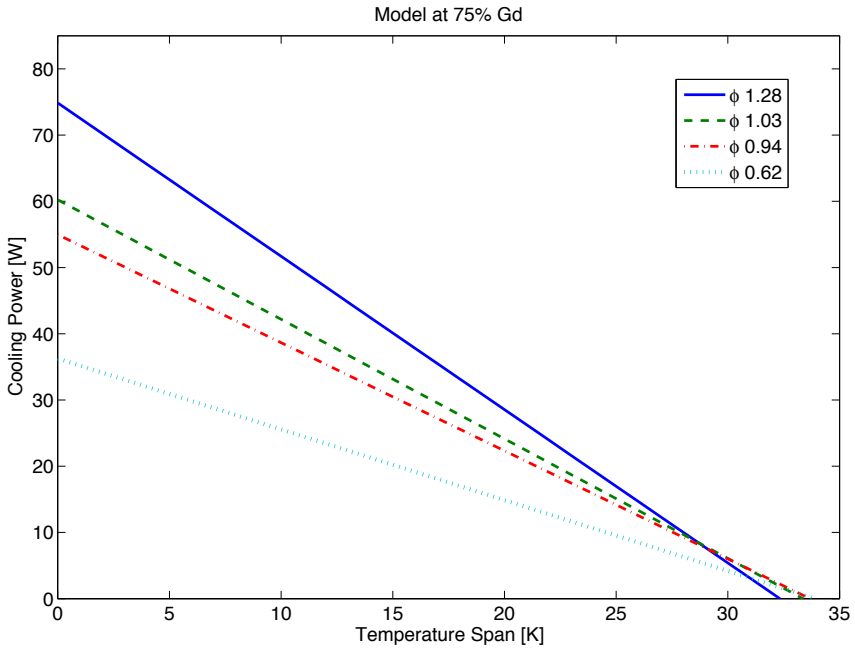

Figure 3: Model results of cooling versus temperature span, where the ideal MCE at 75% of Gd is used.

The model seems to capture the experimental trends. If operating at zero temperature span the real refrigerant is closest to performing like the idealized material as the properties are relatively constant. Under such operating conditions (ΔT = 0) the chosen ideal refrigerant performance produces results similar to the experimental data. Lower utilizations tend to slightly overestimate cooling power for equivalent span, while the reverse is true for the higher utilizations. Thus the model shows less spread as utilization is varied from 0.62 to 1.28. In general, some degree of overestimation by the model is expected for several reasons. Firstly, the model assumes an ideal refrigerant, with an ideal MCE distribution and constant specific heat equal to peak gadolinium's c_B. In addition, it assumes a step wise cycle while the apparatus adopts a pseudo-sinusoidal wave form for the magnetization and fluid blow (this is partially incorporated by using RMS values). Conversely, the experimental apparatus could be underperforming because of flow channeling, air trapped in the system, void volumes, etc. Additionally, if the ideal refrigerant is chosen to perform similarly to the experimental device for $\Delta T = 0$, by intuition it should be less sensitive to the cooling load when $\Delta T \neq 0$. In other words the slope of the load/span line in the plot should not be as pronounced. This can be explained by the fact that gadolinium displays a caret shaped MCE rather than following an ideal linear distribution. It can be clearly observed that, while the trend of the curves in Figure 2 and Figure 3 follow the same pattern, the model is indeed less sensitive to thermal loads showing a maximum span (for $Q_c = 0$) of almost 35 K compared to the actual device, with only 22 K. It is interesting to observe that the impact of changing utilization follows the same trend in all three cases: larger utilizations allowed larger cooling power, but the curves become steeper too, meaning that only lower temperature spans can be achieved. In the experimental case the curves cross over at about ΔT = 16 K , while in the model this happens for ΔT = 30 K. However, as observed earlier, the curves of the model are more closely packed together when compared to the extrapolated experimental data. This can again be explained by the fact that using an ideal MCE distribution makes the AMR less sensitive to the perturbation induced by the fluid pulsations.

Using the definition of the specific exegetic cooling power, μ:

$$\mu = \frac{Ex_Q}{B_0 V_{MCM}}, \quad \text{with} \quad Ex_Q = Q_C \left(\frac{T_H}{T_C} - 1 \right) \tag{17}$$

where H_a is the applied magnetic field and V_{MCM} is the volume of refrigerant, Figure 4 illustrates the estimations made from the model. The 2 Hz operating frequency plot shows that for a 10 K span μ

is varied between 0.055 WT^{-1} cm^{-3} for $\Phi = 0.62$ and a maximum of 0.105 WT^{-1} cm^{-3} for $\Phi = 1.28$. Also, specific exergetic cooling shows a maximum for the temperature span of 17 K for all utilizations, where it is approximately 0.125 WT^{-1} cm^{-3} for $\Phi = 1.28$. For the 4 Hz case (plot to the right), at a T_{span} of 10 K, μ ranges from 0.1 WT^{-1} cm^{-3} to 0.2 WT^{-1} cm^{-3} . The maximum is found for a span between 14.5 K and 17.5 K depending on the utilization used. The experimental results with PMMR I gave $\mu = 0.085$ WT^{-1} cm^{-3} when operating with a 10 K temperature span, 4 Hz and $\Phi = 1.03$ (Tura et al, 2010). Under the same operating condition the model evaluated the specific exergetic cooling to be 0.15 WT^{-1} cm^{-3}, almost twice as much. This is to be expected as the ideal refrigerant cooling power, as already noted, is less sensitive to temperature span.

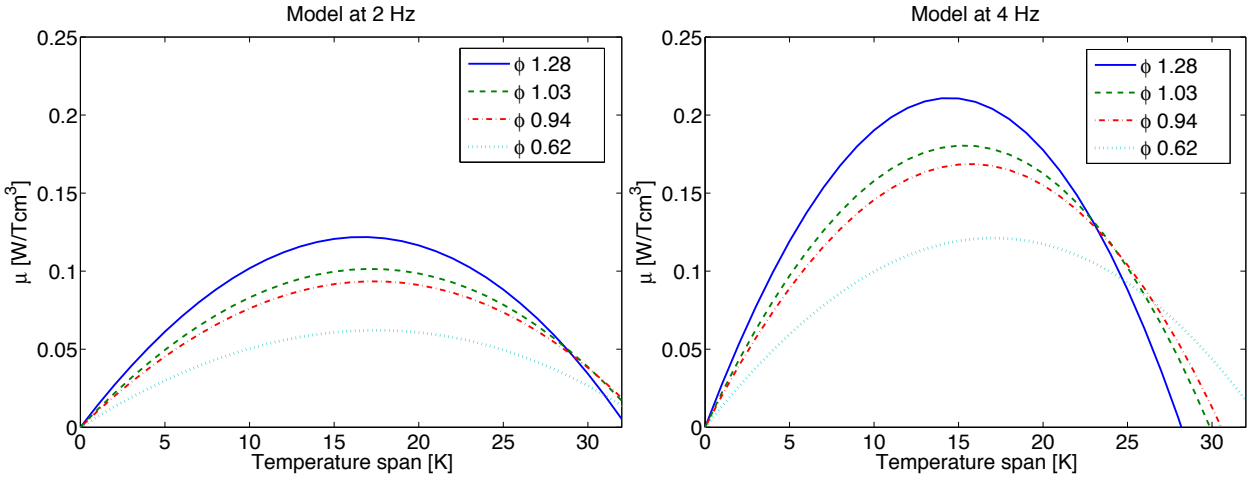

Figure 4: Model specific exegetic specific cooling power for the given parameter sweep, left plot shows 2 Hz operation, right plot 4 Hz.

Figure 5 shows the cost of capacity (equipment) which is merely the cost of refrigerant and magnets divided by cooling power. The costs of magnets and refrigerant are determined by their mass. Cost of refrigerant is assumed to be 150 $\$kg^{-1}$ and the cost of NdFeB is 42 $\$kg^{-1}$. Cost of capacity (for 2 Hz) ranges from a minimum of 10 $\$W^{-1}$ to a maximum of 21 $\$W^{-1}$ at $\Delta T = 0$ K and it grows exponentially as the span approaches the maximum and the cooling power goes to 0 W. Rowe (2011) estimated cost of capacity to be < 2 $\$W^{-1}$ for this type of MR configuration if $\mu > 1$ W T^{-1} cm^{-3} when operating between 7.4 C and 54.4 C with a cooling capacity of 70 W.

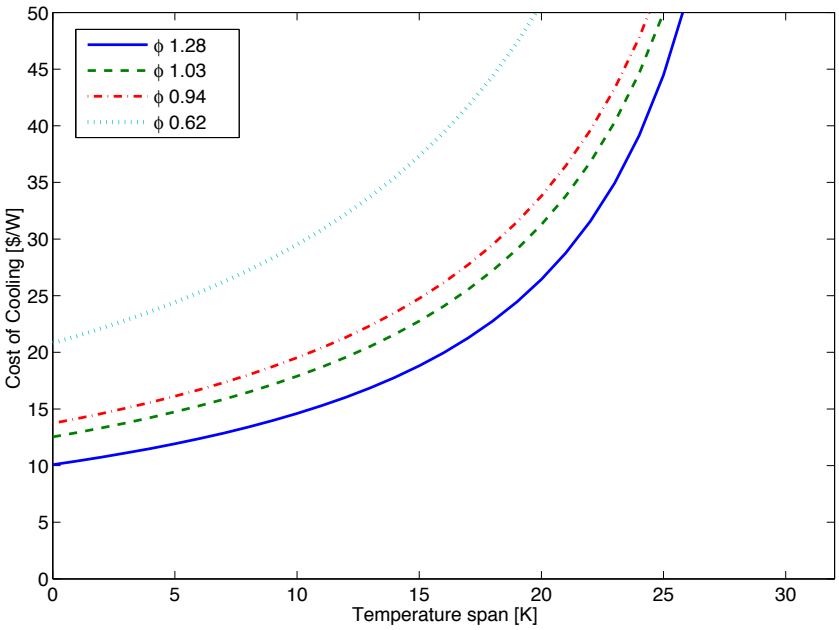

Figure 5: Cost of cooling for the given parameter sweep.

Such analysis raises the question of what kind of performance would be possible if geometry, utilization, and frequency were to be optimized with the objective function minimizing both operating and capital cost. Also it would be valuable to be able to estimate the sensitivity to refrigerant performance and cooling power demand.

3. Optimization Model

3.1. Optimization Routine

An optimization model was constructed in Matlab with the objective of minimizing the total cost rate of a MR. Given the non-linearity of the problem the function *fmincon* was used for the process. The variables in the optimization are utilization Φ, frequency f, outer magnet diameter D_o, inner magnet diameter D_i, and length of the magnet L. The objective function (OF) is the sum of capital cost rate and operating cost rate

$$C_Q = C_{cap} + C_{op} \tag{18}$$

and it uses a number of nested functions governing the physics of the device. Figure 6 illustrates the flowchart of the objective function structure. Capital cost is obtained by simply evaluating the volumes of the magnet and refrigerant, and multiplying them by their cost per weight and the capital recovery factor *CRF,* which is set to 10 years with a discounting rate of 5%. Magnet alloy (NdFeB) cost is fixed to 42 $\$kg^{-1}$ (Gutfleisch et al, 2011) and refrigerant cost to 150 $\$kg^{-1}$, which is quite optimistic when compared to current prices of high purity metallic gadolinium spheres, but pessimistic if compared to the 10-20 $\$kg^{-1}$ price of first order refrigerants or bulk gadolinium. We will see that the refrigerant cost is a fraction of the magnet cost and the optimization results are not very sensitive to refrigerant price. Operating cost is evaluated by multiplying the cost of electricity C_e, by the hourly power consumption W_{tot} and the duty cycle *CF*. Electricity cost is based on an average US household cost of 12 $¢kW^{-1}h^{-1}$ (www.eia.doe.gov), and the duty cycle is set to an arbitrary 0.35. The total power consumption is given by the sum of magnetic thermal cycle W_M, fluid pumping power W_P, and the power required to overcome the drive torque W_{mag}. The total input power includes the motor efficiency, η_{motor}, set to be 85%.

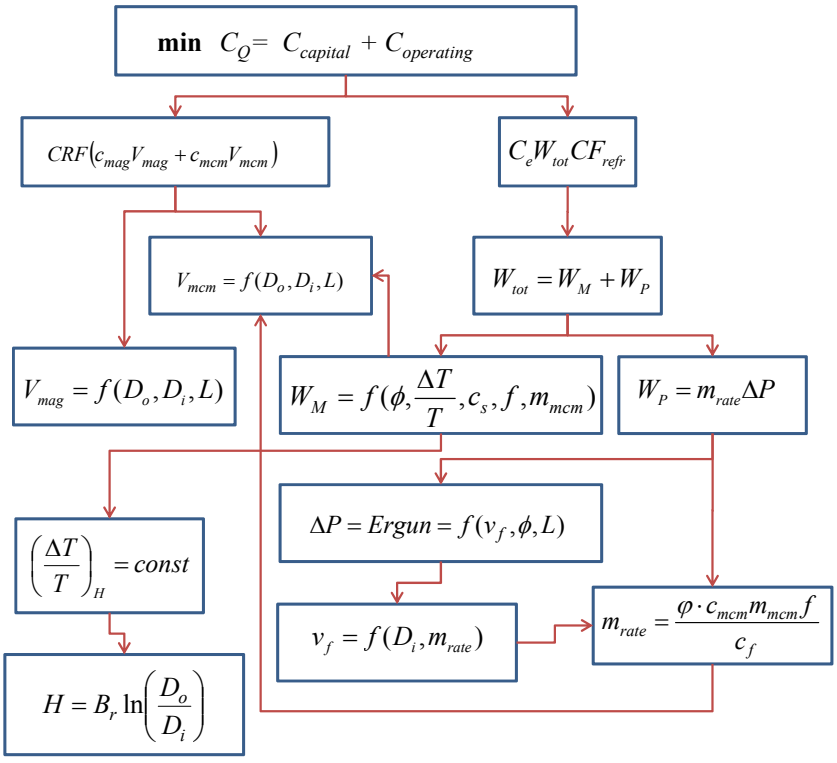

Figure 6: Objective function variable evaluation flowchart.

W_M is derived from the thermodynamics of the magnetic refrigeration cycle and it is function of ΔT_{MCE}, utilization, frequency, mass of the refrigerant and other fixed parameters as expressed in Equation 3. ΔT_{MCE} is obtained from the magnetic field intensity, which is function of the magnet geometry. The mass of the refrigerant also depends on the magnet geometry. W_P represents the hydraulic losses, which are function of the regenerator geometry, utilization, and frequency. Finally W_{mag} is function of the magnet geometry. The cooling capacity is not present in the objective function, but, instead, is a constraint to be met. The optimization problem is formalized as,

$$OF: \quad \textbf{Minimize } C_{tot} = C_{cap} + C_{op} = f(\varphi, f, D_o, D_i, L)$$

$$ST: \quad H_a < 1.5\ T$$
$$Q_c > \text{set value (between 70 W and 400 W)}$$
$$\Delta P < 0.7\ MPa$$

The constraints include the field intensity upper limit, minimum cooling power, and maximum pressure drop. The maximum field constraint is based on limits imposed by the permanent magnet remanence. As shown in Equation 3.2, the field intensity of a Halbach cylinders proportional to the logarithm of the external diameter. As will be shown in the results, in order to be cost effective is *non*-binding at 1.5 T.

The Q_c boundary constraint is necessary to avoid trivial solutions and its range is chosen to match the cooling power requirements for household refrigerators. Larger cooling capacities can be obtained by aggregating a number of pairs of cylinders and regenerators. Under such scenario linear scaling of the results can be applied.

The pressure drop is limited to a maximum of 0.7 MPa, because of design limitations on conventional hydraulic components. Displacers and pumps can be specified to operate at higher pressure drops, however they become more costly and the system less efficient and more prone to wear. As will be shown later, this is not a limiting factor. Also, the pressure drop evaluated by the Ergun correlation is scaled by a factor of 0.7 to account for a regenerator matrix with superior performance than packed spheres (which are generally used for prototyping).

The temperature span chosen is based on CECOMAF high back pressure standards, where T_C is set at a temperature equivalent to an evaporator at 5º C and T_H to a condenser temperature of 55 ºC. Upper and lower bounds are in place for the objective function variables as listed in Table 2. The

optimization search is performed using a number of different start points and all results converge to the same optimized solution, suggesting that the OF is convex in the selected region.

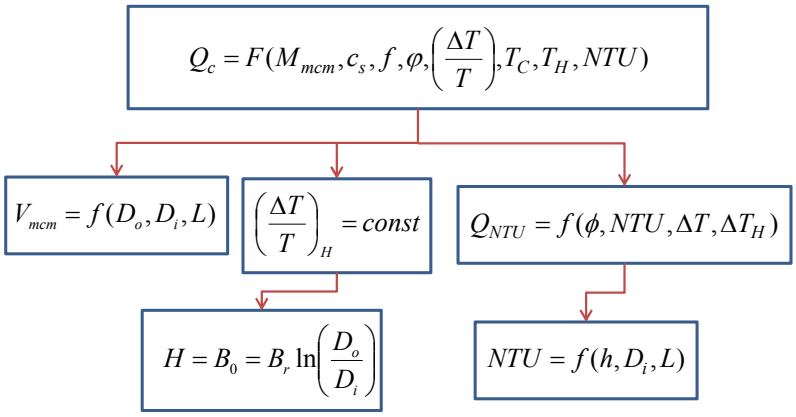

Figure 7: Cooling power derivation flowchart.

The model loops the optimization routine over a range of ideal MCE values and required cooling powers, so that the results can be visualized showing sensitivity in respect to these two parameters. Water is assumed as the heat transfer fluid, while the refrigerant has the thermo-mechanical properties of gadolinium (with the exception of its ideal MCE and a constant c_B). Thermal insulation to the environment is assumed with a heat leak coefficient of 0.2 WK^{-1} (approximately 60% of our first generation permanent magnet magnetic refrigerator). Geometrical demagnetization of the regenerator is reduced from 25% to 15% assuming that improved geometry or effective flux shimming can be implemented (Peksoy and Rowe, 2004). The temperature span chosen is based CECOMAF high back pressure standards, where T_C is set at a temperature equivalent to an evaporator at 5º C and T_H to a condenser temperature of 55 ºC. Parameter values are summarized in Table 2, and upper and lower bounds are in place for the objective function variables as listed in Table 3. The optimization search is performed using a number of different start points and all results converge to the same optimized solution, suggesting that the *OF* is convex in the selected region.

Table 1. Model parameters

Parameter	Value/Range
T_H [ºC]	55
T_C [ºC]	5
Porosity (α) [-]	0.36
Spheres diameter [mm]	0.3
B_r [T]	1.35
Demagnetization factor	15%
R thermal mass ratio [-]	1.7
Q_c [W]	70-400
MCE_{ideal}/MCE_{Gd} @ 22 ºC [-]	0.6-1.1
Q_{amb} heat leak coeff. [W/K]	0.2
Capital Recovery [years]	10

Table 2. OF variable upper and lower bounds

Parameter	Lower Bounds	Upper Bounds
Utilization [-]	0.2	2
Device frequency [Hz]	.5	5
Magnet length [m]	0.02	0.3
Cylinder outside diameter [m]	0.03	0.3
Cylinder inside diameter [m]	0.01	0.1

4. OPTIMIZATION RESULTS

This section presents the estimated cost, size, operating parameters, and efficiency of a dual Halbach cylinder magnetic refrigerator when the sum of operating and capital cost rate is the optimization objective function. Optimized results are determined for a range of values of the design variables $MCE_{ideal}/MCE_{Gd@295K}$ (0.6-1.1, 0.05 increments), and maximum device cooling power (70-400 W, 11 W increments). The results are presented as contour plots with a mesh resolution of 300 optimized points. It is worth noting that throughout the optimization sweep the

pressure drop was the only binding constraint (with the exception of Q_c) and the upper and lower bounds of the *OF* variables were never active. Lagrange multipliers at the solution points are close to zero, suggesting that the optimization results are not strongly limited by the constraints; this is supported by the fact that if the pressure drop limit is removed the solution does not change significantly, favoring slightly higher aspect ratio regenerators with a minor increase in cost. Higher pressure drops are undesirable because of the efficiency loss, therefore a capital cost saving (from higher specific exergetic cooling) would be hampered by a higher operating cost. Regenerator matrix structure plays a critical role in this regard, maximizing heat transfer while minimizing viscous losses. For instance the optimization process showed that if the regenerator was to operate with a pressure drop 50% lower than the 300 μm spheres while maintaining the same heat transfer, we would see approximately 20% savings in both capital and operating cost.

Figure 8 illustrates the cost of the magnets and of the refrigerant. The plots display similar trends and intuitively the system grows larger and more expensive to satisfy larger cooling demand, while larger MCE has an inverse effect, helping the power density, and thus reducing size and cost. For the given variable ranges the cost of the magnets spans from $100 to $ 800 and $50 to $250 for the refrigerant.

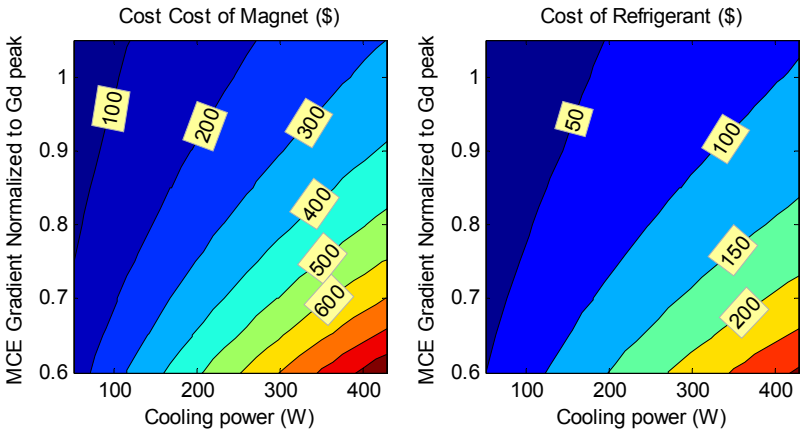

Figure 8: Capital cost of magnets and refrigerant.

Figure 9 (left) shows the cost of refrigeration on a hourly base assuming a life cycle of 10 years and a duty cycle of 0.35. The optimized cost shows a similar trend as the previous plots with values ranging between 0.4 and 2.4 ¢/h. Figure 9 (right) shows the weighting of the capital to operating costs. For high MCE and low cooling demand, capital cost is < 1.5 times the operating cost, while it grows 2-2.5 times for low MCE and high cooling demand. Also, cost ratio is less sensitive to cooling demand as this grows larger.

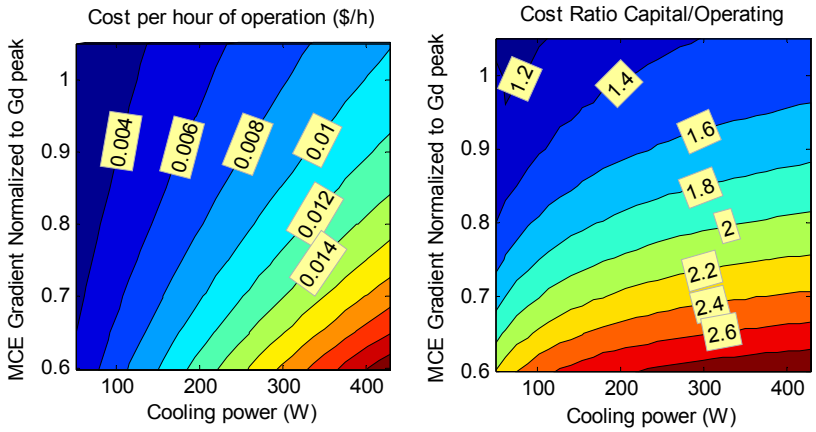

Figure 9: Ratio of capital/operating cost rate and cost per hour of operation.

Looking at the cylinder geometry (Figure 10), the magnet length shows virtually no sensitivity to cooling demand above 200 W. Regenerator length ranges from a minimum of 90 mm to 120 mm. The magnet outer diameter is sensitive to both magnetocaloric properties and cooling demand, ranging from 40 mm to 120 mm, while the inner diameter ranges from 20 mm to 50 mm, following a similar sensitivity pattern as the outer diameter. Although not reported in any of the figures, the regenerator aspect ratio (*L/D*) is insensitive to MCE, while it varies from 5.5 to 2.5 for cooling demands between 70 and 400 W.

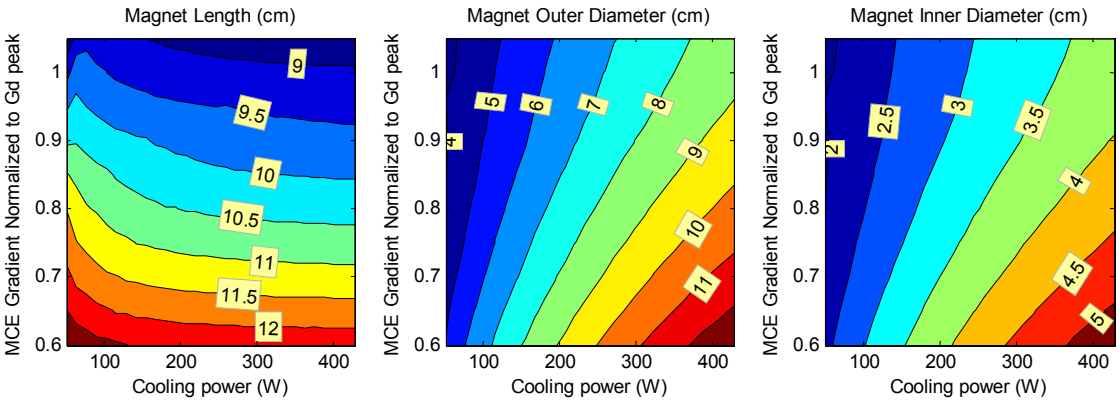

Figure 10: Optimization results for magnet geometry: length, outer diameter and inner diameter.

Peak magnetic field, frequency, and utilization values show some interesting and somewhat unexpected results (Figure 11). The optimization routine suggests that the field should not be maximized, but rather set around 1 T with no more than 15% increase if high cooling demand and low MCE is chosen. This result is quite remarkable because the device magnetization cycle is

sinusoidal and not stepwise, thus the effective field change is even lower (RMS rather than peak value). Maximizing the peak magnetic field would create a more efficient cycle and higher cooling capacity, however it seems that a lower field creates a better balance between operating cost and capital cost. The figure also shows that the optimized frequency is not binding, ranging between 3 and 4.5 Hz; interestingly, lower frequencies are preferred for the higher cooling demands. Finally utilization seems to be optimized for relatively low values, between 0.3 and 0.6. This is due to the large imposed temperature span (ΔT = 50 °C). Higher cooling power demand increases the utilization optimal value with associated reduction in optimized operating frequency (3 Hz vs 4.5 Hz). Also, utilization is seen to be insensitive to the magnetocaloric properties of the refrigerant although currently available refrigerants would likely deviate somewhat from this result, as temperature perturbations induced by the fluid would affect performance more significantly.

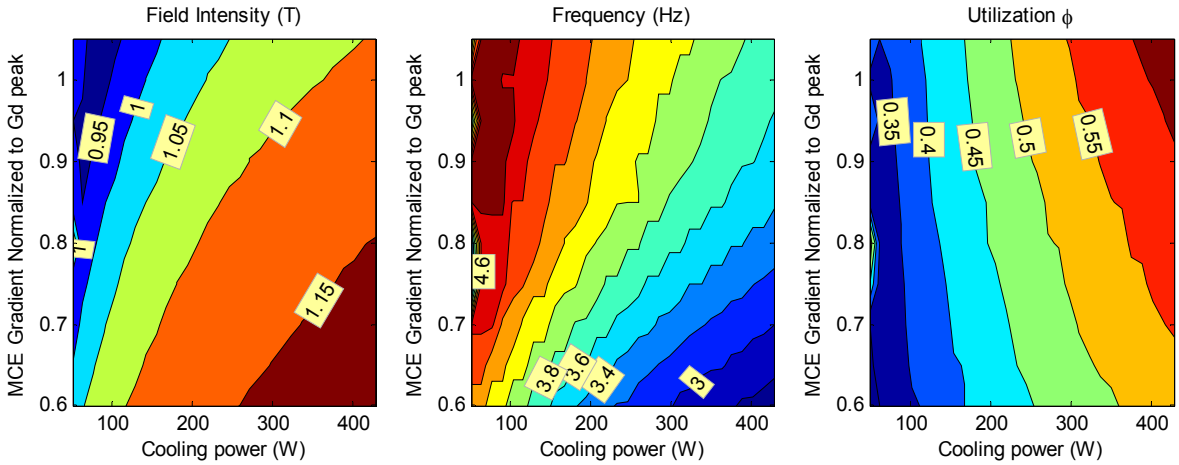

Figure 11: Optimized results for maximum field intensity, frequency, and utilization.

Figure 12 (left) illustrates the expected efficiencies of the optimized system (when operating at the maximum rated cooling power). As expected both higher MCE and rated cooling power promote higher efficiencies. Smaller systems (below 200 W) have a COP not larger than 3.5 while higher capacity systems show COPs up to 4.5. This means that for the specified temperature span the model forecasts predicts between 0.3 and 0.85 of the Carnot efficiency. Although the estimate may seem high, it corroborates theoretical findings by Kitanovski et al. (2009), if considered that here an ideal materials are used in a large MCE range instead of gadolinium. Rowe (2012) also predicted that an ideal MR with low viscous losses should approach the Carnot efficiency.

Figure 12 (center) shows that specific exergetic cooling is mostly sensitive to the refrigerant MCE, while it is does not depend on cooling power as the device's cooling capacity grows larger than 200 W. The specific exergetic cooling is found to range between 0.5 WT^{-1} cm^{-3} and 1.5 WT^{-1} cm^{-3}. Total cost of cooling follows a similar trend ranging between 2.5 $\$W^{-1}$ and 1 $\$W^{-1}$ (Figure 12, right).

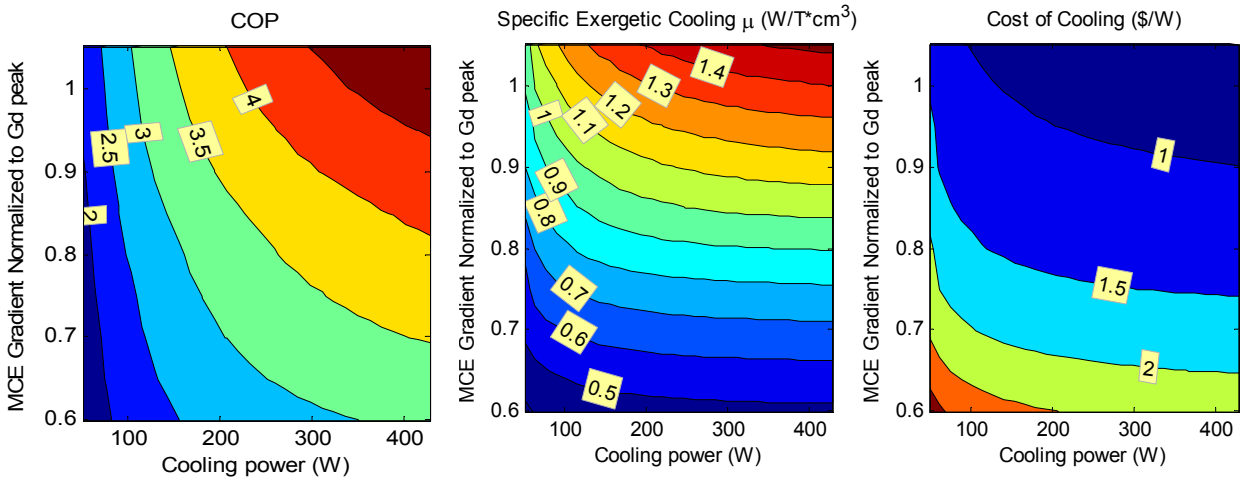

Figure 12: Optimization results for COP specific exergetic cooling and cost of cooling.

It is worth noting that if the cost of refrigerant is reduced to 20 $\$kg^{-1}$ from 150 $\$kg^{-1}$ the results are almost the same for this particular device configuration. In this case, there is a 25% reduction in specific exergetic cooling and a slightly higher COP resulting in approximatively to 20% improvement in cost of cooling.

The magnet figure of merit Λ_{cool} (Bjørk et al, 2009) is a measure of how efficiently the field generator is used,

$$\Lambda_{cool} = \left(H_{\max}^{2/3} - H_{\max}^{2/3} \right) \frac{V_{field}}{V_{mag}} P_{field} \tag{19}$$

where V_{field} is the volume with the high field and V_{mag} is the volume of the magnet itself and P_{field} is the portion of the total cycle period that the magnet is actively used. Given the nature of the cycle under consideration, H_{max} and H_{min} correspond to the for RMS values, while P_{field} is set to 0.5. Λ_{cool} shows small variations (0.03 $T^{2/3}$ - 0.039 $T^{2/3}$) over the full range. In general, smaller cooling power and higher MCE favors better magnet efficiency.

5. Discussion

Due to the approximate nature of the parasitic magnetic torque (Equation 15), the impact of torque on the optimized results was investigated by varying the magnitude from zero to twice the assumed scaling used in Equation 15. Design parameters seemed relatively insensitive to torque variations, while the operating parameters changed so as to optimize efficiency and operating costs. For instance larger torques are acceptable at higher utilizations, as more power can be delivered per cycle; however, because pressure drop is a binding constraint, operating frequency needs to be reduced. As expected efficiency diminishes with larger torques. However for the range of tested torques the overall trends presented in the previous figures did not change significantly with operating parameters and efficiencies varying at the most up to 30%.

Although the optimization results suggest that a field larger than 1 T might not be required for an optimal cost performance for this specific configuration, it is important not to under-estimate the impact of ideal refrigerant properties when compared to real refrigerants, especially if expected to operate over a large temperature span (i.e. low back pressure standards).

As discussed elsewhere (Bjørk et al, 2009), Halbach cylinder configuration is costly because of the ineffective use of large amounts of Nd (relatively low Λ_{cool}). This specific refrigerator configuration was not chosen because of its cost and performance, but rather because its model can be validated against a well characterized experimental device. Additionally, the relatively simple analytical-empirical correlations predicting the system performance, given geometrical and operational parameters, marry well with the simplified analytical AMR model, allowing a sweep thousands of optimized points in a matter of minutes using an average PC.

This work is in very good agreement with the optimization results obtained by Bjørk et al (2011). He estimated the minimum total cost for magnet and refrigerant for a number of regenerator configurations. He considered both Gadolinium and an idealized material with constant ΔT_{ad} (with peak adiabatic temperature change to be the same as Gd) in parallel plates and 300 μm sphere regenerators. Operating conditions are set to 100 W of cooling capacity and 20 °C temperature span. Using the ideal material properties and spheres as the matrix geometry for the regenerator, Bjørk suggested a total cost of $7. The model presented here, under the same conditions, estimates a cost of $15. If we take into account that in the dual Halbach cylinder the magnet is actively used only for 50% of the cycle, while the model used by Bjørk is based on 100% of the cycle, the results are strikingly close. It is interesting to observe that if the model takes into account the operating cost,

the optimized capital cost shifts from $15 to $35 and the COP improves from 1 to 4, while the operating frequency changes from 10 Hz to 2.5 Hz. Bjørk commented in his article that his model did not find an optimum for frequency, which means that in the parameter space explored, the cost of the device monotonically decreases with cycle frequency. However, if operating cost is accounted for, viscous losses degrade the efficiency to a degree that the overall (capital + operating) cost is negatively affected by it and an optimum can be found, well below 10 Hz.

3. CONCLUSION

An optimization model of a dual Halbach cylinder magnetic refrigerator was developed using a simplified analytical method to evaluate the AMR performance. The objective function was the capital and operating cost rate based on a 10 years life cycle, and the constraints were set to be minimum cooling power, maximum pressure drop, and maximum peak field. The model was first validated against extrapolated experimental data. Results show that, under the presented constraints and configuration, cost limiting factors are the permanent magnet size and pressure drop, while, surprisingly, power requirements are achieved with a relatively low magnetic field, operating frequency, and utilization factor. Among all results, it was valuable to observe that if cost rate is to be maximized, the target magnetic field should not be higher than 1.15 T, operating frequency no more than 4.5 Hz and utilization not larger than 0.6. It was also found that cost rate ranges between 0.4 and 2.4¢/h. Finally, even if the constraint of 0.7 MPa is lifted, it seems that the optimization model would generally not choose solutions operating at higher pressure drop because a higher operating cost due to lower efficiency would occur.

REFERENCES

Aprea C., Greco A., and Maiorino A., 2012, A dimensionless numerical analysis for the optimization of an active magnetic regenerative refrigerant cycle, *International Journal of Energy Research*.

Bjørk R., Smith A., Bahl C.R.H., Pryds N., 2011, Determining the minimum mass and cost of a magnetic refrigerator, *International Journal of Refrigeration*, Volume 34, Issue 8, pp 1805-1816.

Bjørk R., Bahl C.R.H., Smith A., Pryds N., 2009, Review and comparison of magnet designs for magnetic refrigeration, *International Journal of Refrigeration*, Volume 33, Issue 3, pp 437-448.

Burdyny T., Rowe A., 2012, Simplified modeling of active magnetic regenerators, *International Journal of Refrigeration*, Available online 31, ISSN 0140-7007.

Dikeos, J. and Rowe, A., 2013, Validation of an Active Magnetic Regenerator (AMR) Test Apparatus Model, *International Journal of Refrigeration*, Vol. 36, Issue 3, pp 921-931.

Grössinger R., Haas M., Turtelli S., 2010, Magnetocaloric versus thermoelectric effect – new systems for thermal applications, *Forth IIF-IIR International Conference on Magnetic Refrigeration at Room Temperature*, Baoutou, pp 15-29.

Gutfleisch O., Willard M. A., Brück E., Chen C. H., Sankar S. G., and Liu J. P., 2010, Magnetic Materials and Devices for the 21st Century: Stronger, Lighter, and More Energy Efficient, *Adv. Mater.,* vol. 23, no. 7, pp. 821–842.

Kaviany M., 1995, Principles of Heat Transfer in Porous Media, Springer.

Kitanovski, A., Egolf, P.W., 2009, Application of magnetic refrigeration and its assessment, *Journal of Magnetism and Magnetic Materials*, vol. 321, Issue 7, pp. 777-781.

Ní Mhíocháin T.R. , Weaire D., McMurry S.M., Coey J.M.D., 1999, Analysis of torque in nested magnetic cylinders, *J. Appl. Phys.,* 86: 6412-6425.

Peksoy O., Rowe A., 2005, Demagnetizing effects in active magnetic regenerators, *Journal of Magnetism and Magnetic Materials* 288, pp 424–432.

Rowe A., 2012, Thermodynamics of active magnetic regenerators: Part I*, Cryogenics*, 52 (2-3): 111-118.

Rowe A., 2012, Thermodynamics of active magnetic regenerators: Part II, *Cryogenics*, 52 (2-3): 119-128.

Rowe A., 2011, Configuration and performance analysis of magnetic refrigerators*, International Journal of Refrigeration*, 34(1): 168-177.

Rowe A. and Barclay J., 2003, Ideal Magnetocaloric Effect for Active Magnetic Regenerators, *J. Appl. Phys,* 93(3): 1672-1676.

Tura A., Rowe A., 2011, Permanent magnet magnetic refrigerator design and experimental characterization, *International Journal of Refrigeration*, 34(3):628-639.

Schmidt F.W. and Wilmott A.J., 1981, Thermal energy storage and regeneration, Hemisphere, Washington DC.

Yu B, Liu M, Egolf P, Kitanovski A, 2010, A review of magnetic refrigerator and heat pump prototypes built before the year 2010*, International Journal of Refrigeration*, 33 (6): 1029-1060.